Memo version 6.6.2

BESIII Analysis Memo

BAM-552

May 30, 2022

Study of decay parameters in $J/\psi \to \Sigma^+\bar{\Sigma}^-$

Yunlong Xiao*[a], Liang Yan†[1a], and Jianyu Zhang[b], Liang Liu[c], Patrik Adlarson[d], Andrzej Kupsc[d], and Haibo Li[b]

[a]*Fudan University, People's Republic of China*
[b]*Institute of High Energy Physics, People's Republic of China*
[c]*University of Science and Technology of China, People's Republic of China*
[d]*Uppsala University, Sweden*

Internal Referee Committee

Guangshun Huang (Chair)[1], Dong Liu[2], and Dexun Lin[3]

[1]*University of Science and Technology of China, People's Republic of China*
[2]*Helmholtz Institute Mainz, Germany*
[3]*Institute of Modern Physics, People's Republic of China*

DocDB : https://docbes3.ihep.ac.cn/cgi-bin/DocDB/ShowDocument?docid=1027

Hypernews : http://hnbes3.ihep.ac.cn/HyperNews/get/paper552.html

Abstract

Using J/ψ data of $(10087.8 \pm 23.8) \times 10^6 J/\psi$ taken with the Beijing Spectrometer (BESIII) at the Beijing Electron-Positron Collider(BEPCII), the process $J/\psi \to \Sigma^+\bar{\Sigma}^-(\Sigma^+ \to p\pi^0, \bar{\Sigma}^- \to \bar{n}\pi^-$ and $\Sigma^+ \to n\pi^+, \bar{\Sigma}^- \to \bar{p}\pi^0)$ has been measured exclusively. By combining two different decay channels($\Sigma^+ \to p\pi^0, \bar{\Sigma}^- \to \bar{n}\pi^-$ and $\Sigma^+ \to n\pi^+, \bar{\Sigma}^- \to \bar{p}\pi^0$), the branching fraction of $J/\psi \to \Sigma^+\bar{\Sigma}^-$ is measured to be $(10.85 \pm 0.01 \pm 0.31) \times 10^{-4}$, with an improved precision compared to previous measurements. By fitting two different decay channels, the parameters $\alpha_{J/\psi}$ and $\Delta\Phi_{J/\psi}$ are improved, as listed below:

- $\alpha_{J/\psi} = -0.5156 \pm 0.0030 \pm 0.0061$
- $\Delta\Phi_{J/\psi} = -0.2772 \pm 0.0044 \pm 0.0041$

The parameter $\alpha_{(\Sigma^+ \to n\pi^+)}$ and $\frac{\alpha_{(\Sigma^+ \to n\pi^+)}}{\alpha_{(\Sigma^+ \to p\pi^0)}}$ are improved significantly, as listed below:

- $\alpha_{(\Sigma^+ \to n\pi^+)} = 0.0481 \pm 0.0031 \pm 0.0019$

- $\frac{\alpha_{(\Sigma^+\to n\pi^+)}}{\alpha_{(\Sigma^+\to p\pi^0)}} = -0.0490 \pm 0.0032 \pm 0.0021$

The parameters $\alpha_{(\bar{\Sigma}^-\to\bar{n}\pi^-)}$ and $\frac{\alpha_{(\bar{\Sigma}^-\to\bar{n}\pi^-)}}{\alpha_{(\bar{\Sigma}^-\to\bar{p}\pi^0)}}$ are measured for the first time, as listed below:

- $\alpha_{(\bar{\Sigma}^-\to\bar{n}\pi^-)} = -0.0565 \pm 0.0047 \pm 0.0022$
- $\frac{\alpha_{(\bar{\Sigma}^-\to\bar{n}\pi^-)}}{\alpha_{(\bar{\Sigma}^-\to\bar{p}\pi^0)}} = -0.0571 \pm 0.0053 \pm 0.0032$

The CP asymmetries are extracted for the first time, as listed below:

- $A_{CP} = \frac{\alpha_{(\Sigma^+\to n\pi^+)}+\alpha_{(\bar{\Sigma}^-\to\bar{n}\pi^-)}}{\alpha_{(\Sigma^+\to n\pi^+)}-\alpha_{(\bar{\Sigma}^-\to\bar{n}\pi^-)}} = -0.08 \pm 0.052 \pm 0.028$

The Q value of "12%" is tested, as listed below:

- $Q = \frac{P_{J/\psi}}{P_{\psi(3686)}} \times \frac{\psi(3686)\to\Sigma^+\bar{\Sigma}^-}{J/\psi\to\Sigma^+\bar{\Sigma}^-} = \frac{1}{1.4194} \times \frac{2.32\pm0.12}{10.85\pm0.29} = 15.1\% \pm 0.9\%$

*xiaoyl20@fudan.edu.cn
†yanl@fudan.edu.cn

Contents

1 ChangeLog

From Memo V6.5 to Memo V6.6.1:

Compared with the Memo V6.5, the difference is that we used the new reconstruction algorithm to replace the old reconstruction algorithm.

The header file of the new reconstruction algorithm: #include "$MDCHOUGHFINDERROOT/share/jobOptions_MdcPatTsfHoughRec.txt"

The header file of the old reconstruction algorithm: #include "$MDCXRECOROOT/share/jobOptions_MdcPatTsfRec.txt".

In fact, the template of the BESIII new reconstruction algorithm have been updated in those versions: BOSS703, BOSS705, BOSS707, and BOSS708. The new reconstruction algorithm corrects some problems of reconstruction in the low momentum charge $\pi^+\pi^-$.

2 Introduction

Hyperon non-leptonic decays have played a vital role in studying CP violation in particle physics [1]. As an ideal probe, it can be used to study strong interaction region from non-perturbation to perturbation. Besides, it can use to test standard model by the production and decay of the hyperon. In spin 1/2 hyperon non-leptonic decay, the angular distribution of the daughter baryon takes the form $\frac{dN}{d\Omega} = \frac{1}{4\pi}(1 + \alpha_\Sigma \vec{P}\hat{p}_d)$, where $\vec{P}$ is the hyperon polarization, $\hat{p}_d$ is the daughter baryon momentum unit vector in its mother's rest frame, and α_Σ is the hyperon asymmetry parameter [2]. Therefore, using α and $\bar{\alpha}$, we can test CP violation by $A_{CP} = \frac{\alpha+\bar{\alpha}}{\alpha-\bar{\alpha}}$. If $A_{CP} = 0$, the CP is conserved. Historically, the Hypercp experimental group has measured the CP destruction of charged Ξ and Λ particles, but no evidence of CP violation has been found [3] [4]. A recent study by the BESIII collaboration have reported $\alpha_{(\Lambda\to p\pi^-)} = 0.750 \pm 0.009 \pm 0.004$ [5], which is significantly different compared to the older value of 0.642 ± 0.013 [6]. Besides, for the Σ particle, the results of $\alpha_{(\Sigma^+\to n\pi^+)}$ come from the measurement results of nearly 50 years ago [7], so it is very meaningful for us to measure $\alpha_{(\Sigma^+\to n\pi^+)}$ independently at BESIII. What's more, so far we have no measurement of $\alpha_{(\bar{\Sigma}^-\to\bar{n}\pi^-)}$ existence. The decay parameters of some Hyperons are listed in the Table. 1. In this work, we want to measure or improve previous measurements for the first time(red words).

Tab. 1: The decay parameters of Hyperon(All information is from PDG [32])

parameters	value	parameters	value
$\alpha_{(\Sigma^+\to p\pi^0)}$	-0.982 ± 0.014	$\alpha_{(\Lambda\to p\pi^-)}$	0.732 ± 0.014
$\alpha_{(\bar{\Sigma}^-\to\bar{p}\pi^0)}$	0.99 ± 0.04	$\alpha_{(\bar{\Lambda}\to\bar{p}\pi^-)}$	-0.758 ± 0.012
$\alpha_{(\bar{\Sigma}^-\to\bar{n}\pi^-)}$	Not be measured	$\alpha_{(\bar{\Lambda}\to\bar{n}\pi^0)}$	-0.692 ± 0.017
$\alpha_{(\Sigma^+\to n\pi^+)}$	0.068 ± 0.013	$\alpha_{(\Lambda\to n\pi^0)}$	Not be measured
$\frac{\alpha_{(\bar{\Sigma}^-\to\bar{n}\pi^-)}}{\alpha_{(\bar{\Sigma}^-\to\bar{p}\pi^0)}}$	Not be measured	$\frac{\alpha_{(\bar{\Lambda}\to\bar{n}\pi^0)}}{\alpha_{(\bar{\Lambda}\to\bar{p}\pi^-)}}$	0.913 ± 0.030
$\frac{\alpha_{(\Sigma^+\to n\pi^+)}}{\alpha_{(\Sigma^+\to p\pi^0)}}$	-0.069 ± 0.013	$\frac{\alpha_{(\Lambda\to n\pi^0)}}{\alpha_{(\Lambda\to p\pi^-)}}$	1.01 ± 0.07
$\alpha_{(\bar{\Sigma}^+\to\bar{n}\pi^+)}$	Not be measured	$\frac{\alpha_{(\Lambda\to n\pi^0)}+\alpha_{(\bar{\Lambda}\to\bar{n}\pi^0)}}{\alpha_{(\Lambda\to n\pi^0)}-\alpha_{(\bar{\Lambda}\to\bar{n}\pi^0)}}$	Not be measured
$\alpha_{(\Sigma^-\to n\pi^-)}$	-0.068 ± 0.008	$\frac{\alpha_{(\Lambda\to p\pi^-)}+\alpha_{(\bar{\Lambda}\to\bar{p}\pi^+)}}{\alpha_{(\Lambda\to p\pi^-)}-\alpha_{(\bar{\Lambda}\to\bar{p}\pi^+)}}$	-0.002 ± 0.012
$\frac{\alpha_{(\Sigma^+\to p\pi^0)}+\alpha_{(\bar{\Sigma}^-\to\bar{p}\pi^0)}}{\alpha_{(\Sigma^+\to p\pi^0)}-\alpha_{(\bar{\Sigma}^-\to\bar{p}\pi^0)}}$	0.00 ± 0.04	$\frac{\alpha_{(\Sigma^+\to n\pi^+)}+\alpha_{(\bar{\Sigma}^-\to\bar{n}\pi^-)}}{\alpha_{(\Sigma^+\to n\pi^+)}-\alpha_{(\bar{\Sigma}^-\to\bar{n}\pi^-)}}$	Not be measured

In the above formula we notice that α (decay parameter) and P (polarization) appear as a product in the angular momentum distribution, which means that we cannot derive the decay parameter from the angular distribution of a single final state particle. However, in the BESIII experiment, Σ^+ and the $\bar{\Sigma}^-$ hyperon are produced by electron-positron annihilation. It provides a unique environment to study the production and decay of hyperons. On the one hand, the parameters $\alpha_{(\Sigma^+\to p\pi^0)}$ and $\alpha_{(\bar{\Sigma}^-\to\bar{p}\pi^0)}$ have been precise measured by the BESIII collaboration [42]. On the other hand, recently, the J/ψ data of 10

billion taken with the Beijing Spectrometer (BESIII) at the Beijing Electron-Positron Collider(BEPCII). It's good for measuring the decay parameters that are about Σ decays into neutron and anti-neutron and the conservation of CP in baryon region will be tested with high accuracy.

To describe the reaction $e^+e^- \rightarrow J/\psi \rightarrow \Sigma^+\bar{\Sigma}^- \rightarrow p\pi^0\bar{n}\pi^-(n\pi^+\bar{p}\pi^0)$, the theoretical formula of differential cross-section [11] we used is

$$\begin{aligned} W(\xi) =& t_0(\xi) + \alpha_\psi t_5(\xi) \\ & \alpha_{\Sigma^+}\alpha_{\bar{\Sigma}^-}(t_1(\xi) + \sqrt{1-\alpha_\psi^2}cos(\Delta\Phi)t_2(\xi) + \alpha_\psi t_6(\xi) \\ & \sqrt{1-\alpha_\psi^2}sin(\Delta\Phi)(\alpha_{\Sigma^+}t_3(\xi) - \alpha_{\bar{\Sigma}^-}t_4(\xi)). \end{aligned} \tag{1}$$

The arguments to the function are

$$\begin{aligned} & t_0(\xi) = 1 \\ & t_1(\xi) = sin^2\theta_\Sigma sin\theta_p sin\theta_{\bar{n}} cos\phi_p cos\phi_{\bar{n}} + cos^2\theta_\Sigma cos\theta_p cos\theta_{\bar{n}} \quad (t_1(\xi) = sin^2\theta_\Sigma sin\theta_n sin\theta_{\bar{p}} cos\phi_n cos\phi_{\bar{p}} + cos^2\theta_\Sigma cos\theta_n cos\theta_{\bar{p}}) \\ & t_2(\xi) = sin\theta_\Sigma cos\theta_\Sigma (sin\theta_p cos\theta_{\bar{n}} cos\phi_p + cos\theta_p sin\theta_{\bar{n}} cos\phi_{\bar{n}}) \quad (t_2(\xi) = sin\theta_\Sigma cos\theta_\Sigma (sin\theta_n cos\theta_{\bar{p}} cos\phi_n + cos\theta_n sin\theta_{\bar{p}} cos\phi_{\bar{p}})) \\ & t_3(\xi) = sin\theta_\Sigma cos\theta_\Sigma sin\theta_p sin\phi_p \quad (t_3(\xi) = sin\theta_\Sigma cos\theta_\Sigma sin\theta_n sin\phi_n) \\ & t_4(\xi) = sin\theta_\Sigma cos\theta_\Sigma sin\theta_{\bar{n}} sin\phi_{\bar{n}} \quad (t_4(\xi) = sin\theta_\Sigma cos\theta_\Sigma sin\theta_{\bar{p}} sin\phi_{\bar{p}}) \\ & t_5(\xi) = cos^2\theta_\Sigma \\ & t_6(\xi) = cos\theta_p cos\theta_{\bar{n}} - sin^2\theta_\Sigma sin\theta_p sin\theta_{\bar{n}} sin\phi_p sin\phi_{\bar{n}} \quad (t_6(\xi) = cos\theta_n cos\theta_{\bar{p}} - sin^2\theta_\Sigma sin\theta_n sin\theta_{\bar{p}} sin\phi_n sin\phi_{\bar{p}}) \end{aligned} \tag{2}$$

In the formula 1 and 2, ξ represents the polar angle and azimuth angle of the particle in its final state. The formula consists of three parts: the first term represents the scattering angle of the Sigma particle, the second term represents the correlation of the spins, and the third term is the independent polarization term. The $\Delta\phi$ represents the strength of hyperonic polarization. It can be seen from the third term that if $\Delta\phi$ is not equal to 0, then we can obtain the decay parameters α_{Σ^+} and $\alpha_{\bar{\Sigma}^-}$ of both Sigma hyperon and anti-sigma hyperon, and further test the conserved quantity of CP. The corresponding parameters in the formula can be obtained by analyzing and fitting the angular distribution information of the data.

The full differential cross-section can be described by the five measured angles $(\theta_\Sigma, \theta_p, \phi_p, \theta_{\bar{n}}, \phi_{\bar{n}})$ and $(\theta_\Sigma, \theta_n, \phi_n, \theta_{\bar{p}}, \phi_{\bar{p}})$. Here θ_Σ is the angle between Σ^+ and the electron (e^-) beam in the reaction center-of-mass frame. The other four angles are the polar and azimuthal angles of the proton and anti-neutron(or anti-proton and neutron) in the helicity frame, respectively [9] [10]. To obtain the helicity angles, one begins from the production scattering plane of $e^+e^- \rightarrow J/\psi \rightarrow \Sigma^+\bar{\Sigma}^- \rightarrow p\pi^0\bar{n}\pi^-(n\pi^+\bar{p}\pi^0)$ the system. This is obtained by considering the centre-of-mass (CM) system where the four-momenta of the electron-

positron and $\Sigma^+\bar{\Sigma}^-$ are given by

$$\begin{aligned} \vec{p}_{\Sigma^+} &= -\vec{p}_{\bar{\Sigma}^-} \\ \frac{\vec{k}_{e^+}}{|\vec{k}_{e^+}|} &= -\frac{\vec{k}_{e^-}}{|\vec{k}_{e^-}|} = \vec{k}. \end{aligned} \tag{3}$$

The xz-scattering plane is defined by the $\vec{p}$ and $\vec{k}$ vectors, while the y-axis is the normal to the plane. From a right-handed coordinate system with the basis vectors

$$\begin{aligned} \vec{e}_x &= \frac{1}{sin\theta_\Sigma}(\vec{p}\times\vec{k})\times\vec{p} \\ \vec{e}_y &= \frac{1}{sin\theta_\Sigma}(\vec{p}\times\vec{k}) \\ \vec{e}_z &= \vec{p}, \end{aligned} \tag{4}$$

the helicity angles are obtained, where $\vec{p}$ and $\vec{k}$ are the unit vectors of $\vec{p}_\Sigma$ and $\vec{k}_e$, respectively. As seen from the basis vector definitions in Fig. 1, the helicity angles are defined with respect to the direction of the outgoing hyperon in the CM frame ($\vec{e}_z$). Technically the helicity angles are obtained by (i) boosting the hyperon(anti-hyperon) in the CM frame and obtain the polar, $\theta^+_\Sigma(\theta_{\bar{\Sigma}^-})$ and $\phi_{\Sigma^+}(\phi_{\bar{\Sigma}^-})$, (ii) by boosting the proton(antiproton) first in the CM frame and then into the hyperon(anti-hyperon) rest frame, (iii) and then by rotating the proton(antiproton) with respect to the boosted z-axis and y-axis with an angle $-\phi_{\Sigma^+}(\phi_{\bar{\Sigma}^-})$ and $-\theta^+_\Sigma(\theta_{\bar{\Sigma}^-})$, respectively. All corresponding symbols are listed in the Table. 2.

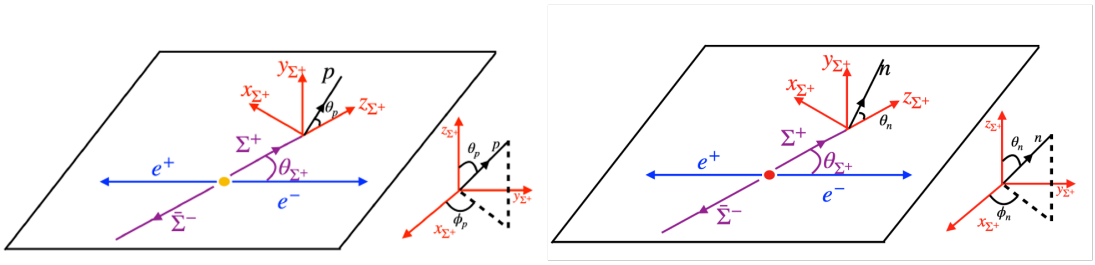

Fig. 1: (left) the helicity frame we used in the $J/\psi \to \Sigma^+\bar{\Sigma}^-$,$\Sigma^+ \to p\pi^0$, $\bar{\Sigma}^- \to \bar{n}\pi^-$,(right) the helicity frame we used in the $J/\psi \to \Sigma^+\bar{\Sigma}^-$,$\Sigma^+ \to n\pi^+$,$\bar{\Sigma}^- \to \bar{p}\pi^0$.

Tab. 2: Meaning of symbol

Symbol	Meaning
α_ψ	Angle distribution parameter
$\Delta\Phi$	Polarization parameter
α_{Σ^+}	Asymmetric parameter
$\alpha_{\bar{\Sigma}^-}$	Asymmetric parameter
θ_Σ	Angle between the electron and the hyperon
θ_p	Polar angle between the p and the Σ^+
$\theta_{\bar{n}}$	Polar angle between the $\bar{n}$ and the Σ^-
ϕ_p	Azimuth angle between the p and the Σ^+
$\phi_{\bar{n}}$	Azimuth angle between the $\bar{n}$ and the Σ^-
$\theta_{\bar{p}}$	Polar angle between the $\bar{p}$ and the Σ^-
θ_n	Polar angle between the n and the Σ^+
$\phi_{\bar{p}}$	Azimuth angle between the $\bar{p}$ and the Σ^-
ϕ_n	Azimuth angle between the n and the Σ^+

Secondly, the angular distribution of the baryon states is also very interesting topic. In general, the angular distribution of a neutral vector resonance V decay into a hadron anti-hadron pair can be described as: Actually, V is instead of a charmonium vector like $J/\psi, \psi(3686)$. The angular distribution of a charmonium vector decay in hyperon and anti-hyperon could be described as $1 + \alpha_\psi cos^2\theta$.(It has been rephrased:Secondly, the angular distribution of the baryon states is also very interesting topic. In general, the angular distribution of a neutral vector resonance $J/\psi, \psi(3686)$ decay into a hadron anti-hadron pair can be described as: $1 + \alpha_\psi cos^2\theta$.) In the limit of infinitely heavy charm mass, the hadron helicity conservation rule implies angular distribution parameter $\alpha_\psi = 1$ [12]. The values of angular distribution of $J/\psi \to \Sigma^+\bar{\Sigma}^-$ have been predicted theoretically based on first order perturbative QCD. In the prediction of Claudson, Glashow and Wise [13], the mass of the final baryon is taken into account as a whole, while the constituent quarks inside the baryon are taken as massless when calculating the decay amplitude. In the prediction of Carimalo [14], mass effects at the quark level are taken into consideration. Experimentally, the related measurements are needed for the test. With the above Eq. 1 and 2, we could measure parameters($\alpha_{J/\psi}, \Delta\Phi_{J/\psi}, \alpha_{(\Sigma^+\to n\pi^+)}, \alpha_{(\bar{\Sigma}^-\to\bar{n}\pi^-)}$) by fitting the five angle distributions. Lastly, Perturbative QCD [15] [16] predicts that the partial widths for J/ψ decays into an exclusive hadronic state h are proportional to the squares of the wave-function, which are well determined from the leptonic widths. And it is also related to the strong coupling constant, which is expected to behave in the same way for the two resonances J/ψ and $\psi(3686)$. From this assumption $J/\psi \to h$ and $\psi(3686) \to h$ can be related via

$$\frac{B(\psi(3686) \to h)}{B(J/\psi \to h)} \approx \frac{B(\psi(3686) \to e^+e^-))}{B(J/\psi \to e^+e^-)} \approx 12\%$$

This relation defines the ”12%rule”, which works reasonably well for many specific decay modes. A large violation of this rule was observed by later experiments [17] [18] [19], particularly in $\rho\ \pi$ decay. Recent reviews [20] [21] of relevant theories and experiments conclude that current theoretical explanations are unsatisfactory. Clearly, more experimental results are desirable. The study of baryon spectroscopy plays an important role in the development of the quark model and in the understanding of QCD [22] [23]. However, our knowledge of baryon is limited. The study of $J/\psi \rightarrow \Sigma^{+}\bar{\Sigma}^{-}$ in BESIII and new method application supply a good opportunity to further study the baryon behaviors.

3 Detector

The BESIII detector [24] records symmetric e^+e^- collisions provided by the BEPCII storage ring [25], which operates with a peak luminosity of 1×10^{33} cm^{-2}s^{-1} in the center of mass energy range from 2.0 to 4.9 GeV. BESIII has collected large data samples in this energy region [26]. The cylindrical core of the BESIII detector covers 93% of the full solid angle and consists of a helium-based multilayer drift chamber (MDC), a plastic scintillator time-of-flight system (TOF), and a CsI(Tl) electromagnetic calorimeter (EMC), which are all enclosed in a superconducting solenoidal magnet providing a 1.0 T (0.9 T in 2012) magnetic field. The solenoid is supported by an octagonal flux-return yoke with resistive plate counter muon identification modules interleaved with steel. The charged-particle momentum resolution at 1 GeV/c is 0.5%, and the dE/dx resolution is 6% for electrons from Bhabha scattering. The EMC measures photon energies with a resolution of 2.5% (5%) at 1 GeV in the barrel (end cap) region. The time resolution in the TOF barrel region is 68 ps, while that in the end cap region is 110 ps. The end cap TOF system was upgraded in 2015 using multi-gap resistive plate chamber technology, providing a time resolution of 60 ps [27].

4 Data and Monte Carlo

4.1 Data

The data sample of $(10087.8\pm23.8)\times10^6$ J/ψ events [28] have been collected with the BESIII detector at the BEPCII collider during 2009, 2012, 2017 and 2018 year.

4.2 Monte Carlo Simulation

Simulated samples produced with the GEANT4-based [29] Monte Carlo (MC) package which includes the geometric description of the BESIII detector and the detector response, are used to determine the detection efficiency and to estimate the backgrounds. The J/ψ resonance is simulated with the KKMC generator [30], which is an event generator based on precise predictions of the Electroweak Standard Model for the process. The beam energy spread and initial state radiation (ISR) are taken into account in the simulation. The software framework used for the data analysis is BOSS(BESIII Offline Software System), which is developed from Gaudi. This work is under BOSS version 7.0.8. About 10000×10^6 J/ψ MC inclusive events is used to investigate possible backgrounds.The known decay modes are modelled with EVTGEN [31] using branching fractions taken from the Particle Data Group [32], and the remaining unknown charmonium decays are modelled with LUNDCHARM [33]. Final state radiation (FSR) from charged final state particles is incorporated using the PHOTOS package.

4.3 Decay chain

In this analysis, the concerned decay channel is $J/\psi \to \Sigma^+\bar{\Sigma}^-$, where $\Sigma^+/\bar{\Sigma}^-$ is reconstructed from $p\pi^0/\bar{n}\pi^-(n\pi^+/\bar{p}\pi^0)$, and π^0 decays to two γ.

5 Event Selection $J/\psi \to \Sigma^+\bar{\Sigma}^-, \Sigma^+ \to p\pi^0, \bar{\Sigma}^- \to \bar{n}\pi^-$

5.1 Track Level Selection

Charged tracks reconstructed by main drift chamber(MDC) hit information must be fitted by Kalman method successfully and come from the interaction region in three dimensions. Due to changing beam conditions, the interaction point (IP) moves. Thus, a separate average IP (beam position) is determined for each run using the VertexDbSvc package. The Σ^+ particle has a longer life time, so it requires a wider distance and the reference we refer to is [37]. Relative to this run-dependent IP, each charged track must satisfy the following requirements:

- $V_{xy} < 2$ cm,
- $|V_z| < 10$ cm,
- $|\cos\theta| < 0.93$,
- Good tracks is required $N = 2$.

Here, θ is the polar angle of the charged track with respect to the beam axis, V_{xy} and $|V_z|$ are the closest approaches of a charged track to the interaction point in the Oxy plane and in the z position.

5.2 Particle identification

The charged π^- and p are identified via ParticleID package by using the TOF and dE/dx measurements with which the combined confidence levels $\mathscr{L}(\pi^-)$, $\mathscr{L}(p)$ and $\mathscr{L}(K)$ for pion, proton and kaon hypotheses are calculated, respectively. The particle is taken as $p(\pi^-)$ if the $Prob_{PID}$ more than any other particle hypothesis. We require the pion and proton candidates satisfy the following criteria:

- π^-: $\mathscr{L}(\pi^-) > \mathscr{L}(p)$ and $\mathscr{L}(\pi^-) > \mathscr{L}(K)$,
- p: $\mathscr{L}(p) > \mathscr{L}(\pi)$ and $\mathscr{L}(p) > \mathscr{L}(K)$.

5.3 $\bar{n}$ Shower Requirement

The cluster in the EMC which satisfies the following criteria is regarded as a good $\bar{n}$ shower.

- barrel EMC, $|\cos\theta| < 0.80$; endcap EMC, $0.86 < |\cos\theta| < 0.92$;
- At least one shower with energy larger than 0.5GeV is required. Fig. 2(right) shows the deposit energy distribution of $\bar{n}$ and γ in the EMC from MC simulation.

- Second moment> 20, the reference we refer is [35] [36](This selection is already one of the standard criteria for the selection of antineutron). Fig. 2(left) shows the secondmoment distribution, which is defined as $\sum_i E_i r_i^2 / \sum_i E_i$, where E_i is the deposit energy in the i_{th} crystal and r_i is the radial distance of the crystal i from the cluster center. Briefly, the EM shower(γ) is more centralized, while other type (involving hadronic interaction)($\bar{n}$) is more spread.

- To suppress electronic noise and showers unrelated to the event, the difference between the EMC time and the event start time is required to be within (0, 700) ns

- To exclude showers that originate from charged tracks, the angle between the position of each shower in the EMC and the closest extrapolated charged track must be greater than 10 degrees.

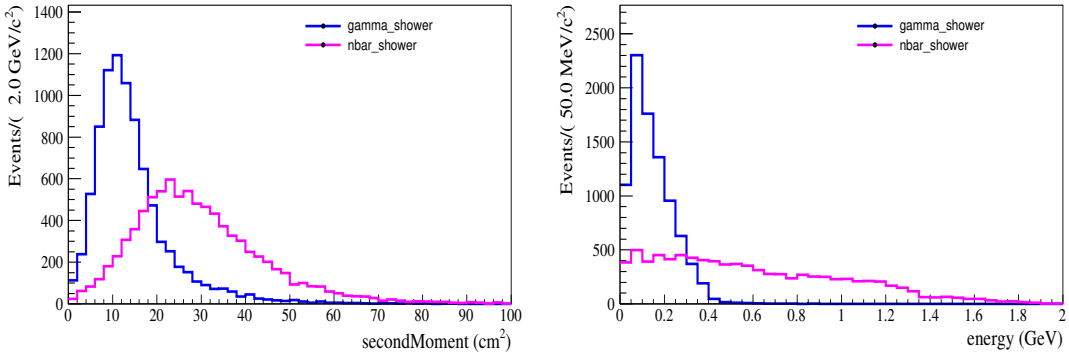

Fig. 2: Left: the distributions of the secondmoment for γ and anti-neutron. Right: the deposition energy distribution in EMC from MC simulation. Histogram and dots denote the γ and $\bar{n}$ respectively. The distribution indicates that E_γ is less than 0.5GeV. So for $\bar{n}$ selection, the energy for the most energetic photon is required larger than 0.5GeV.

5.4 Good photon seclection

- Photon candidates are identified using showers in the EMC. The deposited energy of each shower must be more than 25 MeV in the barrel region ($|\cos\theta| < 0.80$) and more than 50 MeV in the end cap region ($0.86 < |\cos\theta| < 0.92$).

- To suppress electronic noise and showers unrelated to the event, the difference between the EMC time and the event start time is required to be within (0, 700) ns.

- To exclude showers that originate from charged tracks, the angle between the position of each shower in the EMC and the closest extrapolated charged track must be greater than 10°.

- The angle $\theta_{\gamma,\bar{n}}$ between a shower and the $\bar{n}$ track is required to be more than 20°(The reference we refer is [35] [36](Because the anti-neutron will annihilate with the EMC material to generate

showers which are background to select pi0. Therefore, we have to require that the angle between the showers of reconstructive pi0 and anti-neutron is larger than 20°.). This selection is already one of the standard criteria for the selection of antineutron. Because $\bar{n}$ tend to annihilate with matter and produce many false showers on the EMC.).

- The number of good showers $N_\gamma \geq 2$.

5.5 π^0 reconstruction

The π^0 mesons are reconstructed by the decays $\pi^0 \to \gamma\gamma$. To reconstruct π^0 meson, we perform a kinematic fit on $\pi^0 \to \gamma\gamma$. To suppress combinatorial background, we require that the χ^2 of the kinematic fit is less than 25. π^0 candidates are reconstructed from pairs of photons whose invariant mass satisfies $[M_{\pi^0}\text{ -60}] < M_{\gamma\gamma} < [M_{\pi^0}\text{ + 40}]\ MeV/c^2$, where M_{π^0} is the nominal mass of π^0 taken from the PDG. The invariant mass distribution for π^0 and χ^2 distribution for the 1c kinematic fit are shown here in Fig. 3 that we refer this memo [37].

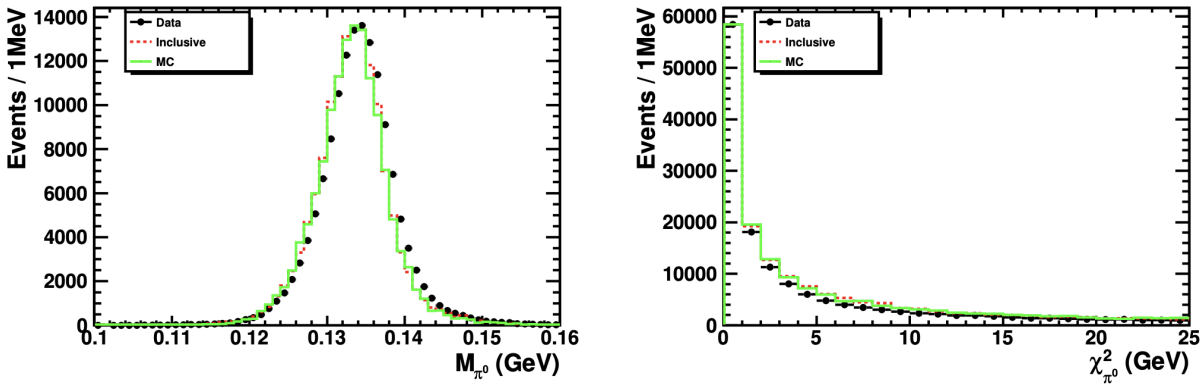

Fig. 3: The left figure is invariant mass distribution for π^0, and the right is χ^2 distribution for the 1c kinematic fit

5.6 kinematic fit

To further remove potential backgrounds and to improve the mass resolution, a four-constraint-energy-momentum conservation kinematic fit (4C fit: the resonance $\bar{\Sigma}^-$ is reconstructed from π^-, a charged track with full momentum information and $\bar{n}$, a neutral track with missing energy information on EMC. The resonance Σ^+ is reconstructed from π^0 and p. Besides, the resonance π^0 is fixed nominal mass, which taken from the PDG.) is performed.

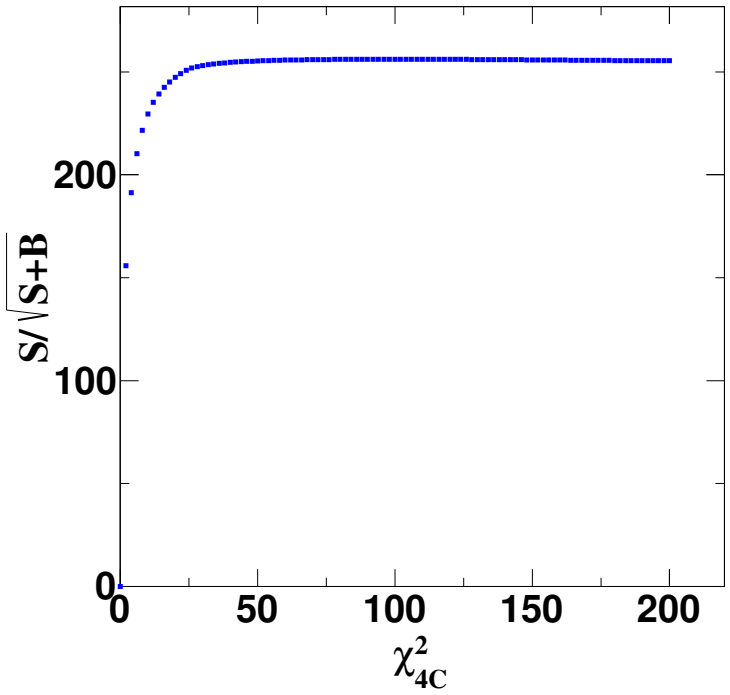

Fig. 4: Figure of merit for the χ^2_{4C} , the figure is for $J/\psi \to \Sigma^+\bar{\Sigma}^-, \Sigma^+ \to p\pi^0, \bar{\Sigma}^- \to \bar{n}\pi^-$, where S is signal MC, and B is the backgrounds from the inclusive MC.

We require that the goodness of fit quality $\chi^2_{4C} < 50$ for $J/\psi \to \Sigma^+\bar{\Sigma}^-, \Sigma^+ \to p\pi^0, \bar{\Sigma}^- \to \bar{n}\pi^-$ decay process. This value is optimized based on the figure of merit as the Fig. 4 shown. In the plot, S is signal MC, and B is the backgrounds from the inclusive MC. Besides, the signal MC has been scaled to luminosity of data via our measurement of branching fracion.

5.7 mass window

The mass window cut is set to be [1.17, 1.2] or [1.18, 1.2] GeV for $\Sigma^+ \to p\pi^0$ ($\bar{\Sigma}^- \to \bar{n}\pi^+ \Longrightarrow \bar{\Sigma}^- \to \bar{n}\pi^-$) signal region which is determined by the fitting of invariant mass of $p\pi^0$ and $\bar{n}\pi^-$ in the Fig. 5. The Crystal-Ball function is used to describe the signals, and the asymmetrical mass window $[M_\Sigma - 4\sigma, M_\Sigma + 3\sigma]$ or $[M_\Sigma - 3\sigma, M_\Sigma + 3\sigma]$([1.17, 1.2] or [1.18, 1.2] GeV) is caused by that the photon energy deposited in EMC has a long tail on the low energy side.

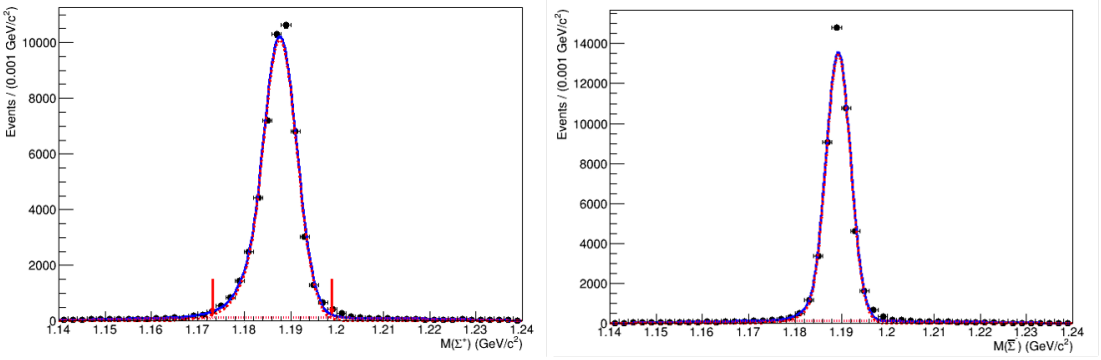

Fig. 5: Figure of Invariant mass, the left figure is for Σ^+, and the right is for $\bar{\Sigma}^-$.

5.8 Background analysis

The background level in this channel is studied based on the J/ψ inclusive samples. There are 67130 events which pass the event selections, and the number of background events is 932. The background level is about 1.4% and the peaking background level is about 0.2%. Besides, the possible peaking background have been studied in this MEMO [37] and it is quite small. The detail background channels could be found in Table. 3.

Tab. 3: Topology of $J/\psi \to \Sigma^+\bar{\Sigma}^-$ in generic J/ψ inclusive MC sample.

rowNo	decay tree	decay final state	iDcyTr	nEtr	nCEtr
1	$J/\psi \to \Sigma^+\bar{\Sigma}^-, \Sigma^+ \to \pi^0 p, \bar{\Sigma}^- \to \pi^-\bar{n}$	$\pi^0\pi^-\bar{n}p$	0	41578	41578
2	$J/\psi \to \Delta^+\bar{\Delta}^+, \Delta^+ \to \pi^0 p, \bar{\Delta}^+ \to \pi^-\bar{n}$	$\pi^0\pi^-\bar{n}p$	4	149	41727
3	$J/\psi \to \pi^-\bar{n}\Delta^+, \Delta^+ \to \pi^0 p$	$\pi^0\pi^-\bar{n}p$	1	128	41855
4	$J/\psi \to \pi^0\pi^-\bar{n}p$	$\pi^0\pi^-\bar{n}p$	3	87	41942
5	$J/\psi \to \pi^-\bar{\Delta}^0 p, \bar{\Delta}^0 \to \pi^0\bar{n}$	$\pi^0\pi^-\bar{n}p$	2	49	41991
6	$J/\psi \to \eta_c\gamma, \eta_c \to \Sigma^+\bar{\Sigma}^-, \Sigma^+ \to \pi^0 p, \bar{\Sigma}^- \to \pi^-\bar{n}$	$\pi^0\pi^-\bar{n}p\gamma$	8	38	42029
7	$J/\psi \to \Lambda\bar{\Lambda}, \Lambda \to \pi^- p, \bar{\Lambda} \to \pi^0\bar{n}$	$\pi^0\pi^-\bar{n}p$	5	28	42057
8	$J/\psi \to \Sigma^+\bar{\Sigma}^-\gamma, \Sigma^+ \to \pi^0 p, \bar{\Sigma}^- \to \pi^-\bar{n}$	$\pi^0\pi^-\bar{n}p\gamma$	6	15	42072
9	$J/\psi \to \Delta^0\bar{\Delta}^0, \Delta^0 \to \pi^- p, \bar{\Delta}^0 \to \pi^0\bar{n}$	$\pi^0\pi^-\bar{n}p$	10	9	42081
10	$J/\psi \to \Sigma^+\bar{\Sigma}^-, \Sigma^+ \to \pi^0 p, \bar{\Sigma}^- \to \pi^-\bar{n}, \pi^0 \to e^+e^-$	$e^+e^-\pi^-\bar{n}p$	17	7	42088
11	$J/\psi \to \pi^0 p\bar{\Delta}^+, \bar{\Delta}^+ \to \pi^-\bar{n}$	$\pi^0\pi^-\bar{n}p$	11	5	42093
12	$J/\psi \to \rho^-\bar{n}p, \rho^- \to \pi^0\pi^-$	$\pi^0\pi^-\bar{n}p$	18	3	42096
13	$J/\psi \to \Sigma^+\bar{\Sigma}^{*-}, \Sigma^+ \to \pi^0 p, \bar{\Sigma}^{*-} \to \pi^-\bar{\Lambda}, \bar{\Lambda} \to \pi^0\bar{n}$	$\pi^0\pi^0\pi^-\bar{n}p$	7	2	42098
14	$J/\psi \to \pi^0\bar{n}\Delta^0, \Delta^0 \to \pi^- p$	$\pi^0\pi^-\bar{n}p$	16	2	42100
15	$J/\psi \to \eta_c\gamma, \eta_c \to \rho^-\bar{n}p, \rho^- \to \pi^0\pi^-$	$\pi^0\pi^-\bar{n}p\gamma$	20	2	42102
16	$J/\psi \to \Lambda\bar{\Lambda}, \Lambda \to \pi^- p, \bar{\Lambda} \to \pi^0\bar{n}, \pi^0 \to e^+e^-$	$e^+e^-\pi^-\bar{n}p$	15	1	42103

rowNo	decay tree	decay final state	iDcyTr	nEtr	nCEtr
17	$J/\psi \to K^*\bar{n}\Lambda, K^* \to \pi^- K^+, \Lambda \to \pi^0 n$	$\pi^0\pi^- K^+ n\bar{n}$	9	1	42104

6 Event Selection of $J/\psi \to \Sigma^+\bar{\Sigma}^-, \Sigma^+ \to n\pi^+, \bar{\Sigma}^- \to \bar{p}\pi^0$

6.1 Track Level Selection

Charged tracks reconstructed by main drift chamber(MDC) hit information must be fitted by Kalman method successfully and come from the interaction region in three dimensions. Due to changing beam conditions, the interaction point (IP) moves. Thus, a separate average IP (beam position) is determined for each run using the VertexDbSvc package. The Σ^+ particle has a longer life time, so it requires a wider distance and the reference we refer to is [34]. Relative to this run-dependent IP, each charged track must satisfy the following requirements:

- $V_{xy} < 2$ cm,
- $|V_z| < 10$ cm,
- $|\cos\theta| < 0.93$.
- Good tracks is required $N = 2$

Here, θ is the polar angle of the charged track with respect to the beam axis, V_{xy} and $|V_z|$ are the closest approaches of a charged track to the interaction point in the Oxy plane and in the z position.

6.2 Particle identification

The charged π^+ and $\bar{p}$ are identified via ParticleID package by using the TOF and dE/dx measurements with which the combined confidence levels $\mathscr{L}(\pi^+)$ and $\mathscr{L}(\bar{p})$ for pion and anti-proton hypotheses are calculated, respectively. The particle is taken as $\bar{p}(\pi^+)$ if the $Prob_{PID}$ more than any other particle hypothesis. We require the pion and anti-proton candidates satisfy the following criteria:

- π^+: $\mathscr{L}(\pi^+) > \mathscr{L}(p)$ and $\mathscr{L}(\pi^+) > \mathscr{L}(K)$,
- $\bar{p}$: $\mathscr{L}(\bar{p}) > \mathscr{L}(\pi)$ and $\mathscr{L}(\bar{p}) > \mathscr{L}(K)$,

6.3 Good photon selection

- Photon candidates are identified using showers in the EMC. The deposited energy of each shower must be more than 25 MeV in the barrel region ($|\cos\theta| < 0.80$) and more than 50 MeV in the end cap region ($0.86 < |\cos\theta| < 0.92$).
- To suppress electronic noise and showers unrelated to the event, the difference between the EMC time and the event start time is required to be within (0, 700) ns.

- To exclude showers that originate from charged tracks, the angle between the position of each shower in the EMC and the closest extrapolated charged track must be greater than 10 degrees.
- The number of good showers $N_\gamma \geq 2$.

6.4 π^0 reconstruction

The π^0 mesons are reconstructed by the decays $\pi^0 \to \gamma\gamma$. To reconstruct π^0 meson, we perform a kinematic fit on $\pi^0 \to \gamma\gamma$. To suppress combinatorial background, we require that the χ^2 of the kinematic fit is less than 25. π^0 candidates are reconstructed from pairs of photons whose invariant mass satisfies $[M_{\pi^0}\text{ -60}] < M_{\gamma\gamma} < [M_{\pi^0} + 40]\ MeV/c^2$, where M_{π^0} is the nominal mass of π^0 taken from the PDG. The invariant mass distribution for π^0 and χ^2 distribution for the 1c kinematic fit are shown here in Fig. 6 that we refer this memo [37].

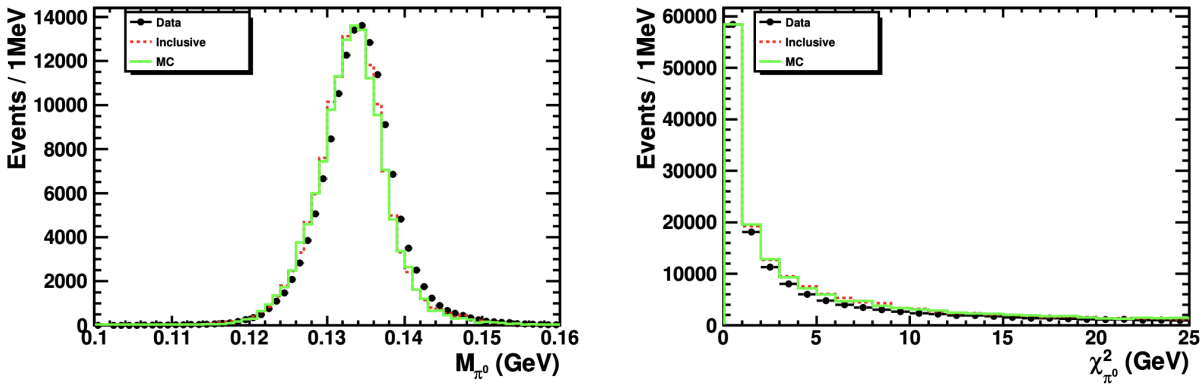

Fig. 6: The left figure is invariant mass distribution for π^0, and the right is χ^2 distribution for the 1c kinematic fit

6.5 kinematic fit

To further remove potential backgrounds and to improve the mass resolution, a four-constraint-energy-momentum conservation kinematic fit (2C fit: the resonance Σ^+ is reconstructed from π^+, a charged track with full momentum information and n, a neutral track with missing momentum and energy information. The resonance $\bar{\Sigma}^-$ is reconstructed from π^- and $\bar{p}$. Besides, the resonance π^0 is fixed nominal mass, which taken from the PDG.) is performed. We did not set any special requirement for neutron, and we treat it as missing particle.

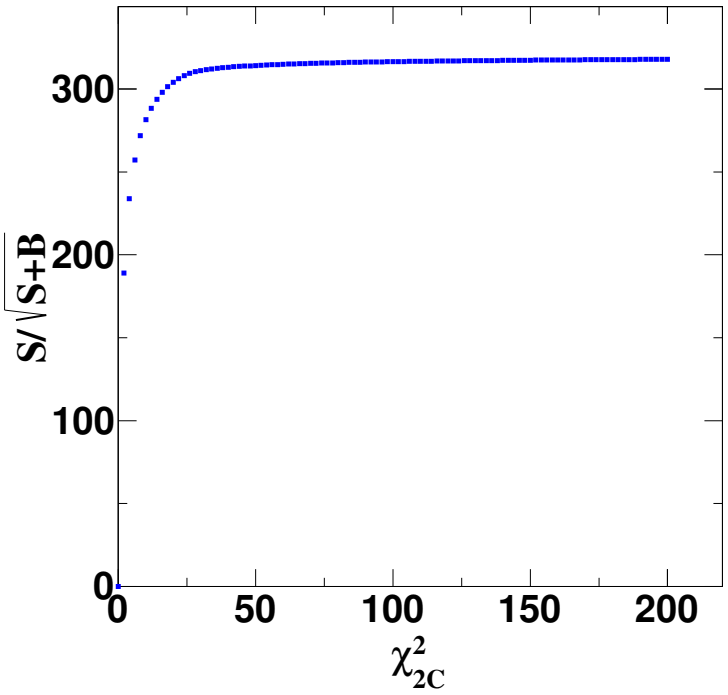

Fig. 7: Figure of merit for the χ^2_{2C} , the figure is for $J/\psi \to \Sigma^+\bar{\Sigma}^-, \Sigma^+ \to n\pi^+, \bar{\Sigma}^- \to \bar{p}\pi^0$, where S is signal MC, and B is the backgrounds from the inclusive MC.

We require that the goodness of fit quality $\chi^2_{2C} < 50$ for $J/\psi \to \Sigma^+\bar{\Sigma}^-, \Sigma^+ \to n\pi^+, \bar{\Sigma}^- \to \bar{p}\pi^0$ decay process. This value is optimized based on the figure of merit as the Fig. 7 shown. In the plot, S is signal MC, and B is the backgrounds from the inclusive MC. Besides, the signal MC has been scaled to luminosity of data via our measurement of branching fracion.

6.6 mass window

The mass window cut is set to be [1.18, 1.2] or [1.17, 1.2] GeV for $\Sigma^+ \to n\pi^+$ ($\bar{\Sigma}^- \to \bar{p}\pi^0$)signal region which is determined by the fitting of invariant mass of $n\pi^+$ and $\bar{p}\pi^0$ as the Fig. 8. The Crystal-Ball function is used to describe the signals, and the asymmetrical mass window $[M_\Sigma - 4\sigma, M_\Sigma + 3\sigma]$ or $[M_\Sigma - 3\sigma, M_\Sigma + 3\sigma]$([1.17, 1.2] or [1.18, 1.2] GeV) is caused by that the photon energy deposited in EMC has a long tail on the low energy side.

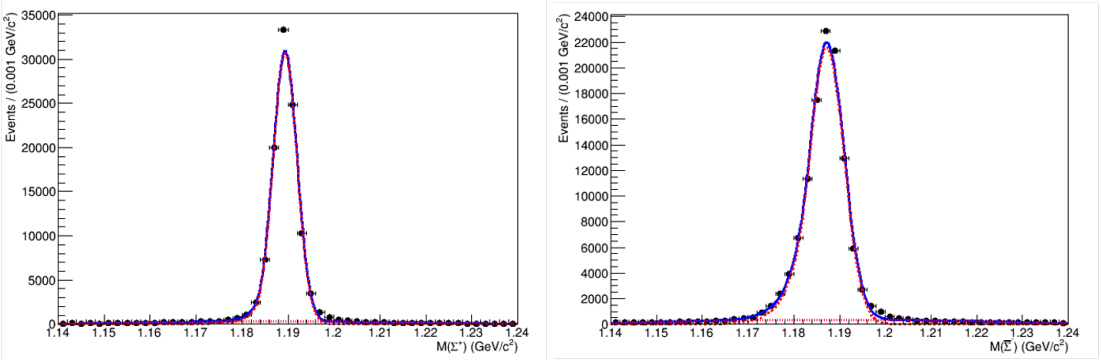

Fig. 8: Figure of Invariant mass, the left figure is for Σ^+, and the right is for $\bar{\Sigma}^-$.

6.7 Background analysis

The background level in this channel is studied based on the J/ψ inclusive samples. There are 98094 events which pass the event selections, and the number of background events is 1569. The background level is 1.6% and the peaking background level is about 0.2%. Besides, the possible peaking background have been studied in this MEMO [37] and it is quite small. The detail background channels could be found in Table. 4.

Tab. 4: Topology of $J/\psi \to \Sigma^+\bar{\Sigma}^-$ in generic J/ψ inclusive MC sample.

rowNo	decay tree	decay final state	iDcyTr	nEtr	nCEtr
1	$J/\psi \to \Sigma^+\bar{\Sigma}^-, \Sigma^+ \to \pi^+ n, \bar{\Sigma}^- \to \pi^0 \bar{p}$	$\pi^0\pi^+ n\bar{p}$	0	100582	100582
2	$J/\psi \to \pi^+ n\bar{\Delta}^+, \bar{\Delta}^+ \to \pi^0 \bar{p}$	$\pi^0\pi^+ n\bar{p}$	8	388	100970
3	$J/\psi \to \Delta^+\bar{\Delta}^+, \Delta^+ \to \pi^+ n, \bar{\Delta}^+ \to \pi^0 \bar{p}$	$\pi^0\pi^+ n\bar{p}$	4	373	101343
4	$J/\psi \to \pi^0\pi^+ n\bar{p}$	$\pi^0\pi^+ n\bar{p}$	13	213	101556
5	$J/\psi \to \eta_c\gamma, \eta_c \to \Sigma^+\bar{\Sigma}^-, \Sigma^+ \to \pi^+ n, \bar{\Sigma}^- \to \pi^0 \bar{p}$	$\pi^0\pi^+ n\bar{p}\gamma$	1	177	101733
6	$J/\psi \to \pi^+\Delta^0\bar{p}, \Delta^0 \to \pi^0 n$	$\pi^0\pi^+ n\bar{p}$	2	147	101880
7	$J/\psi \to \Sigma^+\bar{\Sigma}^-\gamma, \Sigma^+ \to \pi^+ n, \bar{\Sigma}^- \to \pi^0 \bar{p}$	$\pi^0\pi^+ n\bar{p}\gamma$	6	75	101955
8	$J/\psi \to \Lambda\bar{\Lambda}, \Lambda \to \pi^0 n, \bar{\Lambda} \to \pi^+ \bar{p}$	$\pi^0\pi^+ n\bar{p}$	3	48	102003
9	$J/\psi \to \Delta^0\bar{\Delta}^0, \Delta^0 \to \pi^0 n, \bar{\Delta}^0 \to \pi^+ \bar{p}$	$\pi^0\pi^+ n\bar{p}$	7	44	102047
10	$J/\psi \to \pi^+\Delta^0\bar{\Delta}^+, \Delta^0 \to \pi^0 n, \bar{\Delta}^+ \to \pi^0 \bar{p}$	$\pi^0\pi^0\pi^+ n\bar{p}$	25	30	102077
11	$J/\psi \to \pi^0\Delta^+\bar{\Delta}^+, \Delta^+ \to \pi^+ n, \bar{\Delta}^+ \to \pi^0 \bar{p}$	$\pi^0\pi^0\pi^+ n\bar{p}$	20	17	102094
12	$J/\psi \to \Sigma^+\bar{\Sigma}^-, \Sigma^+ \to \pi^+ n, \bar{\Sigma}^- \to \pi^0 \bar{p}, \pi^0 \to e^+e^-$	$e^+e^-\pi^+ n\bar{p}$	22	16	102110
13	$J/\psi \to \bar{\Sigma}^-\Sigma^{*+}, \bar{\Sigma}^- \to \pi^0 \bar{p}, \Sigma^{*+} \to \pi^+\Lambda, \Lambda \to \pi^0 n$	$\pi^0\pi^0\pi^+ n\bar{p}$	31	14	102124
14	$J/\psi \to \pi^0\Delta^0\bar{\Delta}^0, \Delta^0 \to \pi^0 n, \bar{\Delta}^0 \to \pi^+ \bar{p}$	$\pi^0\pi^0\pi^+ n\bar{p}$	26	12	102136
15	$J/\psi \to \eta_c\gamma, \eta_c \to \pi^+ n\bar{p}$	$\pi^+ n\bar{p}\gamma$	19	11	102147
16	$J/\psi \to \pi^0\Sigma^+\bar{\Sigma}^-, \Sigma^+ \to \pi^+ n, \bar{\Sigma}^- \to \pi^0 \bar{p}$	$\pi^0\pi^0\pi^+ n\bar{p}$	29	11	102158
17	$J/\psi \to \Sigma^+\bar{\Sigma}^-, \Sigma^+ \to \pi^+ n, \bar{\Sigma}^- \to \bar{p}\gamma$	$\pi^+ n\bar{p}\gamma$	18	11	102169
18	$J/\psi \to \Lambda\bar{\Lambda}\gamma, \Lambda \to \pi^0 n, \bar{\Lambda} \to \pi^+ \bar{p}$	$\pi^0\pi^+ n\bar{p}\gamma$	5	10	102179
19	$J/\psi \to \pi^+\Lambda\bar{\Sigma}^-, \Lambda \to \pi^0 n, \bar{\Sigma}^- \to \pi^0 \bar{p}$	$\pi^0\pi^0\pi^+ n\bar{p}$	11	9	102188

rowNo	decay tree	decay final state	iDcyTr	nEtr	nCEtr
20	$J/\psi \to \rho^+ n\bar{p}, \rho^+ \to \pi^0\pi^+$	$\pi^0\pi^+ n\bar{p}$	15	8	102196

7 Fitting Method

In the introduction part, the differential cross section could be described by the function of angular distributions including $\theta_{\Sigma^+}, \theta_p, \phi_p, \theta_{\bar{n}}$ and $\phi_{\bar{n}}$ (or $\theta_{\Sigma^+}, \theta_n, \phi_n, \theta_{\bar{p}}$ and $\phi_{\bar{p}}$). The definitions of these helicity parameters could be found in the introduction. The $\alpha, \Delta\Phi, \alpha_{\Sigma^+}$ and $\alpha_{\bar{\Sigma}^-}$ are decay parameters, which are need to be extracted from those angular distribution in the decay channels of $J/\psi \to \Sigma^+\bar{\Sigma}^- \to p\pi^0\bar{n}\pi^-$ and $J/\psi \to \Sigma^+\bar{\Sigma}^- \to n\pi^+\bar{p}\pi^0$.

7.1 Likelihood function construction

The maximum likelihood method is used to fit data to yield the decay parameters. The joint likelihood function is define by

$$\mathscr{L} = \prod_{i=1}^{N} Prob\,(p_i) = \prod_{i=1}^{N} \frac{W_i}{C},$$

$$C = \frac{1}{N_{mc}} \sum_{j=1}^{N_{mc}} W_j^{mc},$$

where Prob(P_i) is the probability to produce event i characterized by the measurements P_i (the solid angles of $\theta_{\Sigma^+}, \theta_p, \phi_p, \theta_{\bar{n}}$ and $\phi_{\bar{n}}$ (or $\theta_{\Sigma^+}, \theta_n, \phi_n, \theta_{\bar{p}}$ and $\phi_{\bar{p}}$), W is the differential cross section, and C is the the normalization factor for the cross section. We generate a large phase space MC samples to estimate the normalization factor, as the above equation shows, N_{mc} is the number of events generated in phase space MC. Here the detector efficiency is included in the W.

Instead of working with the likelihood function $\mathscr{L}$, it is more convenient to work with the logarithm of $\mathscr{L}$,

$$S = -ln\mathscr{L} = -ln \sum_{i=1}^{N} W_i + lnC$$

After the background events are substracted, the objective function is modified to:

$$S = -ln\mathscr{L}_{data} + ln\mathscr{L}_{bg},$$

where $\mathscr{L}_{data}$ is the likelihood function of events selected, and $\mathscr{L}_{bg}$ is the likelihood function of background events. By minimize the S, which equals to maximize $\mathscr{L}$, the decay parameters of $\theta_{\Sigma^+}, \theta_p, \phi_p, \theta_{\bar{n}}$ and $\phi_{\bar{n}}$ (or $\theta_{\Sigma^+}, \theta_n, \phi_n, \theta_{\bar{p}}$ and $\phi_{\bar{p}}$) could be extracted.

7.2 Function Minimization

The package MINUIT available in the CERN library is famous in the field of high energy physics, which is widely used to minimize the objective function in the data analysis to extract the parameters in questions. There are two methods to calculate the extremum: one is the chi-square(binned fit), another

one is the log-likelihood (un-binned fit), which is used in this analysis. In the final output of MINUIT package, we could get the parameter values and error matrix.

7.3 Input/output check

To validate the reliability of the fitting results, 100 times DIY Monte Carlo samples are generated, as Fig 9. In these samples, the amplitude information is based on differential cross section based on the Eq. 1 and 2. And the inputs of decay parameters are from the real data fitting results, which are listed in the Table 9.

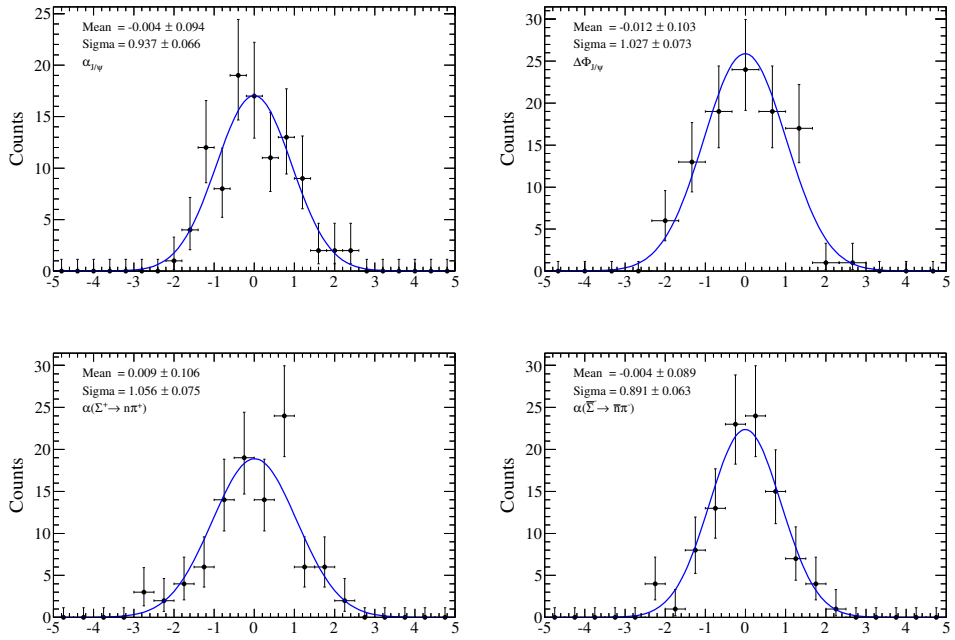

Fig. 9: The pull distributions for fitted parameters $J/\psi \to \Sigma^+\bar{\Sigma}^-, \Sigma^+ \to p\pi^0(n\pi^+), \bar{\Sigma}^- \to \bar{n}\pi^-(\bar{p}\pi^0)$.

8 Decay Parameter Measurement

The same fit procedure as done to the MC samples is applied to the selected data events. In fitting, the detection efficiency has been considered by using the MC sample to calculate the normalization factor in the likelihood definition. Here the MC sample is generated with the phase space model. After the background events are substrated, the objective function is modified to:

$$S = -ln\mathscr{L}_{data}^{\Sigma^+(p\pi^0)\bar{\Sigma}^-(\bar{n}\pi^-)} - ln\mathscr{L}_{data}^{\Sigma^+(n\pi^+)\bar{\Sigma}^-(\bar{p}\pi^0)} + 0.27 \times ln\mathscr{L}_{bg}^{J/\psi} + 0.26 \times ln\mathscr{L}_{bg}^{J/\psi} \quad (5)$$

The background events are estimated by the sideband region of Σ^+ and $\bar{\Sigma}^-$. For the decay channel of $\Sigma^+ \to p\pi^0, \bar{\Sigma}^- \to \bar{n}\pi^-$, the sideband regions are defined [1.13, 1.16] × [1.14, 1.16]GeV, [1.13, 1.16] × [1.22, 1.24] GeV, [1.21, 1.24]× [1.14, 1.16] GeV and [1.21, 1.24]×[1.22, 1.24] GeV mass regions for Σ^+ and $\bar{\Sigma}^-$, as shown in blue squares of Fig. 10 on the left. For the decay channel of $\Sigma^+ \to n\pi^+, \bar{\Sigma}^- \to \bar{p}\pi^0$, the sideband regions are defined [1.13, 1.16] × [1.14, 1.16]GeV, [1.13, 1.16] × [1.22, 1.24] GeV, [1.21, 1.24]× [1.14, 1.16] GeV and [1.21, 1.24]×[1.22, 1.24] GeV mass regions for $\bar{\Sigma}^-$ and Σ^+, as shown in blue squares of Fig. 10 on the right. The background events are estimated by 0.27A and 0.26A, where A are number of events in blue regions.

For the $J/\psi \to \Sigma^+\bar{\Sigma}^-, \Sigma^+ \to p\pi^0, \bar{\Sigma}^- \to \bar{n}\pi^-$, I have checked it and the background formula $N = N_{tot}$–$0.27 \times A$ has been corrected by fitting two dimension invariant mass in the Fig. 32

For the $J/\psi \to \Sigma^+\bar{\Sigma}^-, \Sigma^+ \to n\pi^+, \bar{\Sigma}^- \to \bar{p}\pi^0$, I have checked it and the background formula $N = N_{tot}$–$0.26 \times A$ has been corrected by fitting two dimension invariant mass in the Fig. 33.

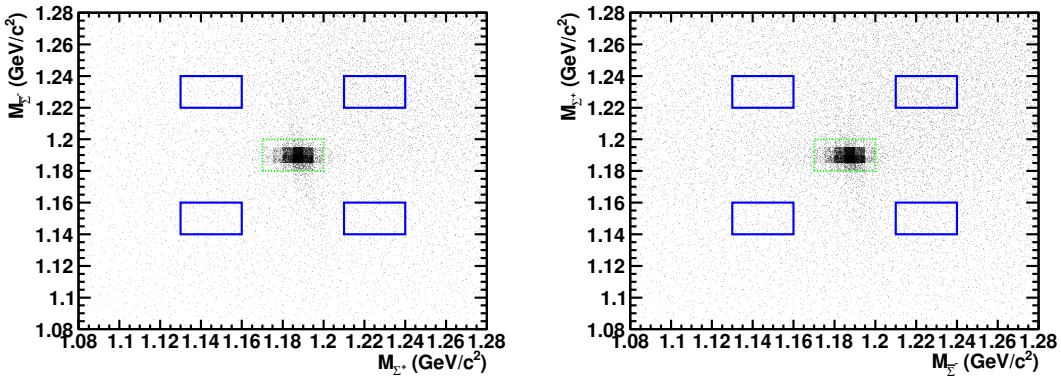

Fig. 10: Left: the scatter plot for the sideband region definition for $J/\psi \to \Sigma^+\bar{\Sigma}^-, \Sigma^+ \to p\pi^0, \bar{\Sigma}^- \to \bar{n}\pi^-$. Right: the scatter plot for the sideband region definition for $J/\psi \to \Sigma^+\bar{\Sigma}^-, \Sigma^+ \to n\pi^+, \bar{\Sigma}^- \to \bar{p}\pi^0$.

8.1 MC efficiency

To extract decay parameters from the decay channels of $J/\psi \to \Sigma^+\bar{\Sigma}^-(\Sigma^+ \to p\pi^0, \bar{\Sigma}^- \to \bar{n}\pi^-$ or $\Sigma^+ \to n\pi^+, \bar{\Sigma}^- \to \bar{p}\pi^0)$, the difference of detection efficiency between MC and data should be considered. In our fitting method, the efficiency is considered in the phase space MC sample which is used to calculate the normalization factors. When we generate the phase space MC sample, we take the detection efficiency difference between data and MC into account. Since the final states are $\pi^\pm$ [38], proton [39], anti-proton [39], $\bar{n}$ [40] and π^0(our results), we compare the detection efficiencies of these particle between MC and real data. To study the π^0 reconstruction efficiency, we choose the $J/\psi \to \Sigma^+\bar{\Sigma}^- \to p\bar{p}\pi^0\pi^0$ as the control sample. By selecting the control samples (the details in Appendix), the efficiencies are compared in different transverse momentums and polar angles for proton and anti-proton in Fig. 12, Fig. 13, Fig. 14 and Fig. 15. For π^+ and π^- detection efficiency in different momentum regions and polar angles, it is drawn in Fig. 16, Fig. 17, Fig. 18 and Fig. 19. For $\bar{n}$ detection efficiency in different momentum regions and polar angles, it is drawn in Fig. 11. For the π^0 detection efficiency, it is drawn in Fig. 33 in different momentum regions and polar angles. Besides, all values and uncertainties of correction factors are also listed in the Appendix. E.

In order to correct the detection efficiency to real data, we did in the following steps. Firstly, for each event, the efficiency ratio between data and MC could be calculated by:

$$r_\epsilon = \frac{\epsilon_p^{data} \times \epsilon_{\bar{p}}^{data} \times \epsilon_{\pi^0}^{data}}{\epsilon_p^{MC} \times \epsilon_{\bar{p}}^{MC} \times \epsilon_{\pi^0}^{MC}}, (\Sigma^+ \to n\pi^+, \bar{\Sigma}^- \to \bar{p}\pi^0)$$

or

$$r_\epsilon = \frac{\epsilon_p^{data} \times \epsilon_{\bar{p}}^{data} \times \epsilon_{\pi^0}^{data} \times \epsilon_{\bar{n}}^{data}}{\epsilon_p^{MC} \times \epsilon_{\bar{p}}^{MC} \times \epsilon_{\pi^0}^{MC} \times \epsilon_{\bar{n}}^{MC}}, (\Sigma^+ \to p\pi^0, \bar{\Sigma}^- \to \bar{n}\pi^-)$$

.

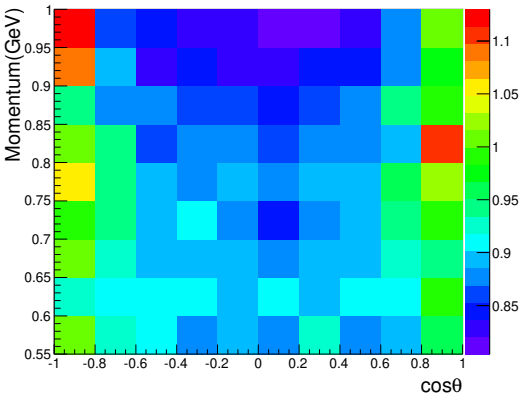

Fig. 11: The correction factor $\epsilon_{\bar{n}}^{data}/\epsilon_{\bar{n}}^{MC}$ in terms of cosθ in different momentum by using control sample $J/\psi \to p\bar{n}\pi^-$.

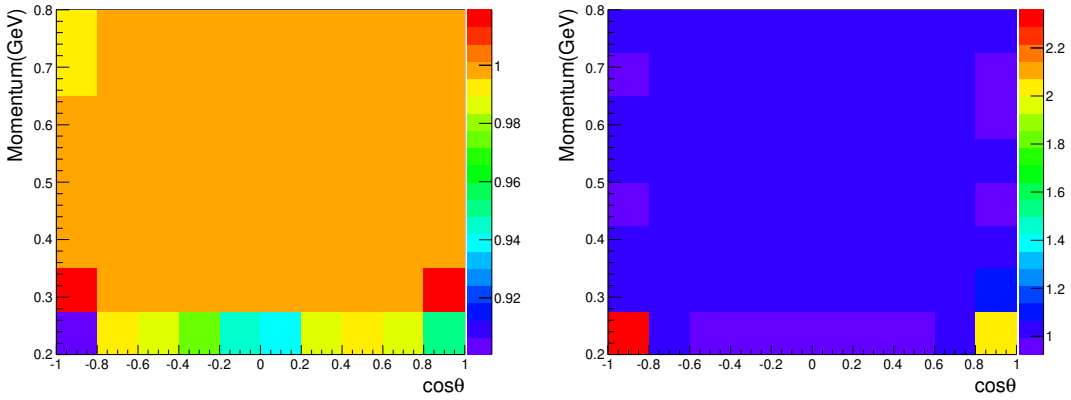

Fig. 12: The correction factor $\epsilon_{\bar{p}}^{data}/\epsilon_{\bar{p}}^{MC}$ in terms of cosθ in different momentum range by using control sample $J/\psi \to p\bar{p}\pi^+\pi^-$(left: 2009 year, right: 2012 year).

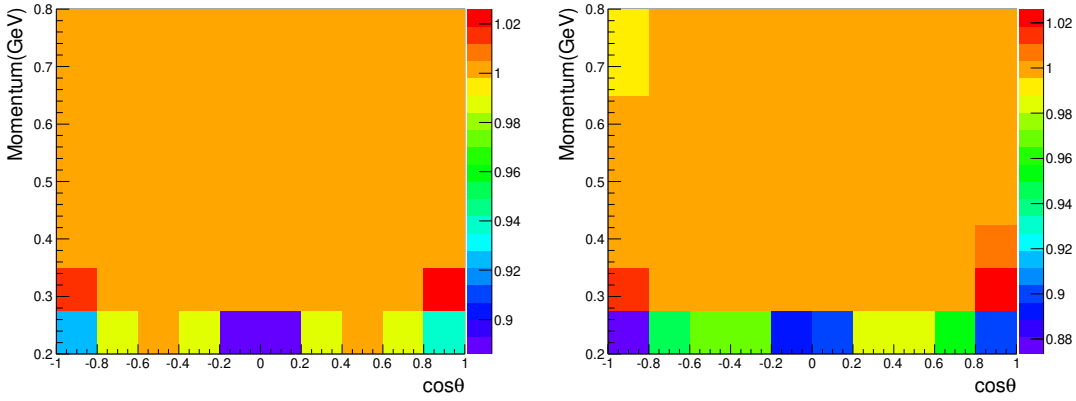

Fig. 13: The correction factor $\epsilon_{\bar{p}}^{data}/\epsilon_{\bar{p}}^{MC}$ in terms of cosθ in different momentum range by using control sample $J/\psi \to p\bar{p}\pi^+\pi^-$(left: 2018 year, right: 2019 year).

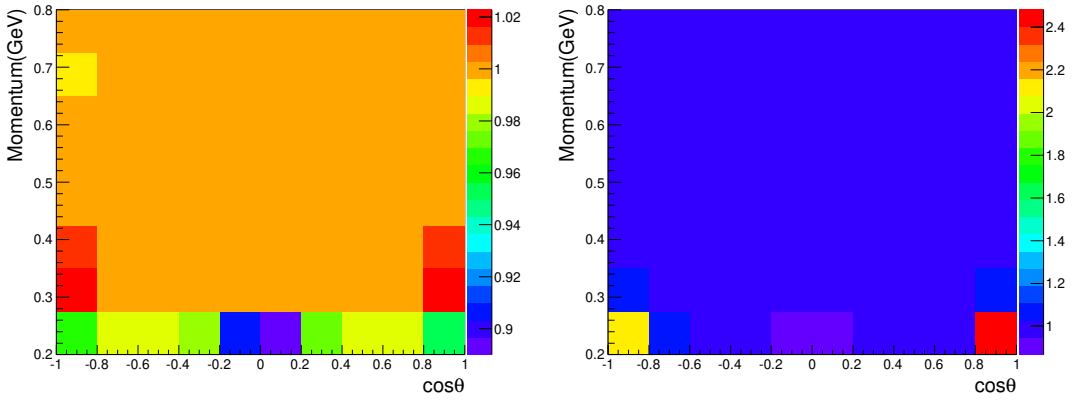

Fig. 14: The correction factor $\epsilon_p^{data}/\epsilon_p^{MC}$ in terms of cosθ in different momentum range by using control sample $J/\psi \to p\bar{p}\pi^+\pi^-$(left: 2009 year, right: 2012 year).

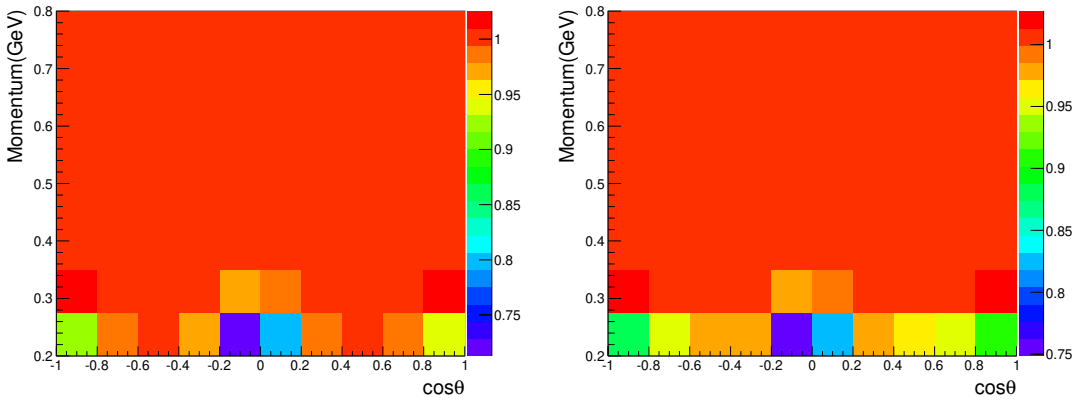

Fig. 15: The correction factor $\epsilon_p^{data}/\epsilon_p^{MC}$ in terms of cosθ in different momentum range by using control sample $J/\psi \to p\bar{p}\pi^+\pi^-$(left: 2018 year, right: 2019 year).

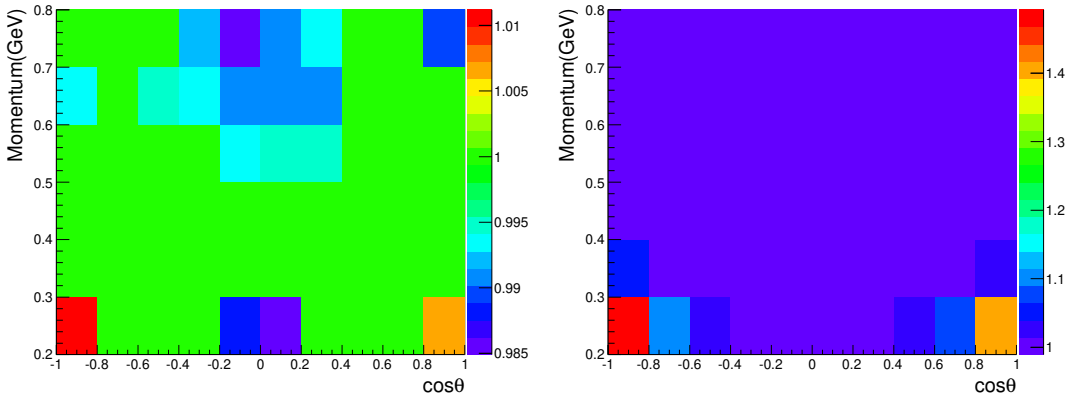

Fig. 16: The correction factor $\epsilon_{\pi^-}^{data}/\epsilon_{\pi^-}^{MC}$ in terms of cosθ in different momentum range by using control sample $J/\psi \to p\bar{p}\pi^+\pi^-$(left: 2009 year, right: 2012 year).

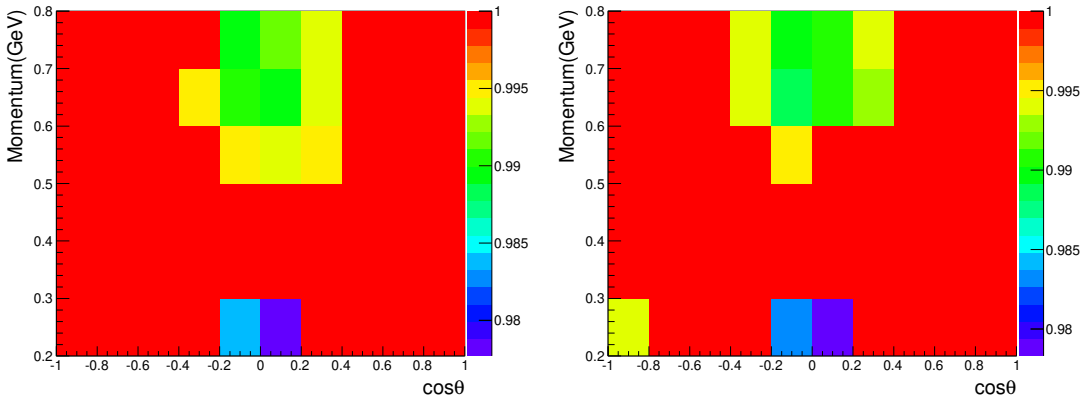

Fig. 17: The correction factor $\epsilon_{\pi^-}^{data}/\epsilon_{\pi^-}^{MC}$ in terms of cosθ in different momentum range by using control sample $J/\psi \to p\bar{p}\pi^+\pi^-$(left: 2018 year, right: 2019 year).

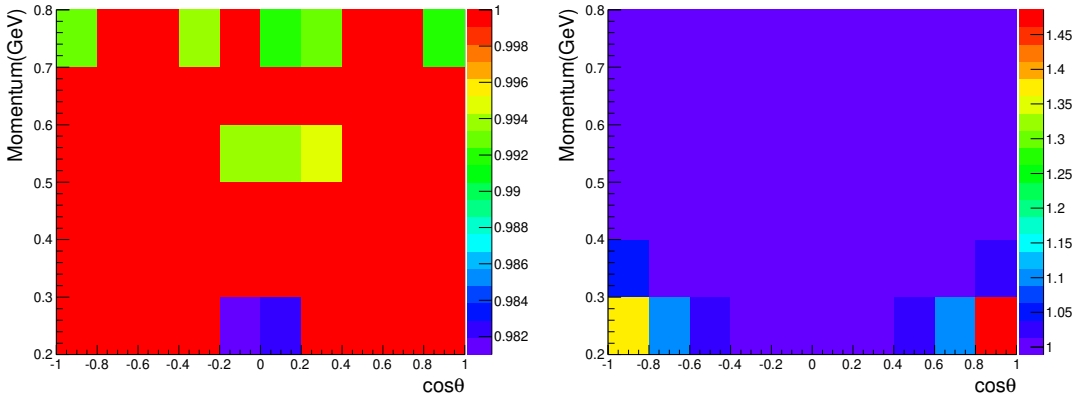

Fig. 18: The correction factor $\epsilon_{\pi^+}^{data}/\epsilon_{\pi^+}^{MC}$ in terms of cosθ in different momentum range by using control sample $J/\psi \to p\bar{p}\pi^+\pi^-$(left: 2009 year, right: 2012 year).

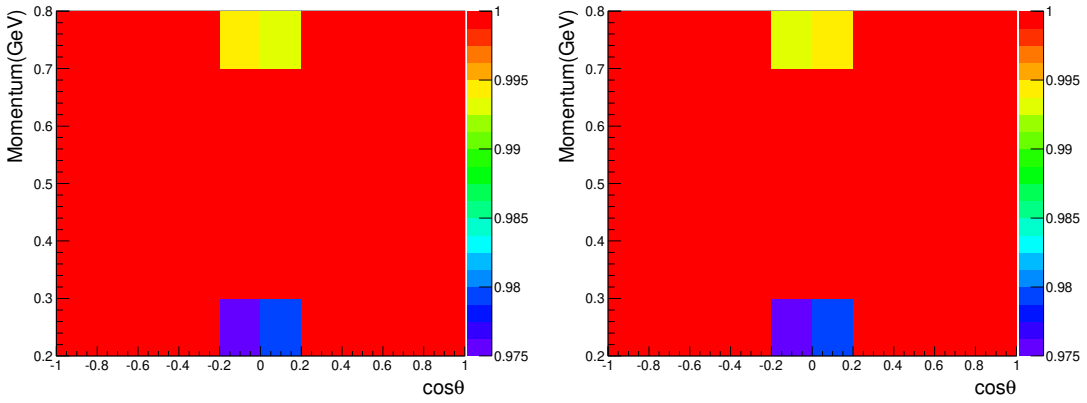

Fig. 19: The correction factor $\epsilon_{\pi^+}^{data}/\epsilon_{\pi^+}^{MC}$ in terms of cosθ in different momentum range by using control sample $J/\psi \to p\bar{p}\pi^+\pi^-$(left: 2018 year, right: 2019 year).

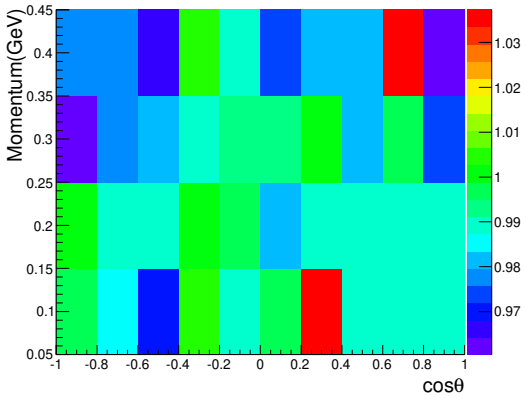

Fig. 20: The π^0 selection efficiency in terms of cosθ in different momentum range.

For the case $r_\epsilon < 1$, a random number η within (0,1) is generated, if $\eta < r_\epsilon$, this event is accepted. If not, this event is rejected. For another case $r_\epsilon > 1$, this event is accepted. To increase the correction procedure, when $r_\epsilon > 1$, we also generate a random number η within (0,1). If $r_\epsilon - 1 > \eta$, this event is accepted twice. By looping all phase space MC events, we could get a new MC sample which the efficiency is corrected to the real data, as Fig. 21.

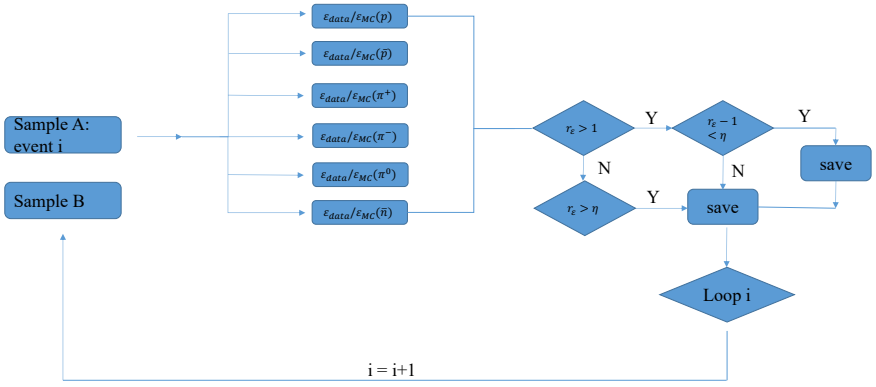

Fig. 21: PHSP MC correction flow

8.2 Fitting results

8.2.1 Sideband of $J/\psi \to \Sigma^+\bar{\Sigma}^-, \Sigma^+ \to p\pi^0, \bar{\Sigma}^- \to \bar{n}\pi^-$

According to the previous section defined S in Eq. 5, using the new phase space MC sample (with efficiency corrected), we did the same process as we did in the input/output check by minimizing the S.

The signal events for J/ψ are selected by requiring the mass region in [1.17, 1.2] GeV and [1.18, 1.2] GeV both for Σ^+ and $\bar{\Sigma}^-$. The signal events are estimated by $N_{tot} - 0.27 \times A$, where A is number of events in the blue regions in Fig. 10 on the left. For the decay channel of $\Sigma^+ \to p\pi^0, \bar{\Sigma}^- \to \bar{n}\pi^-$, the sideband regions are defined:

- The A area: [1.13, 1.16]×[1.14, 1.16] GeV, [1.13, 1.16]×[1.22, 1.24] GeV, [1.21, 1.24]×[1.14, 1.16] GeV and [1.21, 1.24]×[1.22, 1.24] GeV mass regions for Σ^+ and $\bar{\Sigma}^-$.

8.2.2 Sideband of $J/\psi \to \Sigma^+\bar{\Sigma}^-$, $\Sigma^+ \to n\pi^+$, $\bar{\Sigma}^- \to \bar{p}\pi^0$

According to the previous section defined S in Eq. 5, using the new phase space MC sample (with efficiency corrected), we did the same process as we did in the input/output check by minimizing the S. The signal events for J/ψ are selected by requiring the mass region in [1.17, 1.2] GeV and [1.18, 1.2] GeV both for $\bar{\Sigma}^-$ and Σ^+. The signal events are estimated by $N_{tot} - 0.26 \times A$, where A is number of events in the red and blue regions in Fig. 10 on the right. For the decay channel of $\Sigma^+ \to n\pi^+, \bar{\Sigma}^- \to \bar{p}\pi^0$, the sideband regions are defined:

- The A area: [1.13, 1.16]×[1.14, 1.16] GeV, [1.13, 1.16]×[1.22, 1.24] GeV, [1.21, 1.24]×[1.14, 1.16] GeV and [1.21, 1.24]×[1.22, 1.24] GeV mass regions for $\bar{\Sigma}^-$ and Σ^+.

8.2.3 Simultaneous fit by using two decay channels

The simultaneous fit is performed in the real data by:

$$S = -ln\mathscr{L}_{data}^{J/\psi\to\Sigma^+(p\pi^0)\bar{\Sigma}^-(\bar{n}\pi^-)} - ln\mathscr{L}_{data}^{J/\psi\to\Sigma^+(n\pi^+)\bar{\Sigma}^-(\bar{p}\pi^0)} + 0.27 \times ln\mathscr{L}_{bg}^{J/\psi\to\Sigma^+(p\pi^0)\bar{\Sigma}^-(\bar{n}\pi^-)} + 0.26 \times ln\mathscr{L}_{bg}^{J/\psi\to\Sigma^+(n\pi^+)\bar{\Sigma}^-(\bar{p}\pi^0)} \tag{6}$$

The fitting results status for $J/\psi \to \Sigma^+\bar{\Sigma}^-$, $\Sigma^+ \to p\pi^0(n\pi^+)$, $\bar{\Sigma}^- \to \bar{n}\pi^+(\bar{p}\pi^0)$ when the parameter $\alpha_{(\Sigma^+\to p\pi^0)}$ and $\alpha_{(\bar{\Sigma}^-\to\bar{p}\pi^0)}$ are not fixed, as the Fig. 22.

```
FCN=-12389.1 FROM MINOS     STATUS=SUCCESSFUL   1608 CALLS        1850 TOTAL
                     EDM=1.65432e-07    STRATEGY= 1      ERROR MATRIX ACCURATE
 EXT PARAMETER                   PARABOLIC         MINOS ERRORS
 NO.   NAME      VALUE            ERROR      NEGATIVE      POSITIVE
  1  alpha_jpsi  -5.15570e-01   2.96257e-03  -2.95766e-03   2.96763e-03
  2  dphi_jpsi   -2.34886e-01   4.61536e-02  -4.76545e-02   5.85967e-02
  3  aSgm        -1.10108e+00   2.12950e-01  -3.61083e-01   1.83627e-01
  4  aSgmbar      1.19608e+00   2.31292e-01  -1.97892e-01   3.91166e-01
  5  aSgm_n       4.01670e-02   8.13423e-03  -1.00550e-02   8.34407e-03
  6  aSgmbar_nbar  -5.11563e-02   1.05712e-02  -1.11756e-02   1.29805e-02
                               ERR DEF= 0.5
EXTERNAL ERROR MATRIX.    NDIM=  25    NPAR=  6    ERR DEF=0.5
 8.777e-06  1.088e-06 -3.111e-06  4.107e-06  3.530e-07 -3.150e-07
 1.088e-06  2.130e-03 -9.697e-03  1.063e-02 -3.544e-04  4.406e-04
-3.111e-06 -9.697e-03  4.535e-02 -4.838e-02  1.614e-03 -2.061e-03
 4.107e-06  1.063e-02 -4.838e-02  5.350e-02 -1.784e-03  2.199e-03
 3.530e-07 -3.544e-04  1.614e-03 -1.784e-03  6.617e-05 -7.335e-05
-3.150e-07  4.406e-04 -2.061e-03  2.199e-03 -7.335e-05  1.117e-04
PARAMETER  CORRELATION COEFFICIENTS
      NO.  GLOBAL      1      2      3      4      5      6
       1  0.07874   1.000  0.008 -0.005  0.006  0.015 -0.010
       2  0.99669   0.008  1.000 -0.987  0.996 -0.944  0.903
       3  0.98828  -0.005 -0.987  1.000 -0.982  0.932 -0.915
       4  0.99595   0.006  0.996 -0.982  1.000 -0.948  0.899
       5  0.94852   0.015 -0.944  0.932 -0.948  1.000 -0.853
       6  0.91557  -0.010  0.903 -0.915  0.899 -0.853  1.000
```

Fig. 22: The fitting results status for $J/\psi \to \Sigma^+\bar{\Sigma}^-$, $\Sigma^+ \to p\pi^0(n\pi^+)$, $\bar{\Sigma}^- \to n\pi^-(\bar{p}\pi^0)$ when the parameter $\alpha_{(\bar{\Sigma}^-\to\bar{p}\pi^0)}$ is not fixed.

To accurately measure $\alpha_{(\Sigma^+\to n\pi^+)}$ and $\alpha_{(\bar{\Sigma}^-\to\bar{n}\pi^-)}$, the parameter $\alpha_{(\Sigma^+\to p\pi^0)}$ and $\alpha_{(\bar{\Sigma}^-\to\bar{p}\pi^0)}$ is fixed at 0.994, which taken from previous results in Fig. 23.

For $J/\psi \to \Sigma^+\bar{\Sigma}^-$, $\Sigma^+ \to p\pi^0$, $\bar{\Sigma}^- \to \bar{n}\pi^-$(For $J/\psi \to \Sigma^+\bar{\Sigma}^-$, $\Sigma^+ \to n\pi^+$, $\bar{\Sigma}^- \to \bar{p}\pi^0$, the amplitude of polarization is the same), as we know that the term of $\sqrt{1-\alpha_\psi^2}sin(\Delta\Phi)(\alpha_{\Sigma^+}t_3(\xi) - \alpha_{\bar{\Sigma}^-}t_4(\xi))$ represents the polarization contribution(it come from formula 1). Hence, if we did the integration to $sin\theta_p sin\phi_p$ and $sin\theta_{\bar{n}} sin\phi_{\bar{n}}$, we could observed the polarization behavior dependence on $cos\theta_{\Sigma^+}$ which is proportional to $\mu(\cos\theta_{\Sigma^+}) = (\alpha_{\Sigma^+} - \bar{\alpha}_{\bar{\Sigma}^-})\sqrt{1-\alpha_{J/\psi}^2}sin(\Delta\Phi)sin\theta_{\Sigma^+}cos\theta_{\Sigma^+}$. The variable $\mu(cos\theta_{\Sigma^+})$ is calculated by $\frac{m}{N}\sum_i^{N(m)}(sin\theta_p sin\phi_p^{(i)} - sin\theta_{\bar{n}} sin\phi_{\bar{n}}^{(i)})$, where m equals to 40 (40 bins in $cos\theta_{\Sigma^+}$), N is the total number of events in the data sample, $N(m)$ is the number of events in the i_{th} $cos\theta_{\Sigma^+}$ bin and $\theta_p, \phi_p, \theta_{\bar{n}}, \phi_{\bar{n}}$ are the polar and azimuthal angles of proton and anti-neutron.

The distributions are shown in Fig. 24 for $\bar{\Sigma}^- \to \bar{n}\pi^-(\Sigma^+ \to n\pi^+, \bar{\Sigma}^- \to \bar{p}\pi^0)$. Comparing with the phase space distributions(blue ones in the plots), the distributions (black dots) distributed like sine for J/ψ in the real data, respectively, which mean the $\Delta\phi$ is not zero. Based on the differential cross section formulas, if $\Delta\phi$ is not zero, there are polarizations existence.

```
FCN=-12386 FROM MINOS     STATUS=SUCCESSFUL    134 CALLS         203 TOTAL
                     EDM=2.48993e-08    STRATEGY= 1      ERROR MATRIX ACCURATE
 EXT PARAMETER                   PARABOLIC         MINOS ERRORS
 NO.   NAME      VALUE            ERROR      NEGATIVE      POSITIVE
  1  alpha_jpsi  -5.15638e-01   2.96236e-03  -2.95825e-03   2.96640e-03
  2  dphi_jpsi   -2.77235e-01   4.46623e-03  -4.46854e-03   4.46391e-03
  3  aSgm        -9.94000e-01      fixed
  4  aSgmbar      9.94000e-01      fixed
  5  aSgm_n       4.80869e-02   3.09463e-03  -3.09464e-03   3.09467e-03
  6  aSgmbar_nbar  -5.64951e-02   4.70052e-03  -4.70128e-03   4.69989e-03
                               ERR DEF= 0.5
EXTERNAL ERROR MATRIX.    NDIM=  25    NPAR=  4    ERR DEF=0.5
 8.776e-06  3.777e-07  5.803e-07 -4.994e-07
 3.777e-07  1.995e-05  8.569e-08 -7.192e-08
 5.803e-07  8.569e-08  9.577e-06 -3.318e-08
-4.994e-07 -7.192e-08 -3.318e-08  2.209e-05
PARAMETER  CORRELATION COEFFICIENTS
       NO.  GLOBAL      1      2      5      6
        1  0.07790   1.000  0.029  0.063 -0.036
        2  0.02898   0.029  1.000  0.006 -0.003
        5  0.06345   0.063  0.006  1.000 -0.002
        6  0.03595  -0.036 -0.003 -0.002  1.000
```

Fig. 23: The fitting results status for $J/\psi \to \Sigma^+\bar{\Sigma}^-$, $\Sigma^+ \to p\pi^0(n\pi^+)$, $\bar{\Sigma}^- \to n\pi^-(\bar{p}\pi^0)$.

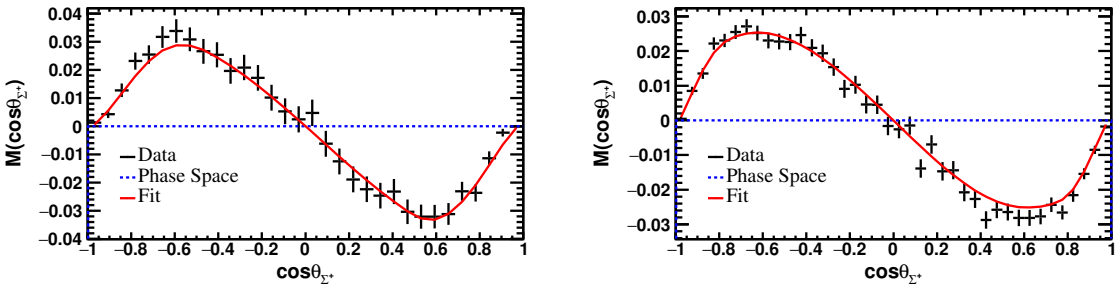

Fig. 24: Left: the fitting result for moment of $sin\theta sin\phi$ for $J/\psi \to \Sigma^+\bar{\Sigma}^-$, $\Sigma^+ \to p\pi^0$, $\bar{\Sigma}^- \to \bar{n}\pi^-$. The black dots are real data, the red cross are fitting results and the blue points are phase space events. Right: the fitting result for moment of $sin\theta sin\phi$ for $J/\psi \to \Sigma^+\bar{\Sigma}^-$, $\Sigma^+ \to n\pi^+$, $\bar{\Sigma}^- \to \bar{p}\pi^0$. The black dots are real data, the red cross are fitting results and the blue points are phase space events.

9 Branching Results

The branch fraction of each channels is calculated according to

$$Br = \frac{N_{sig}(X)}{\varepsilon(X) \times \prod Br_i \times N_{tot}}, \tag{7}$$

where X represents each decay channel, $N_{sig}(X)$ is the signal events by fitting method, $\varepsilon(X)$ is the detection efficiency determined by MC which is generated according to the decay parameters measured in the real data, $\prod Br_i$ is the product branching fractions of all the intermediate states in each channel, N_{tot} is the total number of J/ψ events.

For the subsections 9.1 and 9.2, the fit function PDFs(probability density function) in the fit code are described as:$N_{sig} \times (PDF_{SignalShape} \otimes Gauss(Mean, \sigma)) + N_{bkg} \times PDF_{2nd-OrderPolynomialFunction}$, where N_{sig} represents signal events and N_{bkg} represents background events.

9.1 Branching Ratio of $J/\psi \to \Sigma^+(p\pi^0)\bar{\Sigma}^-(\bar{n}\pi^-)$

To yield the signal events, the fitting of the invariant mass of p and π^0 is performed in the region of [1.14, 1.24] GeV, by requiring that the signal region of $\bar{\Sigma}^-$ lay in [1.18, 1.2] GeV. The signal is described by the MC shape convoluted with Gaussian function which represents the difference between data and MC in the resolution and mean value. The background is described with 2nd order polynomial function. Fig 25 shows the fitting of the $p\pi^0$ invariant mass, where the red solid line is the total fitting function, the red dash line is signal function and blue one is the background function. The fitting results are listed in the Tab. 5, and the branching fractions is measured to be $(10.89 \pm 0.02) \times 10^{-4}$, respectively. Here, we need to consider the efficiency difference between data and MC, which include the detection efficiencies of p, π^-, $\bar{n}$, and π^0.

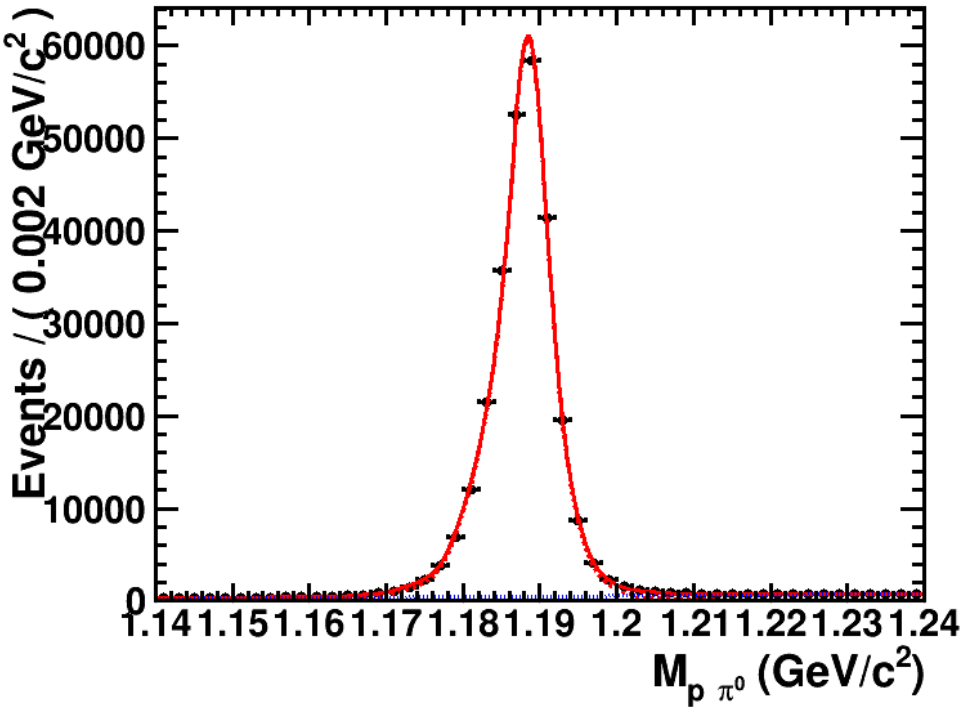

Fig. 25: Fitting $p\pi^0$ of $J/\psi \to \Sigma^+\bar{\Sigma}^-$,$\Sigma^+ \to p\pi^0$, $\bar{\Sigma}^- \to \bar{n}\pi^-$.

Tab. 5: The number of events for $J/\psi \to \Sigma^+\bar{\Sigma}^-$,$\Sigma^+ \to p\pi^0$, $\bar{\Sigma}^- \to \bar{n}\pi^-$

Channel	N_{sig}	ε_{MC}%	ε_{cor}%	$\sigma(Gauss)$ MeV	$Mean(Gauss)$ MeV
$J/\psi \to \Sigma^+\bar{\Sigma}^-$	312136 ± 576	12.50	11.54	0.82 ± 0.02	0.43 ± 0.00

9.2 Branching Ratio of $J/\psi \to \Sigma^+(n\pi^+)\bar{\Sigma}^-(\bar{p}\pi^0)$

Similarly, to yield the signal events, the fitting of the invariant mass of n and π^+ is performed in the region of [1.14, 1.24] GeV, by requiring that the signal region of $\bar{\Sigma}^-$ lay in [1.17, 1.2] GeV. The signal is described by the MC shape convoluted with Gaussian function which represents the difference between data and MC in the resolution and mean value. The background is described with 2nd order polynomial function. Fig 26 shows the fitting of the $n\pi^+$ invariant mass, where the red solid line is the total fitting function, the red dash line is signal function and blue one is the background function. The fitting results are listed in the Tab. 6, and the branching fractions is measured to be $(10.83 \pm 0.01) \times 10^{-4}$, respectively. Here, we need to consider the efficiency difference between data and MC, which include the detection efficiencies of π^+, $\bar{p}$, and π^0. The difference of p, $\bar{p}$, and π^0 have been studied in Appendix.

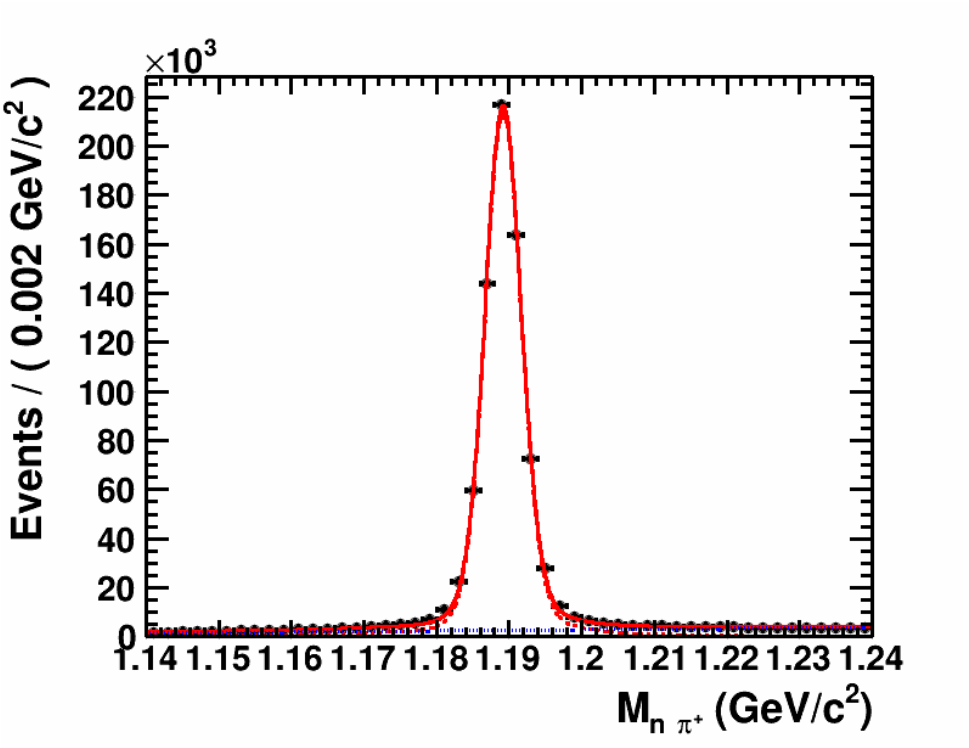

Fig. 26: Fitting $n\pi^+$ of $J/\psi \to \Sigma^+\bar{\Sigma}^-$,$\Sigma^+ \to n\pi^+$,$\bar{\Sigma}^- \to \bar{p}\pi^0$.

Tab. 6: The number of events for $J/\psi \to \Sigma^+\bar{\Sigma}^-$,$\Sigma^+ \to n\pi^+$,$\bar{\Sigma}^- \to \bar{p}\pi^0$

Channel	N_{sig}	$\varepsilon_{MC}\%$	$\varepsilon_{cor}\%$	$\sigma(Gauss)$ MeV	$Mean(Gauss)$ MeV
$J/\psi \to \Sigma^+\bar{\Sigma}^-$	754017 ± 924	27.78	28.02	1.00 ± 0.01	−0.11 ± 0.00

10 Systematic uncertainty

The systematic uncertainties of the decay parameters and branching fractions are studied separately.

10.1 Systematic uncertainties of decay parameters

The systematic uncertainties of decay parameters consist of MC efficiency correction uncertainties, fitting method, kinematic fitting, signal mass window, the background estimation and fixed decay parameter. They are listed in the table 15.

10.1.1 MC efficiency correction

The uncertainties of the MC efficiency correction is studied by considering the uncertainty of the correction factors. In the Section 8.1, we compared the efficiency difference between MC and real data. By changing the correction factor 1σ and the fitting results are listed in the following Table. 7, and take the maximum difference with the nominal values as the uncertainties.

Tab. 7: The uncertainties of MC efficiency correction($\Sigma^+ \to p\pi^0(n\pi^+)$, $\bar{\Sigma}^- \to n\pi^-(\bar{p}\pi^0)$)

Decay Parameters	nominal(correction factor)	$-\sigma$	$+\sigma$	difference
$\alpha_{J/\psi}$	-0.5156 ± 0.0030	-0.5140 ± 0.0030	-0.5215 ± 0.0030	0.0059
$\Delta\Phi_{J/\psi}$	-0.2772 ± 0.0044	-0.2767 ± 0.0044	-0.2776 ± 0.0044	0.0005
$\alpha_{(\Sigma^+\to p\pi^0)}$	-0.994	-0.994	-0.994	–
$\alpha_{(\bar{\Sigma}^-\to \bar{p}\pi^0)}$	0.994	0.994	0.994	–
$\alpha_{(\bar{\Sigma}^-\to \bar{n}\pi^-)}$	-0.0565 ± 0.0047	-0.0581 ± 0.0047	-0.0576 ± 0.0047	0.0016
$\alpha_{(\Sigma^+\to n\pi^+)}$	0.0481 ± 0.0031	0.0492 ± 0.0031	0.0487 ± 0.0031	0.0011

10.1.2 Kinematic fitting

When we use the track correction for the helix parameters, the χ^2_{4C} distribution is more consistent between data and MC in the Fig 27 on the left. Then we could use the difference between before correction and after correction as the systematic uncertainties, and take the values with correction as the nominal one. The results are whether we use the correction or not and it listed in the Table 8.

When we use the track correction for the helix parameters, the χ^2_{2C} distribution is more consistent between data and MC in the Fig 27 on the right. Then we could use the difference between before correction and after correction as the systematic uncertainties, and take the values with correction as the nominal one. The results are whether we use the correction or not and it listed in the Table 8.

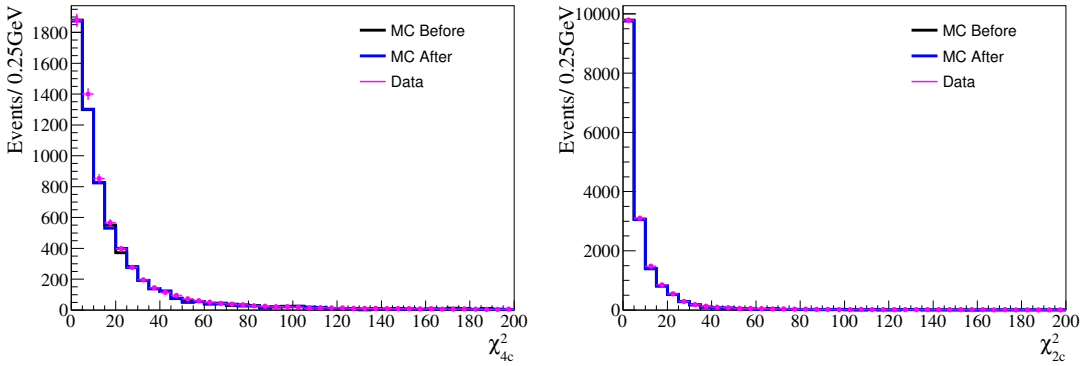

Fig. 27: Left: the χ^2_{4C} distribution for $J/\psi \to \Sigma^+\bar{\Sigma}^-, \Sigma^+ \to p\pi^0, \bar{\Sigma}^- \to \bar{n}\pi^-$. Right: the χ^2_{2C} distribution for $J/\psi \to \Sigma^+\bar{\Sigma}^-, \Sigma^+ \to n\pi^+, \bar{\Sigma}^- \to \bar{p}\pi^0$.

Tab. 8: With or without helix parameter correction for the decay parameters($\Sigma^+ \to p\pi^0(n\pi^+)$, $\bar{\Sigma}^- \to n\pi^-(\bar{p}\pi^0)$).

Decay Parameters	with	without	difference
$\alpha_{J/\psi}$	-0.5156 ± 0.0030	-0.5153 ± 0.0030	0.0003
$\Delta\Phi_{J/\psi}$	-0.2772 ± 0.0044	-0.2768 ± 0.0044	0.0004
$\alpha_{(\Sigma^+\to p\pi^0)}$	-0.994	-0.994	–
$\alpha_{(\bar{\Sigma}^-\to \bar{p}\pi^0)}$	0.994	0.994	–
$\alpha_{(\bar{\Sigma}^-\to \bar{n}\pi^-)}$	-0.0565 ± 0.0047	-0.0572 ± 0.0047	0.0007
$\alpha_{(\Sigma^+\to n\pi^+)}$	0.0481 ± 0.0031	0.0478 ± 0.0031	0.0003

10.1.3 Fitting method

We compared the input values and output values which are listed in the Table 9. The differences are taken as the uncertainties of the fitting method.

Tab. 9: Input/output difference($\Sigma^+ \to p\pi^0(n\pi^+)$, $\bar{\Sigma}^- \to n\pi^-(\bar{p}\pi^0)$).

Decay Parameters	input	output	difference
$\alpha_{J/\psi}$	-0.5100	-0.5093 ± 0.0043	0.0007
$\Delta\Phi_{J/\psi}$	-0.2760	-0.2732 ± 0.0070	0.0028
$\alpha_{(\Sigma^+\to p\pi^0)}$	-0.994	-0.994	–
$\alpha_{(\bar{\Sigma}^-\to \bar{p}\pi^0)}$	0.994	0.994	–
$\alpha_{(\bar{\Sigma}^-\to \bar{n}\pi^-)}$	-0.0510	-0.0517 ± 0.0065	0.0007
$\alpha_{(\Sigma^+\to n\pi^+)}$	0.0510	0.0522 ± 0.0045	0.0012

10.1.4 Signal mass window

We change the size of signal mass box from 30 MeV×20 MeV(1.17 - 1.2 GeV, 1.18 - 1.2 GeV). By make the box smaller (25 MeV×20 MeV)(decreasing 1 σ mass window) and larger (increasing 1 σ mass

window), we compare the fitting results and take the larger difference with the nominal values as the uncertainties. The results are listed in the following Table 10.

Tab. 10: Background uncertainties for the decay parameters($\Sigma^+ \to p\pi^0(n\pi^+)$, $\bar{\Sigma}^- \to n\pi^-(\bar{p}\pi^0)$).

Decay Parameters	nominal	smaller box	larger box	difference
$\alpha_{J/\psi}$	-0.5156 ± 0.0030	-0.5167 ± 0.0030	-0.5141 ± 0.0030	0.0015
$\Delta\Phi_{J/\psi}$	-0.2772 ± 0.0044	-0.2768 ± 0.0045	-0.2751 ± 0.0045	0.0021
$\alpha_{(\Sigma^+\to p\pi^0)}$	-0.994	-0.994	-0.994	–
$\alpha_{(\bar{\Sigma}^-\to \bar{p}\pi^0)}$	0.994	0.994	0.994	–
$\alpha_{(\bar{\Sigma}^-\to \bar{n}\pi^-)}$	-0.0565 ± 0.0047	-0.0575 ± 0.0048	-0.0558 ± 0.0048	0.0010
$\alpha_{(\Sigma^+\to n\pi^+)}$	0.0481 ± 0.0031	0.0490 ± 0.0031	0.0475 ± 0.0031	0.0009

10.1.5 Background estimation

We take the sideband regions of 30×20 MeV as nominal value. Since we use the sideband region of Σ^+ and $\bar{\Sigma}^-$to estimate the background events, we change the sideband regions from 30×20 MeV to 25×20 MeV or 26×20 MeV or 27×20 MeV or 28×20 MeV or 29×20 MeV or 30×20 MeV or 31×20 MeV or 32×20 MeV or 33×20 MeV or 34×20 MeV or 35×20 MeV, as Fig. 28. And we also change the sideband regions from 30×20 MeV to 30×15 MeV or 30×16 MeV or 30×17 MeV or 30×18 MeV or 30×19 MeV or 30×20 MeV or 30×21 MeV or 30×22 MeV or 30×23 MeV or 30×24 MeV or 30×25 MeV, as Fig. 29.

For the different results, they are described by using the first order polynomial, which taken from Barlow method and we take the difference with the nominal values as the uncertainties in the Table. 11. The fitting results are listed in the following Fig. 28 and Fig. 29.

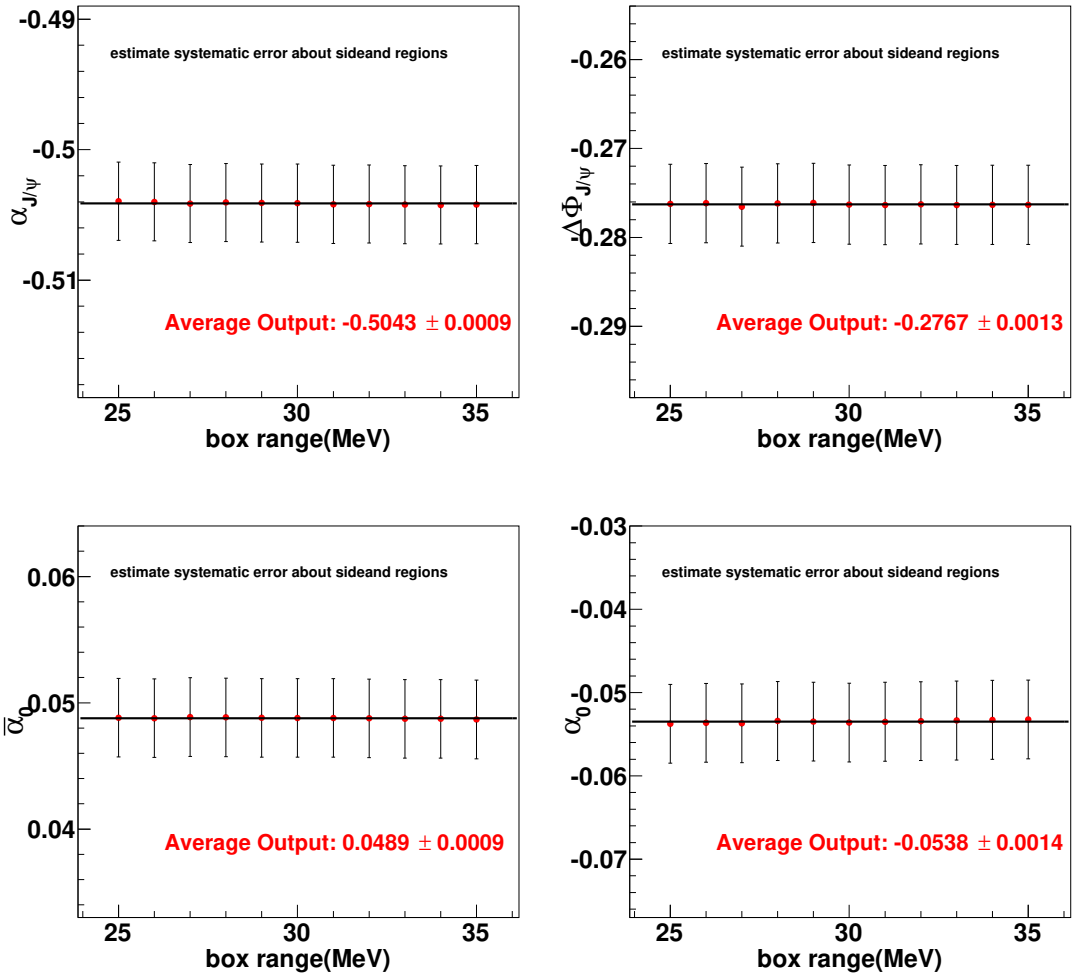

Fig. 28: The systematic uncertainties background estimation have been calculated

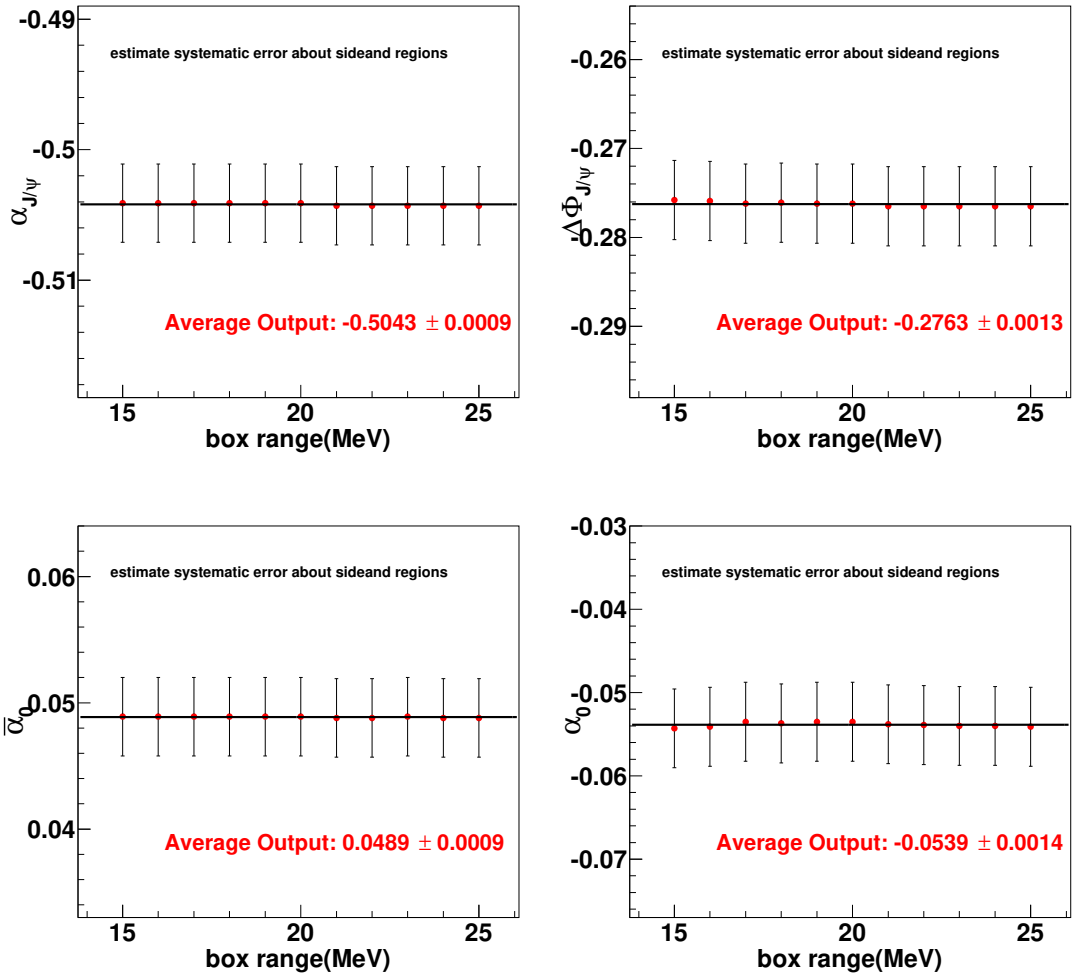

Fig. 29: The systematic uncertainties background estimation have been calculated

Tab. 11: Background uncertainties for the decay parameters($\Sigma^+ \to p\pi^0(n\pi^+)$, $\bar{\Sigma}^- \to n\pi^-(\bar{p}\pi^0)$).

Decay Parameters	nominal	Barlow method	difference
$\alpha_{J/\psi}$	-0.5156 ± 0.0030	-0.5155 ± 0.0030	0.0001
$\Delta\Phi_{J/\psi}$	-0.2772 ± 0.0044	-0.2779 ± 0.0044	0.0007
$\alpha_{(\Sigma^+\to p\pi^0)}$	-0.994	-0.994	–
$\alpha_{(\bar{\Sigma}^-\to \bar{p}\pi^0)}$	0.994	0.994	–
$\alpha_{(\bar{\Sigma}^-\to \bar{n}\pi^-)}$	-0.0565 ± 0.0047	-0.0568 ± 0.0014	0.0003
$\alpha_{(\Sigma^+\to n\pi^+)}$	0.0481 ± 0.0031	0.0484 ± 0.0009	0.0002

10.1.6 Fixed Decay Parameters

To improve our measurements, we fixed the $\alpha_{(\Sigma^+\to p\pi^0)}$ and $\alpha_{(\bar{\Sigma}^-\to \bar{p}\pi^0)}$, which come from previous BES3 results [42]. For $\alpha_{(\Sigma^+\to p\pi^0)} = -0.994 \pm 0.006$ and $\alpha_{(\bar{\Sigma}^-\to \bar{p}\pi^0)} = 0.994 \pm 0.006$. Since we use the

region of $\alpha_{(\Sigma^+\to p\pi^0)}$ and $\alpha_{(\bar{\Sigma}^-\to\bar{p}\pi^0)}$ to estimate the systematic uncertainties, by changing the value from -0.994 to -0.988 or -1.0 for $\Sigma^+ \to p\pi^0, \bar{\Sigma}^- \to \bar{n}\pi^-$, by changing the value from 0.994 to 0.988 or 1.0 for $\Sigma^+ \to n\pi^+, \bar{\Sigma}^- \to \bar{p}\pi^0$. The fitting results are listed in the following table 12, and take the difference with the nominal values as the uncertainties.

Tab. 12: Uncertainties of fixed parameters($\Sigma^+ \to p\pi^0(n\pi^+), \bar{\Sigma}^- \to n\pi^-(\bar{p}\pi^0)$).

Decay Parameters	nominal	smaller value	larger value	difference
$\alpha_{J/\psi}$	-0.5156 ± 0.0030	-0.5122 ± 0.0030	-0.5156 ± 0.0030	0.0000
$\Delta\Phi_{J/\psi}$	-0.2772 ± 0.0044	-0.2792 ± 0.0045	-0.2755 ± 0.0045	0.0020
$\alpha_{(\Sigma^+\to p\pi^0)}$	-0.994	-0.988	-1.0	–
$\alpha_{(\bar{\Sigma}^-\to\bar{p}\pi^0)}$	0.994	0.988	1.0	–
$\alpha_{(\bar{\Sigma}^-\to\bar{n}\pi^-)}$	-0.0565 ± 0.0047	-0.0568 ± 0.0048	-0.0562 ± 0.0047	0.0003
$\alpha_{(\Sigma^+\to n\pi^+)}$	0.0481 ± 0.0031	0.0484 ± 0.0031	0.0478 ± 0.0031	0.0003

10.1.7 Summary of decay parameter uncertainties

All the sources of systematic uncertainties are treated as uncorrelated and summed in quadrature, listed in Table 13.

Table 13: Summary of the systematic uncertainties for the decay parameters

Tab. 13: The total uncertainties of $\Sigma^+ \to n\pi^+, \bar{\Sigma}^- \to \bar{n}\pi^-$

Systematic error	$\alpha_{J/\psi}$	$\Delta\Phi_{J/\psi}$	$\alpha_{(\bar{\Sigma}^-\to\bar{n}\pi^-)}$	$\alpha_{(\Sigma^+\to n\pi^+)}$
MC efficiency correction	0.0059	0.0005	0.0016	0.0011
Kinematic fitting	0.0003	0.0004	0.0007	0.0003
Fitting method	0.0007	0.0028	0.0007	0.0012
Signal mass window	0.0015	0.0021	0.0010	0.0009
Background	0.0001	0.0007	0.0003	0.0002
Fix Decay Parameters	0.0000	0.0020	0.0003	0.0003
Total	0.0061	0.0041	0.0022	0.0019

10.2 Systematic uncertainties of branching fraction measurement

The branching fraction of $J/\psi \to \Sigma^+\bar{\Sigma}^-$ is determined by using simultaneous fit that can be found Appendices. D. The uncertainties of the branching fraction measurement include the uncertainties of MC efficiency correction, the uncertainties of decay parameters, the fitting range, fitting function, background estima tion, kinematic fitting and total number of J/ψ events, which are listed in the Tab. 14.

Tab. 14: The event number of J/ψ data

Source	$J/\psi \to \Sigma^+\bar{\Sigma}^-$
Tracking and PID efficiency	1.7
π^0 reconstruction efficiency	1.2
Decay parameters	1.6
Fitting range	0.3
Fitting function	0.6
Background estimation	0.1
Kinematic fitting	0.5
$\bar{n}$ correction	0.4
Total number	0.6
Total	2.85

10.2.1 MC efficiency correction for charged tracks, $\bar{n}$ and π^0

We use 1,000,000 J/ψ MC DIY event to estimate the event selection efficiencies. The differences of detection efficiencies for proton, anti-proton, π^+, π^-, $\bar{n}$ and π^0 between data and MC have been corrected according to momentums and polar angles.

By changing correction factor $\pm$ 1σ range to get new MC efficiency, the difference of branching fraction is taken as our systematic uncertainty. The uncertainties of charged tracking and PID efficiencies are estimated to 1.7% for $J/\psi \to \Sigma^+\bar{\Sigma}^-$. The uncertainties of π^0 reconstruction efficiencies are estimated to 1.2% for $J/\psi \to \Sigma^+\bar{\Sigma}^-$. The uncertainties of $\bar{n}$ selection efficiencies are estimated to 0.4% for $J/\psi \to \Sigma^+\bar{\Sigma}^-$.

10.2.2 Decay parameters

The efficiency is calculated based on the MC sample which is generated with decay parameters measured by ourselves. By considering the covariance between the fitting parameters. By changing the decay parameters 1σ, we take the maximum difference with the nominal values as the uncertainties, which are 1.6% for $J/\psi \to \Sigma^+\bar{\Sigma}^-$, respectively.

10.2.3 Fitting range

By changing the fitting range from [1.14, 1.24] GeV to [1.15, 1.23] GeV, and considering the fitting results and efficiency, the difference are 0.3% for $J/\psi \to \Sigma^+\bar{\Sigma}^-$.

10.2.4 Fitting function

To estimate the uncertainties of fitting function, we use the Crystal Ball function to describe the signal instead of MC shape convoluted with Gaussian in the Fig 30. To compare the branching fractions

549 with the nominal values, the differences are taken as the systematic uncertainties, 0.6% for $J/\psi \to \Sigma^+\bar{\Sigma}^-$.

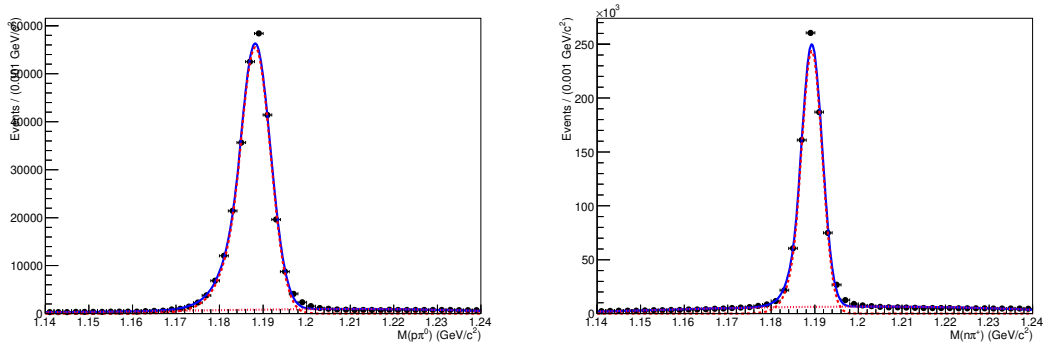

Fig. 30: Left: the $p\pi^0$ invariant mass distribution for $J/\psi \to \Sigma^+\bar{\Sigma}^-, \Sigma^+ \to p\pi^0, \bar{\Sigma}^- \to \bar{n}\pi^-$. Right: the $n\pi^+$ invariant mass distribution for $J/\psi \to \Sigma^+\bar{\Sigma}^-, \Sigma^+ \to n\pi^+, \bar{\Sigma}^- \to \bar{p}\pi^0$.

550 ### 10.2.5 Background estimation

551 To estimate the uncertainties of background events, we changed the order of polynomial functions
552 for background descriptions. The differences are taken as the systematic uncertainties comparing the
553 nominal values, 0.1% for $J/\psi \to \Sigma^+\bar{\Sigma}^-$.

554 ### 10.2.6 Kinematic fitting

555 When we use the track correction for the helix parameters, the χ^2_{4C} and χ^2_{2C} distribution is more con-
556 sistent between data and MC in the Fig 31. Then we could use the difference between before correction
557 and after correction as the systematic uncertainties, and take the value with correction as the nominal
558 one. The differences are taken as the systematic uncertainties, 0.5% for $J/\psi \to \Sigma^+\bar{\Sigma}^-$.

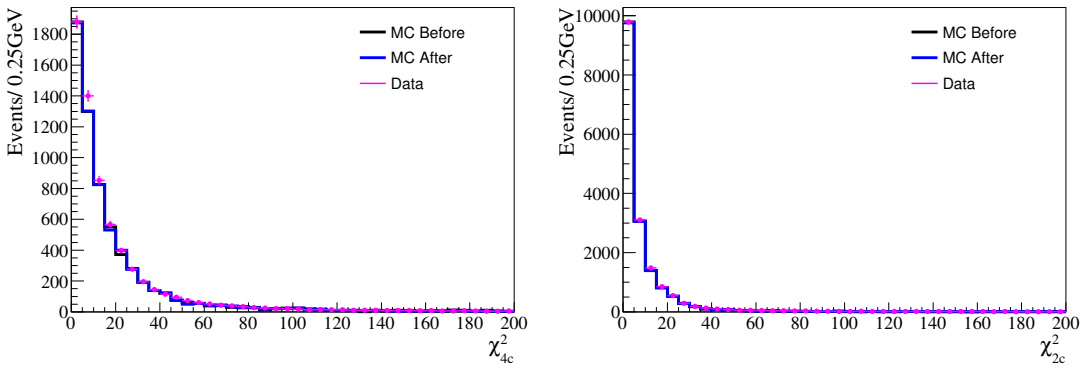

Fig. 31: Left: the χ^2_{4C} distribution for $J/\psi \to \Sigma^+\bar{\Sigma}^-, \Sigma^+ \to p\pi^0, \bar{\Sigma}^- \to \bar{n}\pi^-$. Right: the χ^2_{2C} distribution for $J/\psi \to \Sigma^+\bar{\Sigma}^-, \Sigma^+ \to n\pi^+, \bar{\Sigma}^- \to \bar{p}\pi^0$.

10.2.7 Total number of J/ψ

The total number of J/ψ mesons are based on inclusive hadronic events, as described in [41]. The uncertainties of the total number are determined to be 0.60% for J/ψ events.

11 Summary

In summary, based on the 10087.8×10^6 J/ψ events collected at BESIII detector, the branching fractions and decay parameters of $J/\psi \to \Sigma^+\bar{\Sigma}^-$ ($\Sigma^+ \to p\pi^0, \bar{\Sigma}^- \to \bar{n}\pi^-$ or $\Sigma^+ \to n\pi^+, \bar{\Sigma}^- \to \bar{p}\pi^0$) are measured which are listed in Table 15.

And by comparison the branching fractions of $J/\psi \to \Sigma^+\bar{\Sigma}^-$ and $\psi(3686) \to \Sigma^+\bar{\Sigma}^-$(PDG), the Q value of "12%" is tested to be $Q = \frac{P_{J/\psi}}{P_{\psi(3686)}} \times \frac{\psi(3686)\to\Sigma^+\bar{\Sigma}^-}{J/\psi\to\Sigma^+\bar{\Sigma}^-} = \frac{1}{1.4194} \times \frac{2.32\pm0.12}{10.85\pm0.31} = 15.1\% \pm 0.9\%$, (The $\frac{P_{J/\psi}}{P_{\psi(3686)}}$ is correction factor of the phase space, where $P_{J/\psi}$ or $P_{\psi(3686)}$ is the Σ^- momentum in the J/ψ or $\psi(3686)$ decay process).

For the $\Sigma^+ \to n\pi^+$ and $\bar{\Sigma}^- \to \bar{n}\pi^-$ decays, the value of CP violation is measured for the first time. The polarization is well consistent with previous measurement. The $\alpha_{(\Sigma^+\to n\pi^+)}$ value is improved. The $\alpha_{(\bar{\Sigma}^-\to\bar{n}\pi^-)}$ is measured for the first time. The branching fraction is measured in Table 15, so the branching fraction of $J/\psi \to \Sigma^+\bar{\Sigma}^- = (10.85 \pm 0.01 \pm 0.31) \times 10^{-4}$ is improved by combining two decay channels. We considered systematic and statistical uncertainties, the CP asymmetry $A_{CP} = \frac{\alpha_{(\Sigma^+\to n\pi^+)}+\alpha_{(\bar{\Sigma}^-\to\bar{n}\pi^-)}}{\alpha_{(\Sigma^+\to n\pi^+)}-\alpha_{(\bar{\Sigma}^-\to\bar{n}\pi^-)}} = -0.080 \pm 0.052 \pm 0.028$ is extracted for the first time. The CP violation is still not observed in $\Sigma^+\bar{\Sigma}^-$ decay.

Tab. 15: The decay parameters and branching ratio of $J/\psi \to \Sigma^+\bar{\Sigma}^-, \Sigma^+ \to p\pi^0(n\pi^+), \bar{\Sigma}^- \to \bar{n}\pi^-(\bar{p}\pi^0)$

Decay parameters and branching ratio	Our measurements	Previous measurements
$\alpha_{J/\psi}$	$-0.5156 \pm 0.0030 \pm 0.0061$	$-0.508 \pm 0.006 \pm 0.004$ [42]
$\Delta\Phi_{J/\psi}$	$-0.2772 \pm 0.0044 \pm 0.0041$	$-0.270 \pm 0.012 \pm 0.009$ [42]
$\alpha_{(\bar{\Sigma}^-\to\bar{n}\pi^-)}$	$-0.0565 \pm 0.0047 \pm 0.0022$	Not be measured
$\frac{\alpha_{(\bar{\Sigma}^-\to\bar{n}\pi^-)}}{\alpha_{(\bar{\Sigma}^-\to\bar{p}\pi^0)}}$	$-0.0571 \pm 0.0053 \pm 0.0032$	Not be measured
$\alpha_{(\Sigma^+\to n\pi^+)}$	$0.0481 \pm 0.0031 \pm 0.0019$	0.068 ± 0.013 [32]
$\frac{\alpha_{(\Sigma^+\to n\pi^+)}}{\alpha_{(\Sigma^+\to p\pi^0)}}$	$-0.0490 \pm 0.0032 \pm 0.0021$	-0.069 ± 0.013 [32]
$Br(J/\psi \to \Sigma^+\bar{\Sigma}^-)$	$(10.85 \pm 0.01 \pm 0.31) \times 10^{-4}$	$(15.0 \pm 2.4) \times 10^{-4}$ [43]

References

[1] J. H. Christenson et al., Phys. Rev. Lett. 13, 138 (1964); KTeV Collaboration, A. Alavi-Harati et al., ibid. 83, 22 (1999); NA48 Collaboration, V. Fanti et al., Phys. Lett. B 465, 335 (1999); BABAR Collaboration, B. Aubert et al., Phys. Rev. Lett. 87, 091801(2001); Belle Collaboration, K. Abe et al., ibid. 87, 091802(2001)

[2] M. Tanabashi et al., (Particle Data Group), Phys. Rev. D 98, 030001(2018)

[3] R. Handler, R. Grobel, L. Pondrom, M. Sheaff, C. Wilkinson, P. T. Cox, J. Dworkin, O. E. Overseth, K. J. Heller and T. Devlin, *et al.* Phys. Rev. D **25** (1982), 639-651 doi:10.1103/PhysRevD.25.639

[4] T. Holmstrom *et al.* [HyperCP], Phys. Rev. Lett. **93** (2004), 262001 doi:10.1103/PhysRevLett.93.262001 [arXiv:hep-ex/0412038 [hep-ex]].

[5] M. Ablikim *et al.* (BESIII Collaboration), Nature Phys. **15** (2019), 631-634 doi:10.1038/s41567-019-0494-8 [arXiv:1808.08917 [hep-ex]].

[6] P. Astbury, J. Gallivan, J. Jafar, M. Letheren, V. Steiner, J. A. Wilson, W. Beusch, M. Borghini, D. Websdale and L. Fluri, *et al.* Nucl. Phys. B **99** (1975), 30-52 doi:10.1016/0550-3213(75)90054-1

[7] D. Berley, S. P. Yamin, S. S. Hertzbach, R. R. Kofler, G. W. Meisner, J. Button-Shafer, S. S. Yamamoto, W. Heintzelman, M. Schiff and J. Thompson, *et al.* Phys. Rev. D **1** (1970), 2015-2030 doi:10.1103/PhysRevD.1.2015

[8] M. Ablikim *et al.* (BESIII Collaboration), Phys. Rev. Lett. **125** (2020) no.5, 052004 doi:10.1103/PhysRevLett.125.052004 [arXiv:2004.07701 [hep-ex]].

[9] M. Ablikim *et al.* (BESIII Collaboration), Phys. Rev. Lett. **123** (2019) no.12, 122003 doi:10.1103/PhysRevLett.123.122003 [arXiv:1903.09421 [hep-ex]].

[10] M. Ablikim et al. (BESIII Collaboration), Phys. Rev. D 81 (2010) 012003.

[11] G. Faldt (GF), Eur. Ph. J. A 52 141(2016); GF, A. Kupsc (AK), Phys. Lett. B 772 16(2017); GF, Phys. Rev. D 97 053002 (2018); GF, AK, S. Leupold, E. Perotti, arXiv:1809.04038 (2018).

[12] S. J. Brodsky and G. P. Lepage, Phys. Rev. D 24, 2848 (1981).

[13] M. Claudson, S. L. Glashow and M. B. Wise, Phys. Rev. D 25, 1345 (1982). C. Carimalo, Int. J. Mod. Phys. A2, 249 (1987).

[14] C. Carimalo, Int. J. Mod. Phys. A2, 249 (1987).

[15] T. Appelquist and H. Politzer, Phys. Rev. Lett. 34, 43 (1975).

[16] A. DeRujula and S. Glashow, Phys. Rev. Lett. 34, 46 (1975).

[17] M. E. B. Franklin et al. (MARKII Collaboration), Phys. Rev. Lett. 51, 963 (1983).

[18] M. Ablikim et al. (BESIII Collaboration), Phys. Lett. B 614 37 (2005).

[19] R. A. Briere *et al.* (CLEO Collaboration), Phys. Rev. Lett. **95**, 062001 (2005) doi:10.1103/PhysRevLett.95.062001 [arXiv:hep-ex/0505101 [hep-ex]].

[20] N. Brambilla et al. (Quarkonium Working Group), Eur. Phys. J. C 71 1534 (2011).

[21] Q. Wang, G. Li and Q. Zhao, Phys. Rev. D 85, 074015 (2012).

[22] K. A. Olive et al. (Particle Data Group) Chin. Phys. C 38, 090001 (2014).

[23] K. F. Liu and C. W. Wong, Phys. Rev. D 28, 170 (1983).

[24] M. Ablikim et al. (BESIII Collaboration), Nucl. Instrum. Meth. A 614, 345 (2010).

[25] C. H. Yu et al., Proceedings of IPAC2016, Busan, Korea, 2016, doi:10.18429/JACoW- IPAC2016-TUYA01.

[26] M. Ablikim et al. (BESIII Collaboration), Chin. Phys. C 44, 040001 (2020).

[27] X. Li et al., Radiat. Detect. Technol. Methods 1, 13 (2017); Y. X. Guo et al., Radiat. Detect. Technol. Methods 1, 15 (2017); P. Cao et al., Nucl. Instrum. Meth. A 953, 163053 (2020).

[28] M. Ablikim et al. (BESIII Collaboration), [arXiv:2111.07571 [hep-ex]].

[29] S. Agostinelli et al. (geant4 Collaboration), Nucl. Instrum. Meth. A 506, 250 (2003).

[30] S. Jadach, B. F. L. Ward and Z. Was, Comp. Phys. Commu. 130, 260 (2000); Phys. Rev. D 63, 113009 (2001).

[31] D. J. Lange, Nucl. Instrum. Meth. A 462, 152 (2001); R. G. Ping, Chin. Phys. C 32, 599 (2008).

[32] K. A. Olive et al. (Particle Data Group) Chin. Phys. C 38, 090001 (2014).

[33] J. C. Chen et al., Phys. Rev. D 62, 034003 (2000).

[34] https://hnbes3.ihep.ac.cn/HyperNews/get/AUX/2020/12/24(BAM-00476)

[35] https://docbes3.ihep.ac.cn/DocDB/0002/000250/026/Asymmetry%20Parameters%20Measurement.pdf

[36] M. Ablikim et al. (BESIII Collaboration), Phys. Rev. D **101**, no.9,092002(2020) doi:10.1103/PhysRevD.101.092002 [arXiv:2004.01394 [hep-ex]].

[37] https://docbes3.ihep.ac.cn/DocDB/0005/000574/031/Sigma_memo_v6.0.pdf

[38] https://hnbes3.ihep.ac.cn/HyperNews/get/paper504.html

[39] https://indico.ihep.ac.cn/event/10989/session/19/contribution/141/material/slides/0.pdf

[40] https://indico.ihep.ac.cn/event/11850/contribution/0/material/slides/0.pdf

[41] M. Ablikim et al. (BESIII Collaboration), Chin. Phys. C 37, 063001 (2013).

[42] M. Ablikim *et al.* (BESIII Collaboration), Phys. Rev. Lett. **125** (2020) no.5, 052004 doi:10.1103/PhysRevLett.125.052004 [arXiv:2004.07701 [hep-ex]].

[43] M. Ablikim *et al.* (BESII Collaboration), Phys. Rev. D **78** (2008), 092005 doi:10.1103/PhysRevD.78.092005 [arXiv:0810.1896 [hep-ex]].

Appendices

A π^0 control sample

To study the π^0 reconstruction efficiency, we choose the $J/\psi \to \Sigma^+\bar{\Sigma}^- \to p\bar{p}\pi^0\pi^0$ as the control sample. The π^0 transverse momentum distributed in the region from 0.1 to 0.35 GeV, which could cover our signal area.

Charged tracks reconstructed by main drift chamber(MDC) hit information must be fitted by Kalman method successfully and come from the interaction region in three dimensions. Due to changing beam conditions, the interaction point (IP) moves. Thus, a separate average IP (beam position) is determined for each run using the VertexDbSvc package. Relative to this run-dependent IP, each charged track must satisfy the following requirements:

- $V_{xy} < 2$ cm,
- $|V_z| < 10$ cm,
- $|\cos\theta| < 0.93$,
- Good tracks is required $N \geq 2$ (Because $\bar{n}$ tend to annihilate with matter).

Here, θ is the polar angle of the charged track with respect to the beam axis, V_{xy} and $|V_z|$ are the closest approaches of a charged track to the interaction point in the Oxy plane and in the z position.

A.1 Particle identification

The charged protons are identified via ParticleID package by using the TOF and dE/dx measurements with which the combined confidence levels $\mathscr{L}(p)$ for protons hypotheses are calculated, respectively. The particle is taken as p if the $Prob_{PID}$ more than any other particle hypothesis. We require the pion and proton candidates satisfy the following criteria:

- p: $\mathscr{L}(p) > \mathscr{L}(\pi)$ and $\mathscr{L}(p) > \mathscr{L}(k)$.

A.2 Good shower

- Photon candidates are identified using showers in the EMC. The deposited energy of each shower must be more than 25 MeV in the barrel region ($|\cos\theta| < 0.80$) and more than 50 MeV in the end cap region ($0.86 < |\cos\theta| < 0.92$).
- To suppress electronic noise and showers unrelated to the event, the difference between the EMC time and the event start time is required to be within (0, 700) ns.

- To exclude showers that originate from charged tracks, the angle between the position of each shower in the EMC and the closest extrapolated charged track must be greater than 10 degrees.
- The number of good showers $N_\gamma \geq 4$.

A.3 π^0 reconstruction

The π^0 mesons are reconstructed by the decays $\pi^0 \to \gamma\gamma$. To reconstruct π^0 meson, we perform a kinematic fit on $\pi^0 \to \gamma\gamma$. To suppress combinatorial background, we require that the χ^2 of the kinematic fit is less than 25. π^0 candidates are reconstructed from pairs of photons whose invariant mass satisfies $[M_{\pi^0}\text{ -60}] < M_{\gamma\gamma} < [M_{\pi^0}\text{ + 40}]\ MeV/c^2$, where M_{π^0} is the nominal mass of π^0 taken from the PDG.

A.4 π^0 reconstruction efficiency

- fitting range: $M_{\Sigma^+\bar{p}recoil} \in$ [0.85,1.05] GeV
- π^0 reconstruction efficiency is defined as : $\frac{N_{\pi^0}>=2}{N_{\pi^0}>=1}$.

Appendices

B $\bar{n}$ control sample

To study the $\bar{n}$ reconstruction efficiency, we choose the $J/\psi \to p\bar{n}\pi^-$ as the control sample. The $\bar{n}$ transverse momentum distributed in the region from 0.5 to 1.2 GeV, which could cover our signal area.

Charged tracks reconstructed by main drift chamber(MDC) hit information must be fitted by Kalman method successfully and come from the interaction region in three dimensions. Due to changing beam conditions, the interaction point (IP) moves. Thus, a separate average IP (beam position) is determined for each run using the VertexDbSvc package. Relative to this run-dependent IP, each charged track must satisfy the following requirements:

- $V_{xy} < 0.5$ cm,
- $|V_z| < 5$ cm,
- $|\cos\theta| < 0.93$,
- Good tracks is required $N \geq 2$ (Because $\bar{n}$ tend to annihilate with matter).

Here, θ is the polar angle of the charged track with respect to the beam axis, V_{xy} and $|V_z|$ are the closest approaches of a charged track to the interaction point in the Oxy plane and in the z position.

B.1 Particle identification

The charged pions and protons are identified via ParticleID package by using the TOF and dE/dx measurements with which the combined confidence levels $\mathscr{L}(\pi^-)$ and $\mathscr{L}(p)$ for pion and proton hypotheses are calculated, respectively. The particle is taken as $p(\pi)$ if the $Prob_{PID}$ more than any other particle hypothesis. We require the pion and proton candidates satisfy the following criteria:

- π^-: $\mathscr{L}(\pi^-) > \mathscr{L}(p)$ and $\mathscr{L}(\pi^-) > \mathscr{L}(k)$,
- p: $\mathscr{L}(p) > \mathscr{L}(\pi)$ and $\mathscr{L}(p) > \mathscr{L}(k)$.

B.2 $\bar{n}$ Shower Requirement

The cluster in the EMC which satisfies the following criteria is regarded as a good $\bar{n}$ shower.

- barrel EMC, $|\cos\theta| < 0.80$; endcap EMC, $0.86 < |\cos\theta| < 0.92$;
- At least one shower with energy larger than 0.5GeV is required. Fig. 2 shows the deposit energy distribution of $\bar{n}$ and γ in the EMC from MC simulation.

- Second moment> 20, the reference we refer to is [35] [36](This selection is already one of the standard criteria for the selection of antineutron). The second momentum is defined as $\sum_i E_i r_i^2 / \sum_i E_i$, where E_i is the deposit energy in the i_{th} crystal and r_i is the radial distance of the crystal i from the cluster center.

- To suppress electronic noise and showers unrelated to the event, the difference between the EMC time and the event start time is required to be within (0, 700) ns

- To exclude showers that originate from charged tracks, the angle between the position of each shower in the EMC and the closest extrapolated charged track must be greater than 10 degrees.

B.3 $\bar{n}$ reconstruction efficiency

- fitting range: $M_{p\pi^- recoil} \in$ [0.85,1.05] GeV

- $\bar{n}$ reconstruction efficiency is defined as : $\frac{N_{\bar{n}}>=1}{N_{\bar{n}}>=0}$.

Appendices

C The background formula

For the $J/\psi \to \Sigma^+\bar{\Sigma}^-, \Sigma^+ \to p\pi^0, \bar{\Sigma}^- \to \bar{n}\pi^-$, I have checked it and the background formula N=S – 0.27*A has been corrected by fitting two dimension invariant mass in the Fig. 32 that can be found in our updated memo.

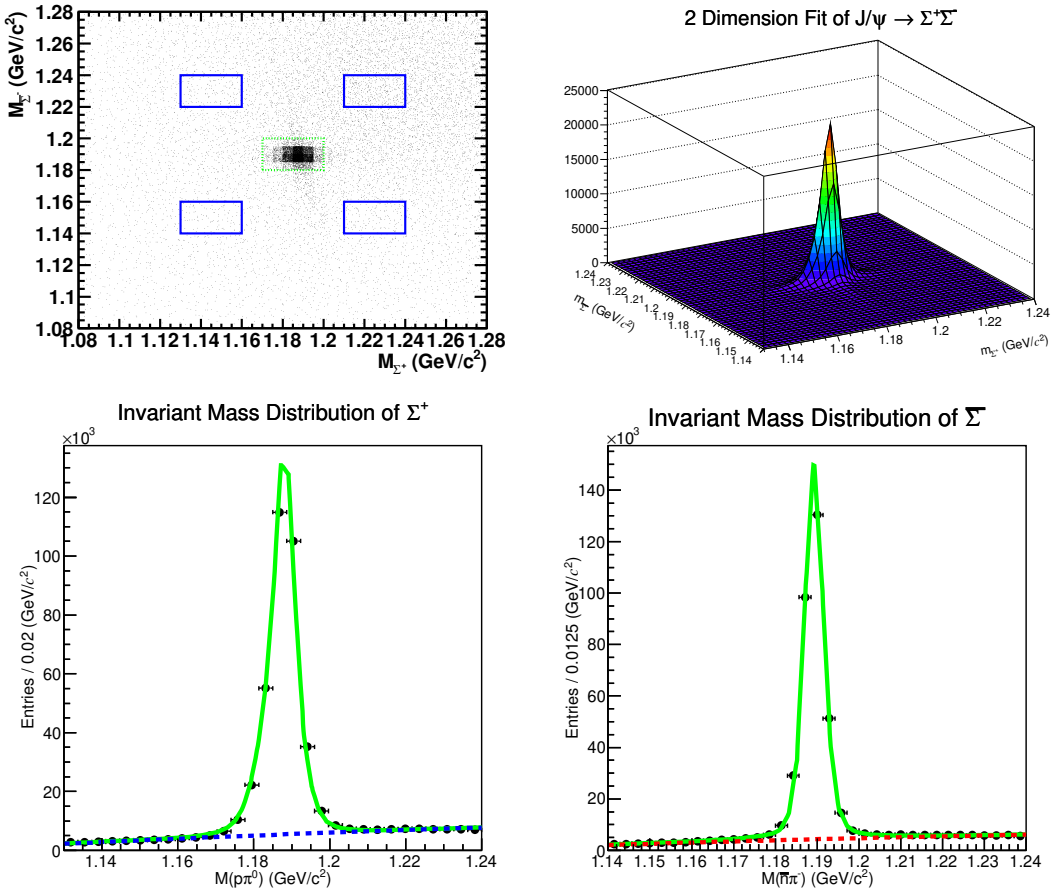

Fig. 32: The scatter plot for the sideband region definition for $J/\psi \to \Sigma^+\bar{\Sigma}^-, \Sigma^+ \to p\pi^0, \bar{\Sigma}^- \to \bar{n}\pi^-$.

For the $J/\psi \to \Sigma^+\bar{\Sigma}^-, \Sigma^+ \to n\pi^+, \bar{\Sigma}^- \to \bar{p}\pi^0$, I have checked it and the background formula N=S – 0.26*A has been corrected by fitting two dimension invariant mass in the Fig. 33 that can be found in our updated memo.

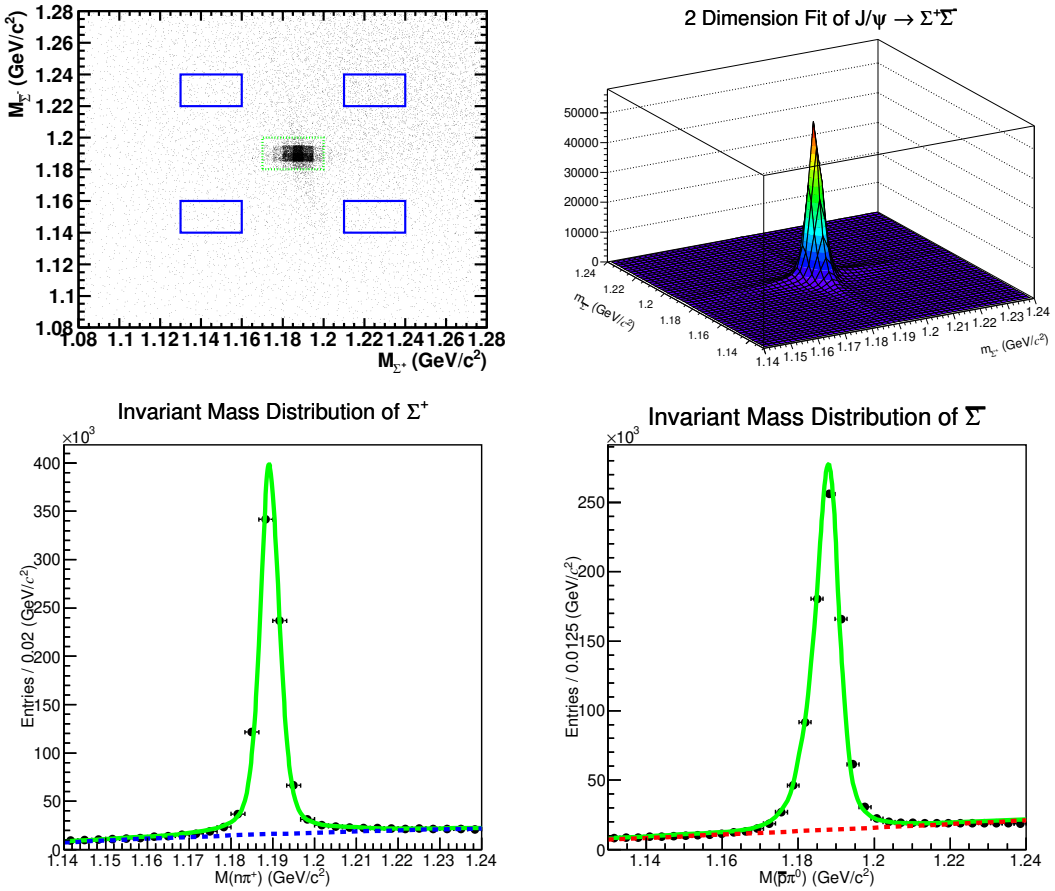

Fig. 33: The scatter plot for the sideband region definition for $J/\psi \to \Sigma^+\bar{\Sigma}^-, \Sigma^+ \to n\pi^+, \bar{\Sigma}^- \to \bar{p}\pi^0$.

Appendices

D combine the two decay modes to determine the BF

The branching fraction of combine fit result in the Fig. 34 are consistent with previous measurements, and corresponding systematic uncertainties have been updated in the memo.

```
COVARIANCE MATRIX CALCULATED SUCCESSFULLY
FCN=-1.88985e+07 FROM HESSE     STATUS=OK             89 CALLS         369 TOTAL
                     EDM=0.0155028    STRATEGY= 1      ERROR MATRIX ACCURATE
 EXT PARAMETER                                   INTERNAL      INTERNAL
 NO.   NAME      VALUE            ERROR          STEP SIZE       VALUE
  1  Branching_fraction   1.08524e-03   1.10845e-06   3.42523e-03   3.71047e-02
  2  n_bk          1.34759e+05   4.81498e+02   5.07627e-03  -6.62354e-01
  3  n_bk2         2.87597e+04   2.19746e+02   5.58825e-03  -1.08641e+00
  4  p0            4.55322e-01   5.28516e-03   1.57531e-03   4.55480e-02
  5  p02           5.29095e-01   1.04885e-02   3.13208e-03   5.29342e-02
  6  resMean1     -1.59505e-04   3.52969e-06   3.53471e-03  -5.31936e-02
  7  resMean2      3.70431e-04   7.40323e-06   7.40461e-03   1.23793e-01
  8  sigma1        1.41896e-03   5.45984e-06   7.20598e-03  -4.47168e-01
  9  sigma2        8.31319e-04   2.18915e-05   3.48732e-02  -7.30809e-01
                               ERR DEF= 0.5
```

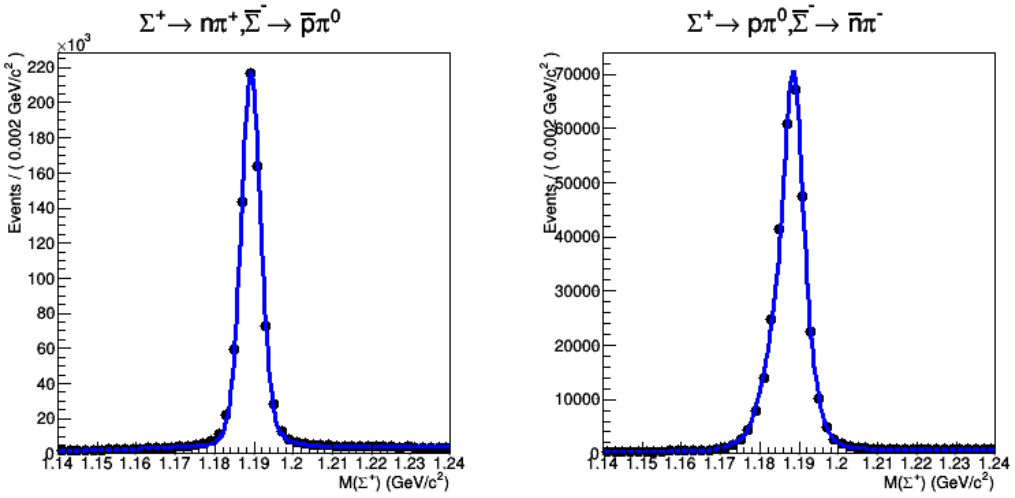

Fig. 34: The branching fraction of combining fit of $J/\psi \to \Sigma^+\bar{\Sigma}^-$.

Appendices

E The ratio of selection between data and MC

Tab. 16: The correction factor $\epsilon_{\bar{n}}^{data}/\epsilon_{\bar{n}}^{MC}$ in terms of cosθ in different momentum by using control sample $J/\psi \to p\bar{n}\pi^-$.

Cosθ	[0.55, 0.6] GeV	[0.6, 0.65] GeV	[0.65, 0.7] GeV	[0.7, 0.75] GeV	[0.75, 0.8] GeV	[0.8, 0.85] GeV	[0.85, 0.9] GeV	[0.9, 0.95] GeV	[0.95, 1.0] GeV
[−1.0, −0.8]	1.001 ± 0.011	0.919 ± 0.010	1.010 ± 0.010	0.988 ± 0.009	1.062 ± 0.009	1.003 ± 0.009	0.939 ± 0.009	1.094 ± 0.009	1.130 ± 0.010
[−0.8, −0.6]	0.925 ± 0.006	0.916 ± 0.005	0.927 ± 0.005	0.948 ± 0.005	0.935 ± 0.004	0.948 ± 0.004	0.872 ± 0.004	0.892 ± 0.004	0.867 ± 0.004
[−0.6, −0.4]	0.902 ± 0.006	0.913 ± 0.005	0.893 ± 0.005	0.895 ± 0.005	0.898 ± 0.004	0.865 ± 0.004	0.870 ± 0.004	0.830 ± 0.003	0.845 ± 0.003
[−0.4, −0.2]	0.874 ± 0.006	0.916 ± 0.005	0.896 ± 0.005	0.904 ± 0.005	0.878 ± 0.004	0.876 ± 0.004	0.864 ± 0.004	0.840 ± 0.003	0.823 ± 0.003
[−0.2, 0.0]	0.897 ± 0.006	0.899 ± 0.005	0.892 ± 0.005	0.881 ± 0.005	0.890 ± 0.004	0.882 ± 0.004	0.857 ± 0.004	0.829 ± 0.003	0.822 ± 0.003
[0.0, 0.2]	0.881 ± 0.006	0.909 ± 0.006	0.884 ± 0.005	0.847 ± 0.005	0.882 ± 0.004	0.867 ± 0.004	0.845 ± 0.004	0.829 ± 0.003	0.813 ± 0.003
[0.2, 0.4]	0.929 ± 0.006	0.889 ± 0.005	0.901 ± 0.005	0.884 ± 0.005	0.896 ± 0.004	0.878 ± 0.004	0.853 ± 0.004	0.827 ± 0.003	0.804 ± 0.003
[0.4, 0.6]	0.885 ± 0.006	0.911 ± 0.005	0.892 ± 0.005	0.901 ± 0.005	0.897 ± 0.004	0.880 ± 0.004	0.870 ± 0.004	0.850 ± 0.003	0.834 ± 0.003
[0.6, 0.8]	0.900 ± 0.006	0.911 ± 0.005	0.934 ± 0.005	0.936 ± 0.005	0.957 ± 0.005	0.899 ± 0.004	0.938 ± 0.005	0.875 ± 0.004	0.877 ± 0.004
[0.8, 1.0]	0.963 ± 0.010	0.996 ± 0.010	0.937 ± 0.009	0.998 ± 0.009	1.029 ± 0.009	1.103 ± 0.009	0.994 ± 0.009	0.976 ± 0.008	1.011 ± 0.009

Tab. 17: The correction factor $\epsilon_{\bar{p}}^{data}/\epsilon_{\bar{p}}^{MC}$ in terms of cosθ in different momentum range by using control sample $J/\psi \to p\bar{p}\pi^+\pi^-$(2009 year).

Cosθ	[0.2, 0.3] GeV	[0.3, 0.4] GeV	[0.4, 0.5] GeV	[0.5, 0.6] GeV	[0.6, 0.7] GeV	[0.7, 0.8] GeV	[0.8, 0.9] GeV	[0.9, 1.0] GeV
[−1.0, −0.8]	0.9005 ± 0.0376	1.0168 ± 0.0092	1.0000 ± 0.0031	1.0000 ± 0.0036	1.0000 ± 0.0013	1.0000 ± 0.0019	0.9919 ± 0.0028	0.9900 ± 0.0038
[−0.8, −0.6]	0.9900 ± 0.0073	1.0000 ± 0.0036	1.0000 ± 0.0009	1.0000 ± 0.0003	1.0000 ± 0.0009	1.0000 ± 0.0010	1.0000 ± 0.0013	1.0000 ± 0.0010
[−0.6, −0.4]	0.9869 ± 0.0042	1.0000 ± 0.0009	1.0000 ± 0.0002	1.0000 ± 0.0003	1.0000 ± 0.0005	1.0000 ± 0.0007	1.0000 ± 0.0006	1.0000 ± 0.0009
[−0.4, −0.2]	0.9756 ± 0.0065	1.0000 ± 0.0004	1.0000 ± 0.0004	1.0000 ± 0.0001	1.0000 ± 0.0006	1.0000 ± 0.0005	1.0000 ± 0.0006	1.0000 ± 0.0010
[−0.2, 0.0]	0.9426 ± 0.0053	1.0000 ± 0.0004	1.0000 ± 0.0004	1.0000 ± 0.0003	1.0000 ± 0.0003	1.0000 ± 0.0007	1.0000 ± 0.0007	1.0000 ± 0.0006
[0.0, 0.2]	0.9389 ± 0.0104	1.0000 ± 0.0005	1.0000 ± 0.0002	1.0000 ± 0.0006	1.0000 ± 0.0003	1.0000 ± 0.0005	1.0000 ± 0.0005	1.0000 ± 0.0018
[0.2, 0.4]	0.9851 ± 0.0029	1.0000 ± 0.0009	1.0000 ± 0.0002	1.0000 ± 0.0003	1.0000 ± 0.0003	1.0000 ± 0.0005	1.0000 ± 0.0006	1.0000 ± 0.0013
[0.4, 0.6]	0.9918 ± 0.0030	1.0000 ± 0.0005	1.0000 ± 0.0005	1.0000 ± 0.0001	1.0000 ± 0.0002	1.0000 ± 0.0004	1.0000 ± 0.0009	1.0000 ± 0.0013
[0.6, 0.8]	0.9877 ± 0.0039	1.0000 ± 0.0025	1.0000 ± 0.0005	1.0000 ± 0.0004	1.0000 ± 0.0011	1.0000 ± 0.0010	1.0000 ± 0.0011	1.0000 ± 0.0012
[0.8, 1.0]	0.9506 ± 0.0286	1.0191 ± 0.0077	1.0070 ± 0.0031	1.0000 ± 0.0036	1.0000 ± 0.0023	1.0000 ± 0.0014	1.0000 ± 0.0046	1.0000 ± 0.0056

Tab. 18: The correction factor $\epsilon_{\bar{p}}^{data}/\epsilon_{\bar{p}}^{MC}$ in terms of cosθ in different momentum range by using control sample $J/\psi \to p\bar{p}\pi^+\pi^-$(2012 year).

Cosθ	[0.2, 0.3] GeV	[0.3, 0.4] GeV	[0.4, 0.5] GeV	[0.5, 0.6] GeV	[0.6, 0.7] GeV	[0.7, 0.8] GeV	[0.8, 0.9] GeV	[0.9, 1.0] GeV
[−1.0, −0.8]	2.3589 ± 0.2068	1.0587 ± 0.0175	1.0000 ± 0.0065	0.9918 ± 0.0019	1.0000 ± 0.0019	1.0000 ± 0.0042	0.9935 ± 0.0014	1.0000 ± 0.0029
[−0.8, −0.6]	1.0142 ± 0.0114	1.0000 ± 0.0025	1.0000 ± 0.0006	1.0000 ± 0.0004	1.0000 ± 0.0003	1.0000 ± 0.0004	1.0000 ± 0.0009	1.0000 ± 0.0010
[−0.6, −0.4]	0.9707 ± 0.0031	1.0000 ± 0.0004	1.0000 ± 0.0004	1.0000 ± 0.0003	1.0000 ± 0.0004	1.0000 ± 0.0005	1.0000 ± 0.0012	1.0000 ± 0.0009
[−0.4, −0.2]	0.9704 ± 0.0033	1.0000 ± 0.0003	1.0000 ± 0.0004	1.0000 ± 0.0002	1.0000 ± 0.0003	1.0000 ± 0.0004	1.0000 ± 0.0005	1.0000 ± 0.0016
[−0.2, 0.0]	0.9238 ± 0.0046	1.0000 ± 0.0019	1.0000 ± 0.0006	1.0000 ± 0.0003	1.0000 ± 0.0004	1.0000 ± 0.0004	1.0000 ± 0.0005	1.0000 ± 0.0008
[0.0, 0.2]	0.9238 ± 0.0047	1.0000 ± 0.0020	1.0000 ± 0.0004	1.0000 ± 0.0004	1.0000 ± 0.0003	1.0000 ± 0.0003	1.0000 ± 0.0006	1.0000 ± 0.0014
[0.2, 0.4]	0.9830 ± 0.0036	1.0000 ± 0.0003	1.0000 ± 0.0002	1.0000 ± 0.0002	1.0000 ± 0.0003	1.0000 ± 0.0004	1.0000 ± 0.0007	1.0000 ± 0.0012
[0.4, 0.6]	0.9815 ± 0.0031	1.0000 ± 0.0008	1.0000 ± 0.0004	1.0000 ± 0.0002	1.0000 ± 0.0002	1.0000 ± 0.0005	1.0000 ± 0.0011	1.0000 ± 0.0015
[0.6, 0.8]	1.0326 ± 0.0097	1.0000 ± 0.0025	1.0000 ± 0.0012	1.0000 ± 0.0002	1.0000 ± 0.0003	1.0000 ± 0.0005	1.0000 ± 0.0006	1.0000 ± 0.0012
[0.8, 1.0]	2.0037 ± 0.1134	1.0687 ± 0.0225	1.0073 ± 0.0062	0.9894 ± 0.0022	1.0000 ± 0.0019	0.9943 ± 0.0007	0.9903 ± 0.0012	1.0000 ± 0.0039

Tab. 19: The correction factor $\epsilon_{\bar{p}}^{data}/\epsilon_{\bar{p}}^{MC}$ in terms of cosθ in different momentum range by using control sample $J/\psi \to p\bar{p}\pi^+\pi^-$(2018 year).

Cosθ	[0.2, 0.3] GeV	[0.3, 0.4] GeV	[0.4, 0.5] GeV	[0.5, 0.6] GeV	[0.6, 0.7] GeV	[0.7, 0.8] GeV	[0.8, 0.9] GeV	[0.9, 1.0] GeV
[−1.0, −0.8]	0.9279 ± 0.0112	1.0156 ± 0.0063	1.0000 ± 0.0049	1.0000 ± 0.0010	1.0000 ± 0.0004	1.0000 ± 0.0005	1.0000 ± 0.0007	1.0000 ± 0.0018
[−0.8, −0.6]	0.9874 ± 0.0022	1.0000 ± 0.0019	1.0000 ± 0.0002	1.0000 ± 0.0001	1.0000 ± 0.0004	1.0000 ± 0.0003	1.0000 ± 0.0007	1.0000 ± 0.0012
[−0.6, −0.4]	1.0000 ± 0.0045	1.0000 ± 0.0008	1.0000 ± 0.0002	1.0000 ± 0.0001	1.0000 ± 0.0006	1.0000 ± 0.0003	1.0000 ± 0.0011	1.0000 ± 0.0014
[−0.4, −0.2]	0.9875 ± 0.0035	1.0000 ± 0.0003	1.0000 ± 0.0002	1.0000 ± 0.0001	1.0000 ± 0.0004	1.0000 ± 0.0004	1.0000 ± 0.0005	1.0000 ± 0.0012
[−0.2, 0.0]	0.8910 ± 0.0042	1.0000 ± 0.0024	1.0000 ± 0.0005	1.0000 ± 0.0002	1.0000 ± 0.0002	1.0000 ± 0.0004	1.0000 ± 0.0006	1.0000 ± 0.0010
[0.0, 0.2]	0.8860 ± 0.0057	1.0000 ± 0.0021	1.0000 ± 0.0003	1.0000 ± 0.0001	1.0000 ± 0.0005	1.0000 ± 0.0003	1.0000 ± 0.0006	1.0000 ± 0.0008
[0.2, 0.4]	0.9863 ± 0.0045	1.0000 ± 0.0002	1.0000 ± 0.0001	1.0000 ± 0.0001	1.0000 ± 0.0006	1.0000 ± 0.0007	1.0000 ± 0.0007	1.0000 ± 0.0012
[0.4, 0.6]	1.0000 ± 0.0028	1.0000 ± 0.0007	1.0000 ± 0.0001	1.0000 ± 0.0000	1.0000 ± 0.0005	1.0000 ± 0.0003	1.0000 ± 0.0009	1.0000 ± 0.0016
[0.6, 0.8]	0.9907 ± 0.0028	1.0000 ± 0.0036	1.0000 ± 0.0002	1.0000 ± 0.0002	1.0000 ± 0.0003	1.0000 ± 0.0003	1.0000 ± 0.0007	1.0000 ± 0.0016
[0.8, 1.0]	0.9394 ± 0.0106	1.0260 ± 0.0081	1.0000 ± 0.0044	1.0000 ± 0.0013	1.0000 ± 0.0016	1.0000 ± 0.0009	1.0000 ± 0.0007	1.0000 ± 0.0043

Tab. 20: The correction factor $\epsilon_{\bar{p}}^{data}/\epsilon_{\bar{p}}^{MC}$ in terms of cosθ in different momentum range by using control sample $J/\psi \to p\bar{p}\pi^+\pi^-$(2019 year).

Cosθ	[0.2, 0.3] GeV	[0.3, 0.4] GeV	[0.4, 0.5] GeV	[0.5, 0.6] GeV	[0.6, 0.7] GeV	[0.7, 0.8] GeV	[0.8, 0.9] GeV	[0.9, 1.0] GeV
[−1.0, −0.8]	0.8734 ± 0.0133	1.0157 ± 0.0057	1.0000 ± 0.0020	1.0000 ± 0.0006	1.0000 ± 0.0007	1.0000 ± 0.0010	1.0000 ± 0.0006	1.0000 ± 0.0006
[−0.8, −0.6]	0.9440 ± 0.0030	1.0000 ± 0.0025	1.0000 ± 0.0003	1.0000 ± 0.0002	1.0000 ± 0.0005	1.0000 ± 0.0006	1.0000 ± 0.0011	1.0000 ± 0.0010
[−0.6, −0.4]	0.9700 ± 0.0017	1.0000 ± 0.0003	1.0000 ± 0.0001	1.0000 ± 0.0001	1.0000 ± 0.0002	1.0000 ± 0.0003	1.0000 ± 0.0006	1.0000 ± 0.0015
[−0.4, −0.2]	0.9718 ± 0.0036	1.0000 ± 0.0002	1.0000 ± 0.0002	1.0000 ± 0.0003	1.0000 ± 0.0004	1.0000 ± 0.0003	1.0000 ± 0.0010	1.0000 ± 0.0007
[−0.2, 0.0]	0.8952 ± 0.0069	1.0000 ± 0.0026	1.0000 ± 0.0003	1.0000 ± 0.0001	1.0000 ± 0.0003	1.0000 ± 0.0005	1.0000 ± 0.0004	1.0000 ± 0.0009
[0.0, 0.2]	0.9031 ± 0.0053	1.0000 ± 0.0016	1.0000 ± 0.0003	1.0000 ± 0.0001	1.0000 ± 0.0003	1.0000 ± 0.0004	1.0000 ± 0.0004	1.0000 ± 0.0011
[0.2, 0.4]	0.9816 ± 0.0033	1.0000 ± 0.0002	1.0000 ± 0.0001	1.0000 ± 0.0001	1.0000 ± 0.0001	1.0000 ± 0.0003	1.0000 ± 0.0006	1.0000 ± 0.0007
[0.4, 0.6]	0.9808 ± 0.0020	1.0000 ± 0.0007	1.0000 ± 0.0001	1.0000 ± 0.0001	1.0000 ± 0.0003	1.0000 ± 0.0004	1.0000 ± 0.0013	1.0000 ± 0.0010
[0.6, 0.8]	0.9563 ± 0.0025	1.0000 ± 0.0026	1.0000 ± 0.0002	1.0000 ± 0.0001	1.0000 ± 0.0002	1.0000 ± 0.0003	1.0000 ± 0.0005	1.0000 ± 0.0017
[0.8, 1.0]	0.9038 ± 0.0163	1.0261 ± 0.0137	1.0059 ± 0.0037	1.0000 ± 0.0019	1.0000 ± 0.0014	1.0000 ± 0.0018	1.0000 ± 0.0013	1.0000 ± 0.0008

Tab. 21: The correction factor $\epsilon_{p}^{data}/\epsilon_{p}^{MC}$ in terms of cosθ in different momentum range by using control sample $J/\psi \to p\bar{p}\pi^+\pi^-$(2009 year).

Cosθ	[0.2, 0.3] GeV	[0.3, 0.4] GeV	[0.4, 0.5] GeV	[0.5, 0.6] GeV	[0.6, 0.7] GeV	[0.7, 0.8] GeV	[0.8, 0.9] GeV	[0.9, 1.0] GeV
[−1.0, −0.8]	0.9631 ± 0.0204	1.0228 ± 0.0085	1.0122 ± 0.0068	1.0000 ± 0.0022	1.0000 ± 0.0013	1.0000 ± 0.0010	0.9919 ± 0.0019	1.0000 ± 0.0044
[−0.8, −0.6]	0.9885 ± 0.0050	1.0000 ± 0.0037	1.0000 ± 0.0015	1.0000 ± 0.0006	1.0000 ± 0.0009	1.0000 ± 0.0014	1.0000 ± 0.0012	1.0000 ± 0.0018
[−0.6, −0.4]	0.9895 ± 0.0031	1.0000 ± 0.0035	1.0000 ± 0.0027	1.0000 ± 0.0033	1.0000 ± 0.0013	1.0000 ± 0.0009	1.0000 ± 0.0010	1.0000 ± 0.0010
[−0.4, −0.2]	0.9820 ± 0.0046	1.0000 ± 0.0027	1.0000 ± 0.0021	1.0000 ± 0.0010	1.0000 ± 0.0017	1.0000 ± 0.0007	1.0000 ± 0.0010	1.0000 ± 0.0005
[−0.2, 0.0]	0.9087 ± 0.0104	1.0000 ± 0.0034	1.0000 ± 0.0030	1.0000 ± 0.0011	1.0000 ± 0.0007	1.0000 ± 0.0006	1.0000 ± 0.0008	1.0000 ± 0.0007
[0.0, 0.2]	0.8990 ± 0.0075	1.0000 ± 0.0018	1.0000 ± 0.0029	1.0000 ± 0.0013	1.0000 ± 0.0007	1.0000 ± 0.0009	1.0000 ± 0.0008	1.0000 ± 0.0007
[0.2, 0.4]	0.9720 ± 0.0049	1.0000 ± 0.0041	1.0000 ± 0.0028	1.0000 ± 0.0016	1.0000 ± 0.0021	1.0000 ± 0.0010	1.0000 ± 0.0008	1.0000 ± 0.0011
[0.4, 0.6]	0.9882 ± 0.0046	1.0000 ± 0.0034	1.0000 ± 0.0025	1.0000 ± 0.0016	1.0000 ± 0.0008	1.0000 ± 0.0009	1.0000 ± 0.0011	1.0000 ± 0.0014
[0.6, 0.8]	0.9867 ± 0.0049	1.0000 ± 0.0037	1.0000 ± 0.0013	1.0000 ± 0.0007	1.0000 ± 0.0009	1.0000 ± 0.0027	1.0000 ± 0.0011	1.0000 ± 0.0012
[0.8, 1.0]	0.9497 ± 0.0192	1.0176 ± 0.0062	1.0099 ± 0.0045	1.0000 ± 0.0017	1.0000 ± 0.0020	1.0000 ± 0.0011	1.0000 ± 0.0017	1.0000 ± 0.0033

Tab. 22: The correction factor $\epsilon_{p}^{data}/\epsilon_{p}^{MC}$ in terms of cosθ in different momentum range by using control sample $J/\psi \to p\bar{p}\pi^+\pi^-$(2012 year).

Cosθ	[0.2, 0.3] GeV	[0.3, 0.4] GeV	[0.4, 0.5] GeV	[0.5, 0.6] GeV	[0.6, 0.7] GeV	[0.7, 0.8] GeV	[0.8, 0.9] GeV	[0.9, 1.0] GeV
[−1.0, −0.8]	2.1201 ± 0.1244	1.0658 ± 0.0188	1.0165 ± 0.0055	1.0085 ± 0.0029	1.0000 ± 0.0034	1.0000 ± 0.0010	1.0000 ± 0.0016	1.0000 ± 0.0044
[−0.8, −0.6]	1.0327 ± 0.0100	1.0000 ± 0.0034	1.0000 ± 0.0022	1.0000 ± 0.0005	1.0000 ± 0.0006	1.0000 ± 0.0008	1.0000 ± 0.0008	1.0000 ± 0.0011
[−0.6, −0.4]	0.9755 ± 0.0030	1.0000 ± 0.0031	1.0000 ± 0.0019	1.0000 ± 0.0017	1.0000 ± 0.0013	1.0000 ± 0.0016	1.0000 ± 0.0012	1.0000 ± 0.0008
[−0.4, −0.2]	0.9839 ± 0.0041	1.0000 ± 0.0021	1.0000 ± 0.0041	1.0000 ± 0.0026	1.0000 ± 0.0006	1.0000 ± 0.0007	1.0000 ± 0.0005	1.0000 ± 0.0004
[−0.2, 0.0]	0.8662 ± 0.0038	1.0000 ± 0.0016	1.0000 ± 0.0027	1.0000 ± 0.0013	1.0000 ± 0.0006	1.0000 ± 0.0005	1.0000 ± 0.0008	1.0000 ± 0.0006
[0.0, 0.2]	0.8843 ± 0.0037	1.0000 ± 0.0013	1.0000 ± 0.0029	1.0000 ± 0.0012	1.0000 ± 0.0009	1.0000 ± 0.0005	1.0000 ± 0.0005	1.0000 ± 0.0005
[0.2, 0.4]	0.9692 ± 0.0047	1.0000 ± 0.0032	1.0000 ± 0.0039	1.0000 ± 0.0015	1.0000 ± 0.0005	1.0000 ± 0.0006	1.0000 ± 0.0011	1.0000 ± 0.0006
[0.4, 0.6]	0.9686 ± 0.0042	1.0000 ± 0.0030	1.0000 ± 0.0036	1.0000 ± 0.0018	1.0000 ± 0.0010	1.0000 ± 0.0015	1.0000 ± 0.0010	1.0000 ± 0.0012
[0.6, 0.8]	1.0000 ± 0.0089	1.0000 ± 0.0047	1.0000 ± 0.0017	1.0000 ± 0.0009	1.0000 ± 0.0006	1.0000 ± 0.0006	1.0000 ± 0.0024	1.0000 ± 0.0008
[0.8, 1.0]	2.4815 ± 0.0940	1.0633 ± 0.0133	1.0170 ± 0.0067	1.0077 ± 0.0019	1.0000 ± 0.0025	1.0000 ± 0.0008	1.0000 ± 0.0014	1.0000 ± 0.0026

Tab. 23: The correction factor $\epsilon_p^{data}/\epsilon_p^{MC}$ in terms of cosθ in different momentum range by using control sample $J/\psi \to p\bar{p}\pi^+\pi^-$(2018 year).

Cosθ	[0.2, 0.3] GeV	[0.3, 0.4] GeV	[0.4, 0.5] GeV	[0.5, 0.6] GeV	[0.6, 0.7] GeV	[0.7, 0.8] GeV	[0.8, 0.9] GeV	[0.9, 1.0] GeV
[−1.0, −0.8]	0.9265 ± 0.0116	1.0255 ± 0.0118	1.0000 ± 0.0047	1.0000 ± 0.0007	1.0000 ± 0.0005	1.0000 ± 0.0005	1.0000 ± 0.0005	1.0000 ± 0.0009
[−0.8, −0.6]	0.9851 ± 0.0012	1.0066 ± 0.0013	1.0000 ± 0.0004	1.0000 ± 0.0005	1.0000 ± 0.0006	1.0000 ± 0.0024	1.0000 ± 0.0011	1.0000 ± 0.0031
[−0.6, −0.4]	1.0000 ± 0.0049	1.0052 ± 0.0009	1.0000 ± 0.0013	1.0000 ± 0.0017	1.0000 ± 0.0010	1.0000 ± 0.0010	1.0000 ± 0.0012	1.0000 ± 0.0013
[−0.4, −0.2]	0.9760 ± 0.0092	1.0000 ± 0.0018	1.0000 ± 0.0027	1.0000 ± 0.0020	1.0000 ± 0.0004	1.0000 ± 0.0005	1.0000 ± 0.0005	1.0000 ± 0.0015
[−0.2, 0.0]	0.7128 ± 0.0052	0.9774 ± 0.0014	1.0000 ± 0.0010	1.0000 ± 0.0015	1.0000 ± 0.0005	1.0000 ± 0.0005	1.0000 ± 0.0010	1.0000 ± 0.0006
[0.0, 0.2]	0.7997 ± 0.0110	0.9864 ± 0.0010	1.0000 ± 0.0010	1.0000 ± 0.0006	1.0000 ± 0.0008	1.0000 ± 0.0005	1.0000 ± 0.0006	1.0000 ± 0.0009
[0.2, 0.4]	0.9824 ± 0.0046	1.0000 ± 0.0027	1.0000 ± 0.0020	1.0000 ± 0.0010	1.0000 ± 0.0005	1.0000 ± 0.0008	1.0000 ± 0.0005	1.0000 ± 0.0007
[0.4, 0.6]	1.0000 ± 0.0050	1.0000 ± 0.0050	1.0000 ± 0.0012	1.0000 ± 0.0011	1.0000 ± 0.0012	1.0000 ± 0.0006	1.0000 ± 0.0018	1.0000 ± 0.0013
[0.6, 0.8]	0.9892 ± 0.0017	1.0000 ± 0.0012	1.0000 ± 0.0004	1.0000 ± 0.0003	1.0000 ± 0.0006	1.0000 ± 0.0013	1.0000 ± 0.0015	1.0000 ± 0.0014
[0.8, 1.0]	0.9382 ± 0.0075	1.0214 ± 0.0083	1.0070 ± 0.0022	1.0000 ± 0.0006	1.0000 ± 0.0009	1.0000 ± 0.0009	1.0000 ± 0.0011	1.0000 ± 0.0012

Tab. 24: The correction factor $\epsilon_p^{data}/\epsilon_p^{MC}$ in terms of cosθ in different momentum range by using control sample $J/\psi \to p\bar{p}\pi^+\pi^-$(2019 year).

Cosθ	[0.2, 0.3] GeV	[0.3, 0.4] GeV	[0.4, 0.5] GeV	[0.5, 0.6] GeV	[0.6, 0.7] GeV	[0.7, 0.8] GeV	[0.8, 0.9] GeV	[0.9, 1.0] GeV
[−1.0, −0.8]	0.8857 ± 0.0094	1.0271 ± 0.0107	1.0055 ± 0.0037	1.0000 ± 0.0015	1.0000 ± 0.0006	1.0000 ± 0.0007	1.0000 ± 0.0009	1.0000 ± 0.0022
[−0.8, −0.6]	0.9453 ± 0.0033	1.0083 ± 0.0011	1.0000 ± 0.0004	1.0000 ± 0.0007	1.0000 ± 0.0005	1.0000 ± 0.0010	1.0000 ± 0.0010	1.0000 ± 0.0018
[−0.6, −0.4]	0.9733 ± 0.0019	1.0000 ± 0.0045	1.0000 ± 0.0016	1.0000 ± 0.0018	1.0000 ± 0.0007	1.0000 ± 0.0007	1.0000 ± 0.0009	1.0000 ± 0.0006
[−0.4, −0.2]	0.9752 ± 0.0072	1.0000 ± 0.0023	1.0000 ± 0.0020	1.0000 ± 0.0014	1.0000 ± 0.0006	1.0000 ± 0.0006	1.0000 ± 0.0007	1.0000 ± 0.0009
[−0.2, 0.0]	0.7486 ± 0.0103	1.9798 ± 0.0017	1.0000 ± 0.0014	1.0000 ± 0.0006	1.0000 ± 0.0011	1.0000 ± 0.0006	1.0000 ± 0.0004	1.0000 ± 0.0005
[0.0, 0.2]	0.8265 ± 0.0116	0.9884 ± 0.0013	1.0000 ± 0.0011	1.0000 ± 0.0016	1.0000 ± 0.0004	1.0000 ± 0.0004	1.0000 ± 0.0005	1.0000 ± 0.0005
[0.2, 0.4]	0.9725 ± 0.0035	1.0000 ± 0.0012	1.0000 ± 0.0022	1.0000 ± 0.0011	1.0000 ± 0.0006	1.0000 ± 0.0006	1.0000 ± 0.0005	1.0000 ± 0.0007
[0.4, 0.6]	0.9672 ± 0.0013	1.0000 ± 0.0043	1.0000 ± 0.0009	1.0000 ± 0.0013	1.0000 ± 0.0005	1.0000 ± 0.0015	1.0000 ± 0.0026	1.0000 ± 0.0010
[0.6, 0.8]	0.9458 ± 0.0031	1.0073 ± 0.0013	1.0000 ± 0.0003	1.0000 ± 0.0003	1.0000 ± 0.0004	1.0000 ± 0.0006	1.0000 ± 0.0015	1.0000 ± 0.0023
[0.8, 1.0]	0.9021 ± 0.0149	1.0173 ± 0.0081	1.0000 ± 0.0018	1.0000 ± 0.0012	1.0000 ± 0.0008	1.0000 ± 0.0012	1.0000 ± 0.0006	1.0000 ± 0.0013

Tab. 25: The correction factor $\epsilon_{\pi^-}^{data}/\epsilon_{\pi^-}^{MC}$ in terms of cosθ in different momentum range by using control sample $J/\psi \to p\bar{p}\pi^+\pi^-$(2009 year).

Cosθ	[0.05, 0.15] GeV	[0.15, 0.25] GeV	[0.25, 0.35] GeV	[0.35, 0.45] GeV	[0.45, 0.55] GeV	[0.55, 0.65] GeV
[−1.0, −0.8]	1.0112 ± 0.0040	1.0000 ± 0.0009	1.0000 ± 0.0013	1.0000 ± 0.0042	0.9937 ± 0.0021	1.0000 ± 0.0061
[−0.8, −0.6]	1.0000 ± 0.0034	1.0000 ± 0.0006	1.0000 ± 0.0005	1.0000 ± 0.0022	1.0000 ± 0.0024	1.0000 ± 0.0020
[−0.6, −0.4]	1.0000 ± 0.0028	1.0000 ± 0.0007	1.0000 ± 0.0009	1.0000 ± 0.0049	0.9942 ± 0.0012	1.0000 ± 0.0021
[−0.4, −0.2]	1.0000 ± 0.0015	1.0000 ± 0.0015	1.0000 ± 0.0009	1.0000 ± 0.0048	0.9938 ± 0.0015	0.9920 ± 0.0022
[−0.2, 0.0]	0.9877 ± 0.0034	1.0000 ± 0.0012	1.0000 ± 0.0013	0.9937 ± 0.0010	0.9902 ± 0.0017	0.9862 ± 0.0025
[0.0, 0.2]	0.9849 ± 0.0038	1.0000 ± 0.0008	1.0000 ± 0.0010	0.9942 ± 0.0010	0.9911 ± 0.0016	0.9902 ± 0.0025
[0.2, 0.4]	1.0000 ± 0.0014	1.0000 ± 0.0008	1.0000 ± 0.0012	0.9949 ± 0.0009	0.9905 ± 0.0014	0.9939 ± 0.0023
[0.4, 0.6]	1.0000 ± 0.0019	1.0000 ± 0.0006	1.0000 ± 0.0005	1.0000 ± 0.0048	1.0000 ± 0.0041	1.0000 ± 0.0042
[0.6, 0.8]	1.0000 ± 0.0032	1.0000 ± 0.0011	1.0000 ± 0.0015	1.0000 ± 0.0019	1.0000 ± 0.0029	1.0000 ± 0.0016
[0.8, 1.0]	1.0061 ± 0.0071	1.0000 ± 0.0010	1.0000 ± 0.0027	1.0000 ± 0.0031	1.0000 ± 0.0027	0.9897 ± 0.0042

Tab. 26: The correction factor $\epsilon_{\pi^-}^{data}/\epsilon_{\pi^-}^{MC}$ in terms of cosθ in different momentum range by using control sample $J/\psi \to p\bar{p}\pi^+\pi^-$(2012 year).

Cosθ	[0.05, 0.15] GeV	[0.15, 0.25] GeV	[0.25, 0.35] GeV	[0.35, 0.45] GeV	[0.45, 0.55] GeV	[0.55, 0.65] GeV
[−1.0, −0.8]	1.4925 ± 0.0349	1.0397 ± 0.0063	1.0101 ± 0.0032	1.0000 ± 0.0036	1.0000 ± 0.0022	1.0000 ± 0.0030
[−0.8, −0.6]	1.1014 ± 0.0192	1.0000 ± 0.0043	1.0000 ± 0.0009	1.0000 ± 0.0010	1.0000 ± 0.0023	1.0000 ± 0.0036
[−0.6, −0.4]	1.0268 ± 0.0077	1.0000 ± 0.0013	1.0000 ± 0.0010	1.0000 ± 0.0027	0.9942 ± 0.0007	0.9943 ± 0.0012
[−0.4, −0.2]	1.0086 ± 0.0042	1.0000 ± 0.0006	1.0000 ± 0.0007	1.0000 ± 0.0049	0.9909 ± 0.0009	0.9931 ± 0.0015
[−0.2, 0.0]	1.0000 ± 0.0056	1.0000 ± 0.0005	1.0000 ± 0.0010	0.9938 ± 0.0005	0.9892 ± 0.0009	0.9908 ± 0.0016
[0.0, 0.2]	1.0000 ± 0.0038	1.0000 ± 0.0011	1.0000 ± 0.0012	0.9943 ± 0.0005	0.9909 ± 0.0010	0.9894 ± 0.0017
[0.2, 0.4]	1.0088 ± 0.0045	1.0000 ± 0.0011	1.0000 ± 0.0005	0.9949 ± 0.0048	0.9904 ± 0.0009	0.9922 ± 0.0015
[0.4, 0.6]	1.0206 ± 0.0070	1.0000 ± 0.0021	1.0000 ± 0.0005	1.0000 ± 0.0030	0.9943 ± 0.0007	0.9948 ± 0.0011
[0.6, 0.8]	1.0872 ± 0.0182	1.0000 ± 0.0035	1.0000 ± 0.0005	1.0000 ± 0.0021	1.0000 ± 0.0030	1.0000 ± 0.0029
[0.8, 1.0]	1.3996 ± 0.0510	1.0364 ± 0.0038	1.0122 ± 0.0016	1.0000 ± 0.0024	1.0000 ± 0.0017	0.9897 ± 0.0037

Tab. 27: The correction factor $\epsilon_{\pi^-}^{data}/\epsilon_{\pi^-}^{MC}$ in terms of cosθ in different momentum range by using control sample $J/\psi \to p\bar{p}\pi^+\pi^-$(2018 year).

Cosθ	[0.05, 0.15] GeV	[0.15, 0.25] GeV	[0.25, 0.35] GeV	[0.35, 0.45] GeV	[0.45, 0.55] GeV	[0.55, 0.65] GeV
[−1.0, −0.8]	1.0000 ± 0.0054	1.0000 ± 0.0010	1.0000 ± 0.0011	1.0000 ± 0.0017	1.0000 ± 0.0015	1.0000 ± 0.0020
[−0.8, −0.6]	1.0000 ± 0.0008	1.0000 ± 0.0004	1.0000 ± 0.0007	1.0000 ± 0.0015	1.0000 ± 0.0025	1.0000 ± 0.0025
[−0.6, −0.4]	1.0000 ± 0.0013	1.0000 ± 0.0006	1.0000 ± 0.0006	1.0000 ± 0.0026	1.0000 ± 0.0043	1.0000 ± 0.0045
[−0.4, −0.2]	1.0000 ± 0.0015	1.0000 ± 0.0004	1.0000 ± 0.0009	1.0000 ± 0.0043	0.9945 ± 0.0008	1.0000 ± 0.0038
[−0.2, 0.0]	0.9835 ± 0.0017	1.0000 ± 0.0004	1.0000 ± 0.0005	0.9947 ± 0.0005	0.9901 ± 0.0008	0.9894 ± 0.0015
[0.0, 0.2]	0.9777 ± 0.0016	1.0000 ± 0.0006	1.0000 ± 0.0005	1.0000 ± 0.0045	0.9899 ± 0.0009	0.9916 ± 0.0015
[0.2, 0.4]	1.0000 ± 0.0012	1.0000 ± 0.0007	1.0000 ± 0.0009	1.0000 ± 0.0028	0.9941 ± 0.0009	0.9943 ± 0.0014
[0.4, 0.6]	1.0000 ± 0.0010	1.0000 ± 0.0004	1.0000 ± 0.0004	1.0000 ± 0.0014	1.0000 ± 0.0043	1.0000 ± 0.0032
[0.6, 0.8]	1.0000 ± 0.0010	1.0000 ± 0.0004	1.0000 ± 0.0007	1.0000 ± 0.0018	1.0000 ± 0.0018	1.0000 ± 0.0014
[0.8, 1.0]	1.0000 ± 0.0056	1.0000 ± 0.0007	1.0000 ± 0.0009	1.0000 ± 0.0014	1.0000 ± 0.0012	1.0000 ± 0.0018

Tab. 28: The correction factor $\epsilon_{\pi^-}^{data}/\epsilon_{\pi^-}^{MC}$ in terms of cosθ in different momentum range by using control sample $J/\psi \to p\bar{p}\pi^+\pi^-$(2019 year).

Cosθ	[0.05, 0.15] GeV	[0.15, 0.25] GeV	[0.25, 0.35] GeV	[0.35, 0.45] GeV	[0.45, 0.55] GeV	[0.55, 0.65] GeV
[−1.0, −0.8]	0.9942 ± 0.0035	1.0000 ± 0.0020	1.0000 ± 0.0015	1.0000 ± 0.0013	1.0000 ± 0.0021	1.0000 ± 0.0031
[−0.8, −0.6]	1.0000 ± 0.0014	1.0000 ± 0.0008	1.0000 ± 0.0007	1.0000 ± 0.0019	1.0000 ± 0.0020	1.0000 ± 0.0021
[−0.6, −0.4]	1.0000 ± 0.0009	1.0000 ± 0.0004	1.0000 ± 0.0005	1.0000 ± 0.0028	1.0000 ± 0.0049	1.0000 ± 0.0021
[−0.4, −0.2]	1.0000 ± 0.0015	1.0000 ± 0.0004	1.0000 ± 0.0005	1.0000 ± 0.0046	0.9938 ± 0.0008	0.9942 ± 0.0015
[−0.2, 0.0]	0.9833 ± 0.0019	1.0000 ± 0.0004	1.0000 ± 0.0008	0.9947 ± 0.0005	0.9890 ± 0.0009	0.9898 ± 0.0015
[0.0, 0.2]	0.9783 ± 0.0027	1.0000 ± 0.0004	1.0000 ± 0.0004	1.0000 ± 0.0044	0.9912 ± 0.0009	0.9907 ± 0.0015
[0.2, 0.4]	1.0000 ± 0.0023	1.0000 ± 0.0005	1.0000 ± 0.0008	1.0000 ± 0.0046	0.9932 ± 0.0008	0.9944 ± 0.0015
[0.4, 0.6]	1.0000 ± 0.0008	1.0000 ± 0.0005	1.0000 ± 0.0008	1.0000 ± 0.0028	1.0000 ± 0.0045	1.0000 ± 0.0033
[0.6, 0.8]	1.0000 ± 0.0023	1.0000 ± 0.0005	1.0000 ± 0.0004	1.0000 ± 0.0018	1.0000 ± 0.0024	1.0000 ± 0.0026
[0.8, 1.0]	1.0000 ± 0.0044	1.0000 ± 0.0015	1.0000 ± 0.0011	1.0000 ± 0.0011	1.0000 ± 0.0009	1.0000 ± 0.0017

Tab. 29: The correction factor $\epsilon^{data}_{\pi^+}/\epsilon^{MC}_{\pi^+}$ in terms of cosθ in different momentum range by using control sample $J/\psi \to p\bar{p}\pi^+\pi^-$(2009 year).

Cosθ	[0.05, 0.15] GeV	[0.15, 0.25] GeV	[0.25, 0.35] GeV	[0.35, 0.45] GeV	[0.45, 0.55] GeV	[0.55, 0.65] GeV
[−1.0, −0.8]	1.0000 ± 0.0051	1.0000 ± 0.0026	1.0000 ± 0.0020	1.0000 ± 0.0033	1.0000 ± 0.0034	0.9931 ± 0.0046
[−0.8, −0.6]	1.0000 ± 0.0042	1.0000 ± 0.0006	1.0000 ± 0.0004	1.0000 ± 0.0010	1.0000 ± 0.0017	1.0000 ± 0.0023
[−0.6, −0.4]	1.0000 ± 0.0041	1.0000 ± 0.0007	1.0000 ± 0.0010	1.0000 ± 0.0018	1.0000 ± 0.0015	1.0000 ± 0.0045
[−0.4, −0.2]	1.0000 ± 0.0025	1.0000 ± 0.0006	1.0000 ± 0.0005	1.0000 ± 0.0014	1.0000 ± 0.0012	0.9936 ± 0.0045
[−0.2, 0.0]	0.9810 ± 0.0046	1.0000 ± 0.0005	1.0000 ± 0.0008	1.0000 ± 0.0023	1.0000 ± 0.0024	1.0000 ± 0.0022
[0.0, 0.2]	0.9826 ± 0.0063	1.0000 ± 0.0005	1.0000 ± 0.0012	1.0000 ± 0.0028	1.0000 ± 0.0027	0.9920 ± 0.0024
[0.2, 0.4]	1.0000 ± 0.0020	1.0000 ± 0.0007	1.0000 ± 0.0006	1.0000 ± 0.0021	1.0000 ± 0.0027	0.9929 ± 0.0039
[0.4, 0.6]	1.0000 ± 0.0012	1.0000 ± 0.0006	1.0000 ± 0.0008	1.0000 ± 0.0009	1.0000 ± 0.0016	1.0000 ± 0.0052
[0.6, 0.8]	1.0000 ± 0.0016	1.0000 ± 0.0008	1.0000 ± 0.0005	1.0000 ± 0.0005	1.0000 ± 0.0016	1.0000 ± 0.0034
[0.8, 1.0]	1.0000 ± 0.0064	1.0000 ± 0.0031	1.0000 ± 0.0021	1.0000 ± 0.0018	1.0000 ± 0.0050	0.9921 ± 0.0043

Tab. 30: The correction factor $\epsilon^{data}_{\pi^+}/\epsilon^{MC}_{\pi^+}$ in terms of cosθ in different momentum range by using control sample $J/\psi \to p\bar{p}\pi^+\pi^-$(2012 year).

Cosθ	[0.05, 0.15] GeV	[0.15, 0.25] GeV	[0.25, 0.35] GeV	[0.35, 0.45] GeV	[0.45, 0.55] GeV	[0.55, 0.65] GeV
[−1.0, −0.8]	1.3848 ± 0.0405	1.0388 ± 0.0074	1.0114 ± 0.0022	1.0000 ± 0.0038	1.0000 ± 0.0037	0.9929 ± 0.0028
[−0.8, −0.6]	1.0940 ± 0.0158	1.0000 ± 0.0039	1.0000 ± 0.0010	1.0000 ± 0.0004	1.0000 ± 0.0009	1.0000 ± 0.0024
[−0.6, −0.4]	1.0217 ± 0.0042	1.0000 ± 0.0017	1.0000 ± 0.0009	1.0000 ± 0.0011	1.0000 ± 0.0030	1.0000 ± 0.0039
[−0.4, −0.2]	1.0091 ± 0.0038	1.0000 ± 0.0009	1.0000 ± 0.0003	1.0000 ± 0.0010	1.0000 ± 0.0030	0.9936 ± 0.0014
[−0.2, 0.0]	1.0000 ± 0.0053	1.0000 ± 0.0003	1.0000 ± 0.0011	1.0000 ± 0.0018	1.0000 ± 0.0021	1.0000 ± 0.0032
[0.0, 0.2]	1.0000 ± 0.0051	1.0000 ± 0.0007	1.0000 ± 0.0012	1.0000 ± 0.0019	1.0000 ± 0.0026	0.9935 ± 0.0016
[0.2, 0.4]	1.0120 ± 0.0039	1.0000 ± 0.0014	1.0000 ± 0.0003	1.0000 ± 0.0015	1.0000 ± 0.0023	0.9928 ± 0.0014
[0.4, 0.6]	1.0225 ± 0.0055	1.0000 ± 0.0009	1.0000 ± 0.0005	1.0000 ± 0.0007	1.0000 ± 0.0020	1.0000 ± 0.0039
[0.6, 0.8]	1.1008 ± 0.0017	1.0000 ± 0.0046	1.0000 ± 0.0008	1.0000 ± 0.0003	1.0000 ± 0.0012	1.0000 ± 0.0027
[0.8, 1.0]	1.4857 ± 0.0715	1.0316 ± 0.0065	1.0093 ± 0.0026	1.0000 ± 0.0047	1.0000 ± 0.0020	1.0000 ± 0.0057

Tab. 31: The correction factor $\epsilon^{data}_{\pi^+}/\epsilon^{MC}_{\pi^+}$ in terms of cosθ in different momentum range by using control sample $J/\psi \to p\bar{p}\pi^+\pi^-$(2018 year).

Cosθ	[0.05, 0.15] GeV	[0.15, 0.25] GeV	[0.25, 0.35] GeV	[0.35, 0.45] GeV	[0.45, 0.55] GeV	[0.55, 0.65] GeV
[−1.0, −0.8]	1.0000 ± 0.0058	1.0000 ± 0.0015	1.0000 ± 0.0012	1.0000 ± 0.0014	1.0000 ± 0.0016	1.0000 ± 0.0019
[−0.8, −0.6]	1.0000 ± 0.0012	1.0000 ± 0.0005	1.0000 ± 0.0003	1.0000 ± 0.0003	1.0000 ± 0.0009	1.0000 ± 0.0014
[−0.6, −0.4]	1.0000 ± 0.0009	1.0000 ± 0.0005	1.0000 ± 0.0003	1.0000 ± 0.0004	1.0000 ± 0.0007	1.0000 ± 0.0014
[−0.4, −0.2]	1.0000 ± 0.0018	1.0000 ± 0.0008	1.0000 ± 0.0008	1.0000 ± 0.0005	1.0000 ± 0.0008	1.0000 ± 0.0022
[−0.2, 0.0]	0.9750 ± 0.0014	1.0000 ± 0.0006	1.0000 ± 0.0008	1.0000 ± 0.0008	1.0000 ± 0.0012	0.9938 ± 0.0050
[0.0, 0.2]	0.9788 ± 0.0022	1.0000 ± 0.0005	1.0000 ± 0.0004	1.0000 ± 0.0006	1.0000 ± 0.0013	0.9929 ± 0.0022
[0.2, 0.4]	1.0000 ± 0.0012	1.0000 ± 0.0003	1.0000 ± 0.0009	1.0000 ± 0.0005	1.0000 ± 0.0010	1.0000 ± 0.0035
[0.4, 0.6]	1.0000 ± 0.0011	1.0000 ± 0.0008	1.0000 ± 0.0012	1.0000 ± 0.0007	1.0000 ± 0.0011	1.0000 ± 0.0014
[0.6, 0.8]	1.0000 ± 0.0013	1.0000 ± 0.0004	1.0000 ± 0.0003	1.0000 ± 0.0005	1.0000 ± 0.0012	1.0000 ± 0.0011
[0.8, 1.0]	1.0000 ± 0.0051	1.0000 ± 0.0009	1.0000 ± 0.0008	1.0000 ± 0.0017	1.0000 ± 0.0019	1.0000 ± 0.0034

Tab. 32: The correction factor $\epsilon_{\pi^+}^{data}/\epsilon_{\pi^+}^{MC}$ in terms of cosθ in different momentum range by using control sample $J/\psi \to p\bar{p}\pi^+\pi^-$(2019 year).

Cosθ	[0.05, 0.15] GeV	[0.15, 0.25] GeV	[0.25, 0.35] GeV	[0.35, 0.45] GeV	[0.45, 0.55] GeV	[0.55, 0.65] GeV
$[-1.0, -0.8]$	1.0000 ± 0.0048	1.0000 ± 0.0008	1.0000 ± 0.0011	1.0000 ± 0.0020	1.0000 ± 0.0022	1.0000 ± 0.0025
$[-0.8, -0.6]$	1.0000 ± 0.0027	1.0000 ± 0.0003	1.0000 ± 0.0003	1.0000 ± 0.0007	1.0000 ± 0.0005	1.0000 ± 0.0010
$[-0.6, -0.4]$	1.0000 ± 0.0014	1.0000 ± 0.00010	1.0000 ± 0.0008	1.0000 ± 0.0007	1.0000 ± 0.0007	1.0000 ± 0.0017
$[-0.4, -0.2]$	1.0000 ± 0.0019	1.0000 ± 0.0003	1.0000 ± 0.0005	1.0000 ± 0.0010	1.0000 ± 0.0009	1.0000 ± 0.0030
$[-0.2, 0.0]$	0.9750 ± 0.0017	1.0000 ± 0.0005	1.0000 ± 0.0003	1.0000 ± 0.0012	1.0000 ± 0.0012	0.9929 ± 0.0014
$[0.0, 0.2]$	0.9788 ± 0.0021	1.0000 ± 0.0004	1.0000 ± 0.0005	1.0000 ± 0.0006	1.0000 ± 0.0017	0.9938 ± 0.0016
$[0.2, 0.4]$	1.0000 ± 0.0019	1.0000 ± 0.0011	1.0000 ± 0.0003	1.0000 ± 0.0006	1.0000 ± 0.0013	1.0000 ± 0.0043
$[0.4, 0.6]$	1.0000 ± 0.0008	1.0000 ± 0.0006	1.0000 ± 0.0006	1.0000 ± 0.0004	1.0000 ± 0.0013	1.0000 ± 0.0020
$[0.6, 0.8]$	1.0000 ± 0.0012	1.0000 ± 0.0004	1.0000 ± 0.0004	1.0000 ± 0.0008	1.0000 ± 0.0008	1.0000 ± 0.0012
$[0.8, 1.0]$	1.0000 ± 0.0054	1.0000 ± 0.0007	1.0000 ± 0.0009	1.0000 ± 0.0015	1.0000 ± 0.0016	1.0000 ± 0.0020

Tab. 33: The correction factor $\epsilon_{\pi^0}^{data}/\epsilon_{\pi^0}^{MC}$ in terms of cosθ in different momentum range

Cosθ	[0.05, 0.15] GeV	[0.15, 0.25] GeV	[0.25, 0.35] GeV	[0.35, 0.45] GeV
$[-1.0, -0.8]$	0.9960 ± 0.0167	1.0003 ± 0.0156	0.9641 ± 0.0214	0.9758 ± 0.0372
$[-0.8, -0.6]$	0.9859 ± 0.0163	0.9908 ± 0.0145	0.9793 ± 0.0153	0.9772 ± 0.0216
$[-0.6, -0.4]$	0.9698 ± 0.0176	0.9897 ± 0.0136	0.9808 ± 0.0105	0.9664 ± 0.0138
$[-0.4, -0.2]$	1.0063 ± 0.0170	0.9990 ± 0.0145	0.9899 ± 0.0113	1.0049 ± 0.0026
$[-0.2, 0.0]$	0.9899 ± 0.0177	0.9950 ± 0.0099	0.9933 ± 0.0123	0.9887 ± 0.0015
$[0.0, 0.2]$	0.9966 ± 0.0178	0.9808 ± 0.0098	0.9914 ± 0.0118	0.9757 ± 0.0057
$[0.2, 0.4]$	1.0373 ± 0.0198	0.9890 ± 0.0046	0.9994 ± 0.0135	0.9797 ± 0.0097
$[0.4, 0.6]$	0.9875 ± 0.0167	0.9909 ± 0.0062	0.9803 ± 0.0152	0.9832 ± 0.0069
$[0.6, 0.8]$	0.9906 ± 0.0163	0.9878 ± 0.0156	0.9975 ± 0.0188	1.0347 ± 0.0123
$[0.8, 1.0]$	0.9889 ± 0.0163	0.9882 ± 0.0166	0.9743 ± 0.0219	0.9604 ± 0.0131